EFFECTS OF VARYING QUANTUM WELL BARRIER HEIGHT AND QUANTUM WELL NUMBER ON THE INTRINSIC FREQUENCY RESPONSE OF InGaAsP/InP MULTIPLE QUANTUM WELL SEMICONDUCTOR LASERS

By

ANTHONY SCOTT VETTER, B.Eng.

A Thesis
Submitted to the School of Graduate Studies
in Partial Fulfillment of the Requirements
for the Degree
Masters of Engineering

McMaster University

MASTERS OF ENGINEERING (1997) McMASTER UNIVERSITY
(Engineering Physics) Hamilton, Ontario

TITLE: Effects of Varying Quantum Well Barrier Height and Quantum Well Number on the Intrinsic Frequency Response of InGaAsP/InP Multiple Quantum Well Semiconductor Lasers

AUTHOR: Anthony Scott Vetter, B.Eng. (McMaster University)

SUPERVISOR: Professor J. G. Simmons

NUMBER OF PAGES: xvii, 137

ABSTRACT

This thesis reports on an extensive investigation into the intrinsic frequency response of various MQW lasers as determined from parasitic-free relative intensity noise (RIN) measurements. Eleven structures were designed, grown and fabricated at Nortel Technology's Advanced Technology Laboratory in Ottawa. Five of the laser structures had active regions containing 10 QWs. The barrier layer composition for these structures was varied such that the emission wavelength corresponding to the barrier band-gap increased from 1.0 μm to 1.2 μm in 0.05 μm steps. The remaining six structures had a constant barrier layer emission wavelength of 1.1 μm but the number of quantum wells was varied from 5, 7, 8 to 14 in 2 well steps. In all structures the QWs were embedded in a graded-index-separate-confinement-heterostructure waveguiding region and were strained to 1.0 percent in compression. The devices processed from these structures were Fabry-Perot type lasers having cavity lengths ranging from 254 μm to 1016 μm. Resonance frequency and damping values as a function of injection current and single facet optical power, as well as optical spectra just below threshold, were obtained for over one hundred devices. From this data the response coefficient D, K factor, group velocity (v_g), photon energy ($h\nu$), mirror loss (α_m), and internal absorption (α_{int}) were characterized. Using these characterized parameters $\partial g/\partial N$, $\partial g/\partial s$, and the maximum theoretical intrinsic 3 dB bandwidth (f_{max}) were calculated. The effects of varying QW number, barrier height, and cavity length on all these parameters was investigated. Limitations with using the single mode rate equation model for these characterizations is discussed. As well, potential limitations with the basic design of the structures studied in this thesis as revealed by the results are explored.

ACKNOWLEDGMENTS

I would very much like to express my appreciation to my supervisor Dr. Simmons for his support, and encouragement, not only for the time that he has served as my supervisor, but for the opportunities he made possible starting in my fourth year of undergraduate studies at McMaster University. I would also like to thank him for providing me with financial support while I conducted this investigation at Nortel Technology's Advanced Technology Lab in Ottawa. Being a member of his research team of students at McMaster University has afforded me the opportunity to work with many other people and facilities of the highest caliber. I would like to acknowledge the support, and encouragement, of three of Dr. Simmon's students, Dr. Jugnu Ohja, Dr. Stephen Kovacic, and Dr. John Evans. Special thanks go to both Steve and Jugnu for giving me the opportunity to assist them with their PhD research during my fourth year of undergraduate studies, and for many engaging scientific conversations that enlightened me to the fact that group interaction can be my most enjoyable intellectual catalyst.

However it is John Evans, to whom I am deeply indebted, who was largely responsible for getting off on the right foot with this thesis. Not only was he incredibly generous with his time, and support, most of the initial device characterization work in this thesis was carried out on experimental apparatus of his making or design at McMaster University. John Evans was also largely responsible for obtaining access to, and permission to, characterize the device structures in this thesis. John Evans was very instrumental in creating the opportunity for me to carry out the majority of this work at

Nortel Technologies Advanced Technology Lab in Ottawa, and acted as my unofficial co-supervisor during my thesis work there.

I would also like to thank all of the other graduate students in Engineering Physics at McMaster University who in one way or another made my stay there one of life's experiences. In particular, special thanks go to John Hazell, Kelvin Prosyk, and Greg Letal for their assistance in the lab at McMaster while I was there, as well while in Ottawa.

I would also like to thank all the members of scientific staff at Nortel Technologies Advanced Technology Lab in Ottawa for their generosity and support. In particular I would like to thank Dr. T. Makino and Dr. H. Lu for allowing me to work at the Advanced Technology Lab as a visiting scientist, for allowing access to the material characterized in this thesis, and for giving me access to their characterization facilities. I would also like to thank Dr. C. Blaauw for the growth, and F. Shepherd for the processing of the laser structures. Special thanks also go to L. Raine and Z. Husain for cleaving and bonding the laser devices, as well as to L. Raine for her assistance in the lab. I would also like to thank D. Adams, G. Mak, J. Goodwin, H. Kim for their theoretical, and technical support on many occasions.

In addition, financial support from the Natural Sciences and Engineering Research Council of Canada, and the Ontario Center for Material Research is also gratefully acknowledged.

Special thanks go to my family and friends who supported me throughout my graduate work. In particular I would like to acknowledge Nathalie Cloutier who helped me maintain mental and emotional balance while I was finishing the writing of this thesis. Finally, thanks to Nicholas Cardone for reasons that he would find self evident.

TABLE OF CONTENTS

LIST OF FIGURES

LIST OF TABLES

CHAPTER 1: INTRODUCTION

1.0 1.3 μm WAVELENGTH LASERS

Two important things need to be considered when developing a long-haul optical fiber communication system: the distance after which an optical signal weakened by fiber loss needs to be regenerated, often referred to as the repeater spacing distance; and the transmission capacity of the signal, often referred to as the bit rate. Fiber-chromatic dispersion, which causes the broadening of optical pulses propagating in a fiber, is the main fiber-related factor limiting bit rate. The objective of any long-haul communication system is to maximize the bit-rate-distance product by taking advantage of the loss and dispersion characteristics of optical fiber. The two wavelength regions of choice for commercially available single-mode silica fibers are 1.3 μm and 1.55 μm. At 1.3 μm transmission commonly used silica fiber has almost negligible fiber-chromatic dispersion; however, the fiber absorption loss at this wavelength limits the repeater spacing significantly. At 1.55 μm there exists an advantageous minimum in the fiber loss, but the bit rate is significantly limited by fiber dispersion. Up till now silica fiber with these material properties has been predominantly deployed in the field. Optical fiber communication systems operating in these two wavelength regions have been realized with the development of commercially viable semiconductor lasers with these emission wavelengths. However, due to the numerous ways that the limitations which exist at these two wavelength regions could potentially be overcome, intense debate over which system will ultimately prove to have the greatest commercial potential continues.

When a semiconductor laser is directly modulated a significant variation in the refractive index occurs with the changing carrier concentration in the active region. This causes a dynamic shift of the lasing frequency, commonly referred to as frequency chirping. Even with recent laser designs, frequency chirp continues to be a major limiting factor of the maximum bit rate achievable in optical fiber communication systems, and it is proving to be a difficult phenomenon to minimize practically. This is magnified by the unavoidable dispersion penalty of the 1.55 μm window of common silica fibers, making the negligible fiber dispersion of the 1.3 μm window attractive. This has given purpose to improving the bandwidth performance of lasers with emission wavelengths of 1.3 μm, as well as the development of higher power lasers to extend the repeater spacing distance at this wavelength.

1.1 USE OF QUANTUM-WELL LASERS FOR HIGH-SPEED APPLICATIONS

Since their introduction two decades ago, quantum-well lasers have received much attention as the beneficial effects of quantization have been realized. Early theoretical work on quantum-well structures predicted enhanced differential gain over bulk lasers [1]-[7]. From the modeling of the high speed dynamics of semiconductor lasers, it has been shown that higher differential gain is expected to result not only in higher resonance frequency as a function of power, but in reduced damping. This was in turn shown to predict bandwidth performance [8]-[10]. As processing techniques improved and viable and reliable QW lasers were developed, it became apparent that the hopes of devices with much higher modulation bandwidth were not to be fulfilled.

The material gain of a laser is postulated to depend on photon density and carrier density in the active region of a semiconductor laser [11]. This dependency on photon population, characterized by the gain derivative with respect to photon density, is referred to as gain suppression, or nonlinear gain, and is usually negative. When included in the rate equation analysis, nonlinear gain also appears to play an important role in the frequency response of semiconductor lasers. Many studies have shown that this factor is typically much higher in quantum-well lasers than in bulk lasers, which could account for why a significant improvement in the modulation bandwidth was not observed [1] [2] [12]-[18]. It has also been suggested that long carrier transport delays in the undoped regions of the laser, as in the separate-confinement heterostructure, introduces a low frequency parasitic-like rolloff which severely limits the maximum possible modulation bandwidth [1] [19]-[22]. Also, carrier transport effects in the quantum-well active region may in fact be responsible for a direct reduction of the effective differential gain via a transport factor, χ, and not an enhancement of ε [22].

Much recent work has focused on using strain to further improve the benefits of quantization in quantum-well lasers. Early theoretical work predicted that the introduction of strain to a QW active layer would increase differential gain due to changes in the valence band structure [7] [23] [24]. Some work did not show any beneficial effect of strain on differential gain [25] [26], but a large number of studies have shown encouraging results [1] [12] [13] [27]-[29]. However, this increase in differential gain has not always resulted in an increase of the modulation bandwidth, as strain has been shown to increase nonlinear gain in some cases [30] [31]. Other results have shown that this may be debatable and that strain has no effect on nonlinear gain [22] [32].

Based on the results achieved to date, improvement in the frequency response of semiconductor lasers is not going to be realized by simply replacing a bulk active region with an arbitrarily strained multiple quantum-well structure. Many technologically important parameters must be simultaneously considered, for example: QW number and width; barrier and width; separate confinement structure; active region optical confinement; and strain of the active region. Careful device design is required in order to maximize the enhancement in differential gain, obtained by the use of quantum wells, and minimize the increase in nonlinear gain and other effects due to carrier transport mechanisms.

1.2 MEASURING THE INTRINSIC FREQUENCY RESPONSE

Measurements of the intrinsic frequency response of semiconductor lasers permit the study of the dynamic operation of a device without being limited by the RC parasitics introduced by electrical contacts and device packaging. They therefore provide a very powerful characterization of the interplay between the optical field and the carrier population inversion in the laser active region. Based on commonly accepted theoretical models and characterization methodologies, access to parameters such as differential gain and nonlinear gain, and the effect that changing structural parameters such as quantum-well number, depth, and optical confinement has on these has been demonstrated. The simplicity with which the intrinsic frequency response can be measured, combined with the range of device parameters this characterization theoretically offers access to, makes this type of characterization a potentially powerful tool for offering insight to semiconductor laser design considerations.

1.3 OBJECTIVE OF THESIS

In this thesis an extensive study of multiple quantum well (MQW) lasers is reported.

In Chapter 2 of this thesis the theoretical concepts of intensity noise in semiconductor lasers, the nature of relative intensity noise (RIN) spectra, and the parametric forms that relaxation oscillation frequency and damping factor take with reference to RIN spectra are examined. How the parameters that contribute to the relaxation oscillation frequency and damping factor are related to the intrinsic bandwidth of semiconductors, which are studied in this thesis, is developed.

In Chapter 3 a description of the laser structures that are studied in this thesis is presented. Following this, an explaination as to how the design variations are expected to impact the parameters being characterized, especially the intrinsic bandwidth, is given.

In Chapter 4 a detailed explaination of the experimental apparatus and techniques used in the characterization of the laser structures studied in this thesis is given.

In Chapter 5 the results of the experimental investigations to extract parameter values from RIN spectrum as a function of injected current are presented. Values for the D coefficient are calculated from the comparison of RIN and L-I characterizations. As well, further information is obtained from the RIN data by examining how the damping factor, K, values varied with the square of the resonance frequency. Utilizing the interrelationship between the D and K coefficients allows for a calculation the differential gain, g_n, and non-linear gain coefficient, ε. Finally, the trends observed in g_n and ε as a function of barrier height, QW number, and cavity length are presented.

In Chapter 6 deviations in resonance frequency near threshold and how this may be related to increased spontaneous emission with increasing temperature is discussed. As well the physical relevance of the values D and f_{max} with respect to the expected bandwidth performance of a laser are discussed. Explanations for the observed deviations of the differential gain results from that expected by theory are explored. As well, exploration of the dependence of ε on other performance parameters leads to the suggestion that nonlinear gain linearly approximated with respect to photon density may not be well founded. Then the influence of the photon lifetime on fmax is demonstrated followed by an investigation into the role that differential gain, g_n, and nonlinear gain, g_s, play in f_{max}. Finally, with the understanding of how the relative contributions of each parameter influence bandwidth performance having been developed, an investigation into how changing key design parameters can be used to improve on the overall design of the laser is presented.

In Chapter 7 the conclusions of this thesis is presented.

CHAPTER 2: INTRINSIC NOISE OF SEMICONDUCTOR LASERS

2.0 INTRODUCTION

In this chapter the theoretical concepts of intensity noise in semiconductor lasers, the nature of relative intensity noise (RIN) spectra, and the parametric forms that relaxation oscillation frequency and damping factor take with reference to RIN spectra are presented. As well a derivation for the maximum theoretical intrinsic bandwidth is presented. How the parameters that contribute to the relaxation oscillation frequency and damping factor are related to the intrinsic bandwidth of semiconductors, and the relative importance of their characterization to this study is discussed.

2.1 ORIGINS OF INTENSITY NOISE IN SEMICONDUCTOR LASERS

After a semiconductor laser is turned on, the output of the laser exhibits fluctuations as the interplay between the photon and carrier populations approach a steady state. However, a true steady state is never reached, due to the presence of noise resulting from the quantum nature of the lasing process itself [33] [34]. Photons arising from spontaneous emission are a source of quantum shot noise as they are emitted in a random direction and phase. Also, there is quantum shot noise associated with injected carriers, because their passage across heterojunction interfaces is a random event which depends on carrier energy. The recombination of carriers in the active layer being a random event is also a source of quantum shot noise. As well, absorption and scattering mechanisms within the laser cavity have a noise effect on the lasing process.

These noise sources all combine to create a white-noise effect on the photon and carrier populations in the laser active region. The interdependence between the photon and carrier populations are typically modeled by single-mode rate equations. The effect of the noise sources can be included in these rate equations [15]:

$$\frac{ds}{dt} = \left(\Gamma v_g g(n,s) - \frac{1}{\tau_{ph}}\right) s + \frac{\Gamma R_{sp}}{V} + F_s(t) \qquad (2.1.1)$$

$$\frac{dn}{dt} = \frac{I}{qV} - \frac{n}{\tau_e} - v_g g(n,s)\, s + F_n(t) \qquad (2.1.2)$$

where $F_s(t)$ and $F_n(t)$ are Langevin noise terms which mathematically model the white noise effect on the photon and carrier populations respectively. Other terms shown are the photon and carrier densities, s, n, the material gain, g(n,s), the spontaneous emission rate, R_{sp}, the injected current captured in the active region, I, the active region volume, V, the confinement factor, Γ, the electron and photon decay times, τ_e, τ_{ph}, and the group velocity, v_g. The resulting intensity noise in the output of a semiconductor laser comes from the interdependence between the photon and carrier populations, represented by (2.1.1) and (2.1.2), and their drive towards a steady-state condition which can never be reached due to the continuous white noise inherent in the process itself.

2.2 RELATIVE INTENSITY NOISE

Relative intensity noise (RIN) is a frequency dependent value defined by the following ratio

$$\mathrm{RIN} = \frac{\left\langle |\Delta P(\omega)| \right\rangle^2}{\langle P \rangle^2} \tag{2.2.1}$$

where $\langle P \rangle$ is the mean optical power and $\left\langle |\Delta P(\omega)| \right\rangle$ is the intensity noise power spectral density. RIN is a measure of the contribution that the intrinsic noise of a semiconductor laser makes to the signal-to-noise ratio of a communication system. If the laser intensity noise were the dominant noise source then the RIN quantity would represent the maximum signal-to-noise ratio possible in a fiber optic system. If this were the case, the signal-to-noise level could be calculated from RIN using the following relationship [35]

$$\frac{S}{N} = \frac{m^2}{2^*B^*\mathrm{RIN}} \tag{2.2.2}$$

where m is the optical modulation and B is the noise bandwidth.

Using standard small-signal analysis, with the Langevin noise terms in (2.1.1) and (2.1.2) replaced by the diffusion coefficients associated with the corresponding noise sources, an expression for the RIN is found to be [11] [15] [37]

$$\mathrm{RIN} = \frac{A + B\omega^2}{\left(\omega^2 - \omega_0^2\right)^2 + \omega^2\Gamma_0^2} \tag{2.2.3}$$

where ω_0 is the resonant frequency, and Γ_0 is the damping. The RIN spectrum represented by (2.2.3) describes how the Langevin white noise is selectively enhanced by the intrinsic resonance of the lasing process. The enhanced response has the transfer characteristic similar to a second-order low-pass network with a resonance at the frequency ω_0, which is damped by Γ_0 [11].

One assumption that should be acknowledged immediately is that this analysis is appropriate for single-mode operation only. The limitations resulting from this assumption will be addressed throughout this work. It would be more appropriate to use a multi-mode rate equation model [36] [37], which unfortunately is beyond the scope of this work, since there is an intensity noise associated with each lasing longitudinal mode and a photon population associated with each lasing and nonlasing longitudinal mode. When the photon population is associated with more than one lasing mode a breakdown of the single-mode theoretical representation occurs, which is usually the case near threshold where multi-mode operation is common. In fact, coupling occurs between longitudinal modes which can renormalize the resonance frequency of the individual modes to very low values, resulting in a lower resonance for a total photon density [34] [37].

2.3 RELAXATION OSCILLATION FREQUENCY AND DAMPING FACTOR

The relaxation oscillation frequency, or resonance frequency, is the frequency at which a resonance peak appears in the modulation response of a semiconductor laser. The damping characterizes the rise in the response spectrum at the resonance peak. The intrinsic frequency response of the laser, as derived from the small-signal solutions to equations (2.1.1) and (2.1.2), minus the Langevin noise terms, is given by [10]

$$R_{int} = \frac{\omega_o^4}{(\omega^2 - \omega_o^2)^2 + \omega^2\Gamma_o^2} \tag{2.3.1}$$

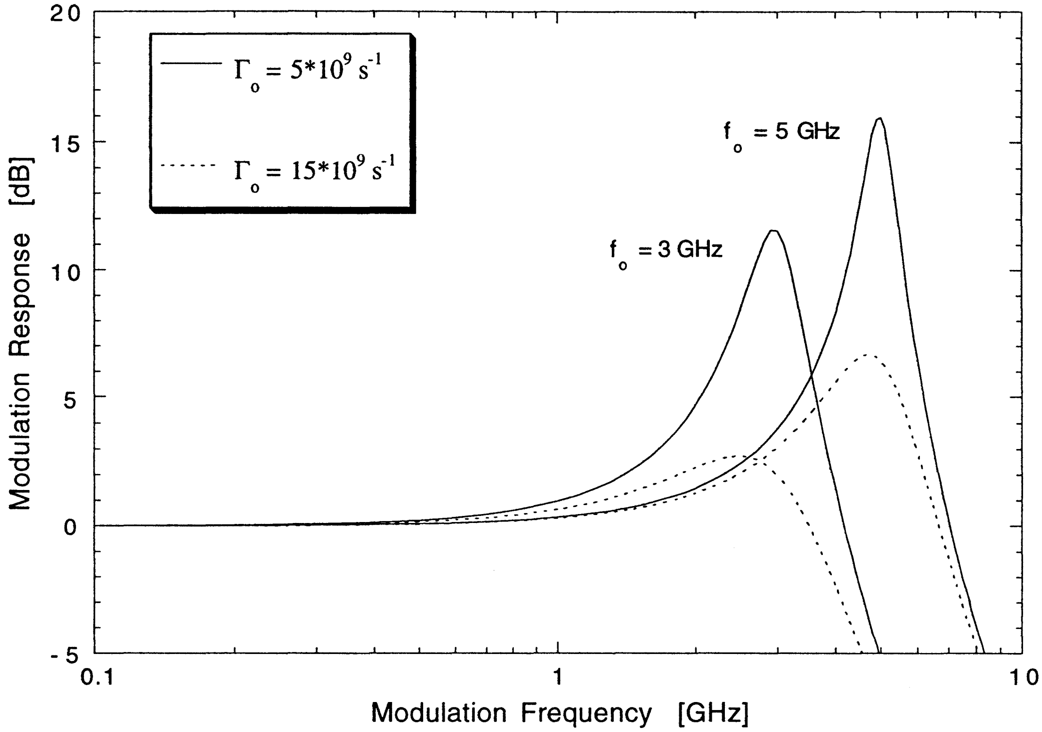

Fig 2.1: Calculated small-signal intrinsic modulation response, R_{int}, showing the relaxation-oscillation peak at f_o and the effect of damping, Γ_o, on the peak height.

The intrinsic modulation bandwidth of a semiconductor laser is the frequency range over which it will respond to current modulation. Its value is usually defined by the frequency at which its intrinsic response has dropped by 3 dB from the dc value [11]. The resonance frequency and damping limit the useful modulation bandwidth of lasers according to their effect on the response (see Fig 2.1). Therefore, a goal in designing high speed lasers is to extend this bandwidth to the highest value possible by increasing the resonance frequency and decreasing the damping.

The resonance frequency and damping parameters appearing in the small-signal modulation response of the laser are the same as those appearing in RIN spectrum. The resonant frequency, in equation (2.2.3), is given by [15]

$$\omega_o^2 = \Gamma_s\Gamma_n + \left(v_g g_n s + \frac{1}{V}\frac{dR_{sp}}{dn}\right)\left(\Gamma v_g g + \Gamma v_v g_s s\right) \tag{2.3.2}$$

and the damping is given by

$$\Gamma_o = \Gamma_s + \Gamma_n = \left(\frac{\Gamma R_{sp}}{sV} - \Gamma v_g g_s s\right) + \left(v_g g_n s + \frac{d}{dn}\left(\frac{n}{\tau_e}\right)\right) \tag{2.3.3}$$

where $g_n = \partial g(n,s)/\partial n$ is the differential gain and $g_s = \partial g(n,s)/\partial s$ is the nonlinear gain. To a good approximation the resonant frequency may be written as [15]

$$\omega_o = \left(v_g g_n s \,.\, \Gamma v_g g\right)^{1/2}$$

or

$$f_o = \frac{1}{2\pi}\left(v_g g_n s \,/\, \tau_{ph}\right)^{1/2} \tag{2.3.4}$$

From this approximation a relationship between the relaxation oscillation frequency and the damping can be established by rewriting the second and third terms of equation (2.3.3) in terms of equation (2.3.4) such that [38]

$$\Gamma_o = K f_o^2 + \frac{1}{\tau'} + \frac{\Gamma R_{sp}}{sV} \tag{2.3.5}$$

where $1/\tau'$ is the differential carrier lifetime at threshold. Further substitution of (2.3.4) into the third term of (2.3.5) gives an equation for Γ_o with its dependence on f_o

$$\Gamma_o = K f_o^2 + \frac{1}{\tau'} + \frac{\Gamma}{V}\frac{v_g g_n R_{sp}}{4\pi^2 \tau_{ph}}\frac{1}{f_o^2} \tag{2.3.6}$$

where K is given by [15]

$$K = (2\pi)^2 \tau_{ph}\left(1 - \frac{\Gamma g_s}{g_n}\right) \tag{2.3.7}$$

and the photon lifetime, τ_{ph}, is given by [11]

$$\tau_{ph}^{-1} = v_g\left(\alpha_m + \alpha_{int}\right) \tag{2.3.8}$$

where α_m is the mirror losses and α_{int} is the internal absorption. Sometimes the nonlinear gain is approximated to further simplify the model by expressing the material gain g(n, s) as [15]

$$g(n,s) = g_o(n)(1 - \varepsilon s) \tag{2.3.9}$$

where g_o is the carrier dependency of the material gain, and ε is the nonlinear gain coefficient. Using the threshold gain condition a more simplified expression for the value K is derived [15]

$$K = (2\pi)^2 (\tau_{ph} - \varepsilon / v_g g_n) \tag{2.3.10}$$

A linear relationship between f_o^2 and Γ_o was first empirically demonstrated by Olshansky [10] which was simply stated as $\Gamma_o = K f_o^2$. As the ability to experimentaly determine the resonance frequency and damping improved, the trends observed were found to conform well with theory validating the inclusion of the differential carrier lifetime term and the spontaneous emission term, the second and third terms seen in equation (2.3.5) [15]. The spontaneous emission term only causes a departure from linearity at low bias levels [36] [38].

The correlation between the resonant frequency and photon density shown in equation (2.3.4) can be expressed in terms of the current injected above threshold, or ($I-I_{th}$) giving a direct relationship between easily characterisable parameters. The photon density can be estimated by [11]

$$s = \frac{\Gamma}{V}\frac{\tau_{ph}\eta_{int}}{q}\left(I - I_{th}\right) \tag{2.3.11}$$

where η_{int} is the internal quantum efficiency, I is the total injected current, and I_{th} is the threshold current of the laser. The accuracy of the estimation of the photon density in (2.3.11) relies heavily on the characterization of the photon lifetime, τ_{ph}, which includes the mirror losses, α_m, and the internal absorption, α_{int}, and the internal quantum efficiency. Substituting (2.3.11) into (2.3.4) results in

$$f_o = \frac{1}{2\pi}\left\{\frac{\Gamma}{V}\frac{\eta_{int} v_g g_n}{q}\left(I - I_{th}\right)\right\}^{1/2} \tag{2.3.12}$$

Rewriting (2.3.12) as a relationship between resonant frequency and current injected above threshold allows for the creation of the slope parameter D' as shown here

$$f_o = D'\left(I - I_{th}\right)^{1/2} \tag{2.3.13}$$

where D' is given by

$$D' = \frac{1}{2\pi}\left\{\frac{\Gamma}{A\,L}\frac{\eta_{int} v_g g_n}{q}\right\}^{1/2} \tag{2.3.14}$$

where the active region cross sectional area is given by $A = n_w\, d_w\, w$, n_w is the number of quantum wells, d_w is the quantum well width, and w is the width of the stripe contact.

The correlation between the resonant frequency and photon density shown in equation (2.3.4) can also be expressed in terms of the facet output power, or P_f, giving an another direct relationship between easily characterisable parameters. The photon density can be estimated by [11]

$$s = 2\frac{\Gamma}{V}\frac{P_f}{h\upsilon\, v_g \alpha_m} \tag{2.3.15}$$

where P_f is the single facet ouput power of the laser, and $h\nu$ is the photon energy. In this case the accuracy of the estimation of the photon density in (2.3.15) relies more heavily on the characterization of the single facet ouput power, P_f, and the mirror losses, α_m. Substituting (2.3.15) into (2.3.4) results in

$$f_o = D\,\sqrt{P_f} \tag{2.3.16}$$

where P_f is the single facet power, and D is given by [15] [26]

$$D = \frac{1}{2\pi}\left[2\,\frac{\Gamma}{A\,L}\frac{v_g g_n}{h\nu}\left(\frac{\alpha_{int}}{\alpha_m} + 1\right)\right]^{\frac{1}{2}} \tag{2.3.17}$$

The values D', D, and K have been used to characterize the frequency response of semiconductor lasers [15]. The value D' describes the rate at which the resonance frequency increases with injected current above threshold. The value D describes the rate at which the resonance frequency increases with output power. The value K is usually used to characterize the intrinsic bandwidth, as will be explained in the next section. High speed performance is expected from devices with a higher value of D' or D, and lower value of K [15].

2.4 MAXIMUM INTRINSIC BANDWIDTH

The maximum intrinsic bandwidth of a semiconductor laser is the damping limited modulation rate theoretically achievable ignoring RC parasitics, device heating, and maximum power of the laser [39]. At a sufficiently high photon densities the damping rate becomes large enough that the resonance is critically damped. The intrinsic bandwidth can be determined by setting the intrinsic frequency response function, equation (2.3.1), equal to 1/2, which is equivalent to the 3-dB definition of bandwidth [10]:

$$\frac{\omega_o^4}{\left(\omega^2 - \omega_o^2\right)^2 + \omega^2\Gamma_o^2} = \frac{1}{2} \tag{2.4.1}$$

The maximum intrinsic bandwidth is then found by taking the derivative of this relationship with respect to optical power, P. Using $\Gamma_o = K\,f_o^2$, an approximation of equation (2.3.5), to equate the power dependence of the damping and the resonant frequency, and setting $d\omega/dP = 0$, results in the relationship

$$\omega_o^4 + \omega_o^2\omega_m^2 = \omega_m^2\Gamma_o^2 \tag{2.4.2}$$

where ω_m is the maximum angular intrinsic bandwidth. When equation (2.4.2) is combined with equation (2.4.1) the relationship $\omega_o = \omega_m$ is established. Applying this to equation (2.4.2) gives

$$2\omega_m^2 = \Gamma_o^2$$

Using the approximation $\Gamma_o = K\,f_o^2$, the maximum intrinsic bandwidth, f_{max}, is

$$f_{max} = \frac{\sqrt{2}\;2\pi}{K} \tag{2.4.3}$$

Combining equation (2.4.3) with equation (2.3.10) gives an expression for f_{max} in terms of physical parameters

$$f_{max} = \frac{1}{\sqrt{2}\pi(\tau_{ph} - \varepsilon / v_g g_n)} \cong - \frac{v_g g_n}{\sqrt{2}\pi\varepsilon} \tag{2.4.4}$$

This characteristic parameter should only be used for comparing the intrinsic behavior of semiconductor lasers, and not as an indication of what the expected bandwidth of the laser may be, for a number of reasons. Two laser structures may have the same intrinsic bandwidth and yet very different true maximum bandwidths due to different thermally limited maximum powers. The maximum intrinsic bandwidth is determined by the limitations of the damping experienced in the carrier-photon interactions occuring in the active region of the laser structure. As demonstrated in §2.3 this damping is dependent on photon density and therefore optical output power. As well, since the damping is characterized in this study using RIN versus frequency values it only represents the damping experienced by the carrier-photon interactions based on the quantum fluctuations occuring in the two populations under dc conditions. Under ac conditions the carriers will be effected by carrier transport times as they travel from their perspective contacts through the material to the active region of the laser. Carrier transport times do not affect the maximum intrinsic modulation determined through the measurement of RIN because it is measured under dc conditions so the actual maximum bandwidth will fall short of that predicted by the intrinsic value [20] [21] [39].

2.5 PARAMETERS TO BE CHARACTERIZED

By fitting the theoretical expression for the RIN spectrum shown in equation (2.2.3) with experimentally obtained RIN values as a function of frequency, ω_o and Γ_o can be characterized as a function of injection current levels. Once these values have been obtained, several other important parameters become available from expressions (2.3.3) - (2.3.17).

2.5.1 Response coefficients D' and D

The response coefficients D' and D are important to characterize because they allow for a direct comparison of the speed performance of the lasers. Also, the differential gain, g_n, can eventually be obtained through additional characterization of other parameters. Plotting resonance frequency values, f_o, obtained as a function of drive current from RIN data versus the root of injected current above threshold should result in a linear trend as predicted by equation (2.3.13). The slope of this line yields the value D'. Plotting the same resonance frequency values versus the root of single facet output values as a function of drive current from light-current (L-I) data should result in a linear trend as predicted by equation (2.3.16) yielding a slope of the value D.

2.5.2 Response parameter K factor

The response parameter K is also important to characterize because it also serves as a comparative value for the speed performance of semiconductor lasers. Also the nonlinear gain coefficient, ε, can eventually be obtained through further characterization. Plotting damping values, Γ_o, obtained as a function of drive current versus resonance frequency values, f_o, obtained as a function of drive current from RIN data should result in a linear trend as predicted by equation (2.3.5). However, this will not be the case for values obtained near threshold as explained in §2.3. The slope of this line will have the value of K.

2.5.3 Group velocity, v_g, and photon energy, $h\nu$

The group velocity and the photon energy are not obtainable from the resonance frequency and damping data. However, their values are required for the characterization of the differential gain parameter, g_n. The group velocity is given by [11]

$$v_g = 2L(\Delta\nu) \tag{2.5.1}$$

where $\Delta\nu$ is the longitudinal mode spacing which can be determined from the spectral output data of the lasers. The photon energy will be estimated using the peak wavelength obtained from the spectral output data of the lasers.

2.5.4 Optical-Confinement-Factor, Γ

Optical confinement in a semiconductor structure occurs when a region of dielectric material is surrounded dielectric of lower index of refraction resulting in the total internal reflection of photon energy. The optical confinement factor, Γ, is typically determined with an optical mode model which is used to spatially determine the photon distribution in the optical confinement region of the dielectric waveguide. Several different approaches can be taken to mathematically represent the optical mode and these are usually tailored to find the easiest solution for a particular dielectric waveguide structure. One such approach was developed for multilayer index profiles, such as those found in multiple quantum well lasers, by L.M. Walpita [56]. This partical approach uses the condition that certain elements in the transfer matrix must be zero. The resulting numerical techique is simpler to solve than eigenvalue equations and thus requires the computational effort. An appropriate algorithm based on Walpita's approach has been programed in the mainframe computer at Nortel Technologies by Dave Adams and it was this software that was used to calculate the optical confinement factor for the laser structures studied in this work.

2.5.5 Mirror loss, α_m, and internal absorption, α_{int}

Both α_m and α_{int} are important to know for the characterization of the differential gain parameter, g_n and are best characterized from L-I data of the lasers. The slope of the L-I curve can be used to characterize the differential quantum efficiency of a device using the following relationship [11]

$$\eta_d = \frac{2q}{h\nu}\frac{dP_{out}}{dI} \tag{2.5.2}$$

The differential quantum efficiency can also be written in terms of the internal quantum efficiency and the photon escape and generation rates as [11]

$$\eta_d = \eta_{int}\frac{\alpha_m}{\alpha_m + \alpha_{int}} \tag{2.5.3}$$

The mirror losses, α_m, are given by

$$\alpha_m = L^{-1}\ln\left(R^{-1}\right) \tag{2.5.4}$$

where L is the laser cavity length and R is the facet reflectivity, which on substitution in (2.5.3) yields

$$\eta_d^{-1} = \eta_{int}^{-1}\left[1 + \frac{\alpha_{int}L}{\ln(1/R)}\right] \tag{2.5.5}$$

Plotting η_d^{-1} versus L obtained for devices of the same active region design should result in a linear trend according to equation (2.5.5). The slope of this plot will characterize the inverse internal efficiency, η_{int}^{-1}, and the intercept will be the term $\alpha_{int}/\ln(1/R)$ containing the internal absorption. The facet reflectivity, R, according to Fresnel's formulae assuming normal incidence, is given by

$$R = \left(\frac{n_g - 1}{n_g + 1} \right)^2 \tag{2.5.7}$$

where, n_g, the group index is given by

$$n_g = \frac{c}{v_g} \tag{2.5.8}$$

Having obtained a value for the facet reflectivity, R, the internal absorption, α_{int}, can be extracted from the value of the intercept. The photon lifetime, τ_{ph}, as described in equation (2.3.8), can now be determined by calculating the mirror losses using equation (2.5.4).

It should be mentioned that this characterization of η_{int} and α_{int} is based on the assumption that they are independent of threshold carrier density which typically changes with device length. Unfortunately, the threshold carrier density of quantum well lasers can increase dramatically for shorter device lengths. It has been shown that α_{int} and η_{int} are dependent on carrier concentration; therefore, some caution must used when using the shorter cavity length lasers in fitting the data to equation (2.5.5) [40].

2.5.6 Differential gain, g_n

The differential gain, g_n, is an extremely useful parameter to characterize since it plays a vital role in the high speed performance of semiconductor lasers. Knowledge of how this value changes as a function of device structure could be extremely useful to future design considerations. The differential gain, g_n, can be obtained from the characterizations of D' and D, as shown in equations (2.3.13) and (2.3.17). Because the values D' and D are obtained by fitting from the threshold condition over the linear region of the dependency of resonance frequency on the injected current, or single facet power, the resulting diffential gain value is a characterization of the rate of change of the material gain dependency on carrier concentration, $\partial g(n,s)/\partial n$, near threshold. An explanation of how

g_n is expected to vary with varying QW barrier height and QW number will be discussed in §3.2. Additional parameters required for this purpose are the active region cross section A, and the device L, which can be estimated from the design parameters of the laser to within reasonable accuracy. Using these values, along with v_g, $h\nu$, Γ, η_{int}, α_{int}, and α_m characterized earlier, the value of g_n can be determined from D.

2.5.7 Nonlinear gain coefficient, ε

Nonlinear gain also plays a vital role in the high-speed performance of semiconductor lasers. Very little conclusive evidence of how this parameter is expected to change with device structure has been presented to date. This study will hopefully reveal some trends that will be useful to future design considerations by revealing structual modifications that would result in a minimizing the magnitude of ε. The nonlinear gain coefficient, ε, can be obtained from the characterization of K, as shown in equation (2.3.10). Using the values obtained for v_g from (2.5.1), and g_n as described above, while the photon lifetime can be calculated using equation (2.3.8).

2.5.8 Maximum intrinsic bandwidth, f_{max}

The maximum intrinsic bandwidth, f_{max}, of a semiconductor laser provides a general overview of the resulting contribution of all of the parameters important for high speed laser performance. The same information is provided by the K factor; however, f_{max} has immediate physical meaning as a bandwidth value. How this parameter varies with quantum well barrier height, QW number, and cavity length could provide useful information for future design considerations. The value f_{max} can be obtained from the characterization of K as shown in equation (2.4.3).

2.6 SUMMARY

In this chapter the theoretical concepts of intensity noise in semiconductor lasers, the nature of relative intensity noise (RIN) spectra, and the parametric forms that relaxation oscillation frequency and damping factor take with reference to RIN spectra were presented. How the parameters that contribute to the relaxation oscillation frequency and damping factor are related to the intrinsic bandwidth of semiconductors, and the relative importance of their characterization to this study was also discussed.

CHAPTER 3: LASER STRUCTURES

3.0 INTRODUCTION

In this chapter details of the design parameters of the eleven laser structures examined in this study are presented. As well the materials growth and processing procedures followed in their construction are briefly covered. In this study information on how the intrinsic modulation response of 1.3 μm InGaAsP/InP compressively strained MQW lasers are affected by changes in the structural parameters of the QW active region was sought, with the objective of optimizing the structural parameters for incorporation into future semiconductor laser designs. The three most important physical parameters to be considered when optimizing the intrinsic frequency response of semiconductor lasers are the differential gain, g_n, the nonlinear gain coefficient, ε, and the photon lifetime, τ_{ph} (see equation 2.4.4). In the final sections of this chapter the expected effect of varying the QW barrier height, number of QWs, and cavity length on these parameters will be considered.

3.1 DEVICE STRUCTURES

Eleven laser structures, which were designed, grown, and fabricated at the Advanced Technology Laboratory of Bell Northern Research (BNR) in Ottawa, were considered for the purposes of this study. All of the structures were single-step index-guided compressively strained MQW ridge waveguide lasers, designed to have an emission wavelength of approximately 1.3 μm. One group of five structures focused on the effect of varying QW barrier height, and the other six of varying the QW number (see Table 3.1). There were slight differences in the thicknesses and doping levels of the GRINCH regions, and the doping levels used in the barrier layers of the structures in the two groups. However, the same well and barrier layer widths were targeted in the growth of all the structures. The device comparison in this study is unique to that of other previous studies in that it simultaneously considers the effect of varying two important QW physical parameters, the number of wells and the barrier height, in the same basic laser structure.

The basic layer structure, common to both sets of devices is shown in Fig. 3.1. The values corresponding to the layer composition and structural variables appearing in Fig. 3.1 are given in Table 3.1.

	cap layer	GaInAs		0.2 μm		[p_{Zn}] = 1×10^{19}
	buffer layer	InP		1.6 μm		[p_{Zn}] = 1×10^{18}
	buffer layer	InP		0.2 μm		[p_{Zn}] = 4×10^{17}
	etch stop	$In_{1-x}Ga_xAs_yP_{1-y}$	1.3 Q	30 Å		[p_{Zn}] = 4×10^{17}
	grinsch layer	InP		0.1 μm		[p_{Zn}] = 4×10^{17}
	grinsch layer	$In_{1-x}Ga_xAs_yP_{1-y}$	1.0 Q	G Å		[p_{Zn}] = 4×10^{17}
	grinsch layer	$In_{1-x}Ga_xAs_yP_{1-y}$	X Q	G Å		[p_{Zn}] = d_{G1}
N wells, N-1 barrier layers	well layer	$In_{1-x}Ga_xAs_yP_{1-y}$	1.3 μm	35 Å	1% Strained	undoped
	barrier layer	$In_{1-x}Ga_xAs_yP_{1-y}$	X Q	100 Å	Unstrained	[p_{Zn}] = d_B
	grinsch layer	$In_{1-x}Ga_xAs_yP_{1-y}$	X Q	G Å		[n_{Si}] = d_{G2}
	grinsch layer	$In_{1-x}Ga_xAs_yP_{1-y}$	1.0 Q	G Å		[n_{Si}] = d_{G2}
	buffer layer	InP		1.5 μm		[n_{Si}] = 2×10^{18}

Figure 3.1: Layer composition and arrangement common to device structures in both sets of MQW ridge waveguide laser structures.

3.1.1 Materials Growth and Processing

The structures from both sets described above were grown by low-pressure metalorganic vapor phase epitaxy (LP-MOVPE) on (100) Si-doped n-type InP substrates. The lasers were processed to have a 2 μm wide ridge structure. The lasers were then fabricated with patterned metal on the p-side of the device. Devices were cleaved from all the wafer samples with cavity lengths of 10 mil, 15 mil, 20 mil, 30 mil, and 40 mil. These were then bonded p-side up onto SiC heat sinks mounted on copper blocks which, in turn, were mounted onto ceramic sub-carriers to facilitate device testing.

Sample Number	Number of QWs	Barrier Q 'X'	Barrier doping 'd_B'	grinsch thickness 'G'	grinsch doping 'd_{G1}'	grinsch doping 'd_{G2}'
			Varying Number of Wells			
S1-349	5	1.10	8 x 10^{17}	400 Å	4 x 10^{17}	4 x 10^{17}
S1-341	7	1.10	8 x 10^{17}	300 Å	4 x 10^{17}	4 x 10^{17}
S1-340	8	1.10	8 x 10^{17}	200 Å	4 x 10^{17}	4 x 10^{17}
S1-429	10	1.10	8 x 10^{17}	200 Å	4 x 10^{17}	4 x 10^{17}
S1-418	12	1.10	8 x 10^{17}	200 Å	4 x 10^{17}	4 x 10^{17}
S1-422	14	1.10	8 x 10^{17}	200 Å	4 x 10^{17}	4 x 10^{17}
			Varying Barrier Height			
S1-591	10	1.00	1 x 10^{18}	200 Å	1 x 10^{18}	8 x 10^{17}
S1-593	10	1.05	1 x 10^{18}	200 Å	1 x 10^{18}	8 x 10^{17}
S1-588	10	1.10	1 x 10^{18}	200 Å	1 x 10^{18}	8 x 10^{17}
S1-590	10	1.15	1 x 10^{18}	200 Å	1 x 10^{18}	8 x 10^{17}
S1-592	10	1.20	1 x 10^{18}	200 Å	1 x 10^{18}	8 x 10^{17}

Table 3.1: Description of the laser structures from which processed devices were selected for study. The values shown correspond to the layer composition and structural variables appearing in Fig. 3.1.

3.1.2 Description of varying barrier height structures

The group of structures in which the quantum well barrier height was varied were numbered S1-588, 590 to 593. As outlined in Table 3.1 the number of quantum wells for these structures was fixed at 10. The barrier layers and upper GRINSCH layer were p-doped using zinc at a concentration of 1 x 10^{18} cm^{-3}. The thickness of the GRINSCH layers was 200 Å with the lower layers n-doped with silicon to a concentration of 8 x 10^{17} cm^{-3}. The barrier layer composition of the five structures was varied such that the emission wavelength corresponding to the barrier band-gap increased from 1.0 μm to 1.2 μm in 0.05 μm step.

3.1.3 Description of varying quantum well number structures

The group of structures in which the quantum well number was varied were numbered S1-340, 341, 349, 418, 422, and 429. As outlined in Table 3.1 the barrier layer composition of the six structures was kept constant such that the emission wavelength corresponding to the barrier band-gap number of quantum wells for these structures was fixed at 1.3 μm. The barrier layers and upper GRINSCH layer were p-doped using zinc at a concentration of 1 x 10^{18} cm^{-3} and 4 x 10^{17} cm^{-3} respectively. The thickness of the GRINSCH layers was 200 Å, with the exception of S1-341 with thickness 300 Å, and S1-349 with thickness 400 Å. As well the lower GRINSCH layers were n-doped with silicon to a concentration of 4 x 10^{17} cm^{-3}. The quantum well number was varied for the six structures with the following sequence; 5, 7, 8, 10, 12, and 14.

3.2 EFFECT OF VARYING THE QUANTUM-WELL PARAMETERS

3.2.1 Expected Effect Of Varying QW Barrier Height On Physical Parameters

A deeper quantum well is expected to result in a higher differential gain. This is because a larger valence band barrier height and, hence, greater quantum confinement increases the heavy hole energy level - light hole energy level (hh-lh) separation which in turn augments the parabolicity of the hh band [41]. The more parabolic the hh band the greater the energy range over which the Fermi-level moves for a given carrier injection rate which is indicative of high differential gain. This effect is more pronounced in compressively strained wells, like those found in the structures in this work, than in lattice-matched or tensile strained wells because the hh-lh separation is greater in compressively strained wells than in lattice-matched wells [41].

As mentioned in §1.2, it has been found that quantum well lasers generally exhibit higher nonlinear gain than bulk lasers. It has been suggested that this is a result of the enhancement of the non-linear gain by the quantum confinement of carriers [18]. However, the wide range of differences between published values of ε for QW and bulk lasers suggests that ε has a dependence on QW structure that is not well understood. Several theories have been published that indicate that nonlinear gain may depend strongly on QW structure parameters such as barrier height, well width, and well number [17]. Some studies have reported observing ε increasing with g_n, suggesting that similar mechanisms may be involved with both physical parameters [13] [15] [17] [18].

From equation (2.4.4) it can be seen that a change in τ_{ph} with varying the quantum well barrier height would have an impact on f_{max}. According to equation (2.3.8), the only physical parameter that could effect τ_{ph} with any active region design variation would be the internal absorption, α_{int}. However the band edge of the range of barrier heights being studied here are energetically far from the emission wavelength of the quantum well regions so little change in internal absorption is expected to be observed. Therefore, it is expected that α_{int} will remain relatively constant with increasing barrier height resulting in little change in τ_{ph}.

According to equation (2.4.4), an increase in the QW barrier height that is expected to result in an increase in g_n should benefit the intrinsic modulation bandwidth, f_{max}. However, the potential increase in ε, would act to decrease f_{max} according to equation (2.4.4). Hence, the optimum barrier height will depend on the relative dependence of f_{max} on these physical parameters.

3.2.2 Expected Effect Of Varying QW Number On Physical Parameters

It has been theoretically demonstrated that the differential gain, g_n, of a QW laser is expected to increase with the number of QWs [42] [43]. This makes sense phenomenologically, since the carrier concentration required to achieve threshold should decrease with increasing quantum well number. The internal absorption of a multiple quantum well laser is expected to increase with increasing quantum well number because of the increased photon/carrier interaction resulting from the greater optical mode overlap with the quantum well region. This will result in an increase in the modal threshold gain condition. However the increase in the active area volume with QW number will result in an increase in the modal gain for a given carrier concentration. This increase in modal gain will more than compensate for the increase in the modal threshold gain condition and result in the expected decrease in the threshold carrier concentration [40]. This increase in g_n

with QW number has been experimentally demonstrated by several authors [15] [26] [42] [44].

Conclusive evidence has not been reported on how ε changes with number of QWs, although, as was mentioned in §3.3.1, a strong dependence may exist. On the one hand, two studies on how the damping coefficient K varies with g_n as a result of varying QW number in 1.5 μm InGaAs/InGaAsP MQW lasers report values of ε that are relatively constant with QW number [15] [26]. This is supported by the findings of a investigation of InGaAs/InGaAsP MQW lasers showing ε to be almost independent of QW number varying from 4 to 20 [45]. On the other hand, an investigation of ε involving InGaAs/InGaAsP MQW lasers reports a regular decrease of ε as the number of wells is increased from 3 to 7, suggesting a dependence of ε on carrier density since a lower carrier density is required to reach threshold as QW number is increased [44].

The effect of the number of QWs on τ_{ph} is expressed implicitly by equation (2.3.8) through α_{int}. Since α_{int} is expected to increase with increasing QW number as a consequence of the increase in the optical mode overlap with the quantum well region a corresponding decrease in τ_{ph} will be observed.

An inspection of equation (2.4.4) indicates the intrinsic modulation bandwidth, f_{max} is augmented by an increase in g_n and decrease in τ_{ph} with number of QWs. Although the trends in the literature of the dependence of ε on QW number are inconclusive, if ε does indeed decrease with increasing QW number, as the most direct study suggests [44], then a substantial increase in the intrinsic modulation bandwidth should be observed.

3.3 VARYING THE DEVICE CAVITY LENGTH

For a given QW active region structure the threshold gain condition is expected to decrease with increasing cavity length, due to the decrease of the mirror loss distribution $\alpha_m = L^{-1}\ln(R^{-1})$, as shown by the relationship [11]:

$$\Gamma g_{th} = \alpha_{int} + \frac{1}{L}\ln\left(\frac{1}{R}\right) \tag{3.3.1}$$

The carrier concentration at threshold decreases as the modal gain, $g_m = \Gamma g_{th}$, required to reach threshold decreases with increasing cavity length. Since the modal gain is logarithmically dependent on carrier concentration, g_n is higher at the lower carrier concentrations required of a lower threshold gain [40]. Therefore g_n is expected to increase with increasing cavity length.

No studies were found in the literature dealing with how the gain saturation, ε, is expected to change with cavity length. Some studies have assumed that ε remains constant with cavity length [15] [26] [41]; however, there is no solid reason for assuming this to be true. This conclusion seems to be based on the results of other works suggesting ε has no dependence on semiconductor structural parameters [22] [32] [41] [45]; however, cavity length was not one of the parameters investigated.

Based on equation (2.3.8), the photon lifetime, τ_{ph}, contains two length-dependent parameters: the mirror losses, α_m, and the group velocity, v_g (see equations (2.5.4) and (2.5.1) respectively). Since the mirror losses are theoretically distributed over the length of the cavity their contribution to the photon lifetime will decrease with increasing cavity length. This will tend to increase the photon lifetime with increasing cavity length. The group velocity dependence on cavity length, based on changes in group index with carrier concentration, will be much weaker than the expected change in the mirror losses.

Increasing the cavity length will benefit the intrinsic modulation bandwidth by increasing g_n; however according to equation (2.4.4), the increase in τ_{ph} due to decreasing mirror losses will have a competing effect. As discussed above, the effects of cavity length on ε are unknown, but based on the changes in g_n and τ_{ph} some optimum cavity length may exist, depending on the relative dependence of f_{max} on these physical parameters [15] [41].

3.4 SUMMARY

In summary, this chapter outlined the design parameters of the eleven laser structures examined in this study. As well the materials growth and processing procedures flowed in their construction were briefly covered. Finally the expected effect of varying the QW barrier height, number of QWs, and cavity length on the differential gain, g_n, the nonlinear gain coefficient, ε, and the photon lifetime, τ_{ph}, were discussed.

CHAPTER 4: EXPERIMENTAL SETUP

4.0 INTRODUCTION

This chapter describes the experimental apparatus and configurations used to measure the relative intensity noise (RIN), continuous wave (CW), and spectral characteristics of devices from the laser structures outlined in Table 3.1. RIN measurements provide a parasitic-free means of observing the dynamic operation of a laser, as mentioned in §1.2. The parameters that define the useful modulation bandwidth of a semiconductor laser also determine the shape of its RIN spectrum, as shown in §2.2.

Using a simple experimental technique, the RIN spectrum for a given level of current injection was obtained, and by fitting the measured spectrum to equation (2.2.3) the resonant frequency and damping values were obtained. Because the laser output had to be coupled into a fiber for the measurement of the RIN spectra, due to the uncertainty of the fiber coupling efficiency the absolute power for each measurement was unknown. Therefore, the CW characteristics of the laser were measured in order to obtain calibrated power values for the laser output as a function of injection current. Then, in order to compare the resonant frequency and damping values obtained from the RIN spectra with output power, the results as a function of injection current for the RIN and CW measurements were simply matched.

The spectral characteristics of the devices were measured to determine the peak wavelength and longitudinal modal spacing of the output of the lasers. The peak wavelength was required to determine the responsivity of the detector used in the CW measurements to allow for a calibration of the results. The peak wavelength, as well as the longitudinal modal spacing, were necessary to calculate the differential gain, g_n, and the nonlinear gain coefficient, ε, from the characterized values of D and K using equations (2.3.17) and (2.3.10) as described in §2.5.7 and §2.5.6.

4.1 RELATIVE INTENSITY NOISE MEASUREMENTS

4.1.1 Theory Of Relative Intensity Noise Measurements

Relative intensity noise as a function of frequency is defined as the ratio of the noise power spectral density to the mean optical power (see §2.1). The noise power spectral density of a semiconductor laser can be measured by focusing its output when dc biased above threshold onto a high-speed p-i-n photodiode, typically one with a 20 GHz bandwidth. The resulting photocurrent is then amplified using a low-noise detector circuit. The spectral density of the RF noise component of the amplified photocurrent can then be measured using a spectrum analyzer. The resulting electrical noise power spectrum consist of noise from three sources; thermal noise in the photodiode amplifier, $\langle i_{th}^2 \rangle$, photodiode shot noise, $\langle i_{shot}^2 \rangle$, and the laser intensity noise, $\langle i_{RIN}^2 \rangle$. Therefore the detected electrical noise power can be represented by [15]

$$\langle P_N \rangle = \frac{Z_T^2}{50} \left\{ \langle i_{th}^2 \rangle + \langle i_{shot}^2 \rangle + \langle i_{RIN}^2 \rangle \right\} \cdot \Delta f \tag{4.1.1}$$

where Z_T is the amplifier trans-impedance and Δf is the noise bandwidth. The trans-impedance of the detector circuit is included in this relationship to relate the voltage generated by the photocurrent terminated with a 50 Ω load to the actual voltage measured at the spectrum analyzer. Defining the dc photocurrent generated by the photodiode as I, the last two terms of equation (4.2.1) are then given by [15]

$$\left\langle i_{shot}^2 \right\rangle = 2qI \tag{4.1.2}$$

and

$$\left\langle i_{RIN}^2 \right\rangle = RIN \cdot I^2 \tag{4.1.3}$$

where the relative intensity noise of the laser, RIN, is given by equation (2.2.1).

4.1.2 RIN Experimental Apparatus

The equipment used perform the RIN characterizations of the laser structures in this study was made available at the Advanced Technology Laboratory of Bell Northern Research (BNR) in Ottawa. The main component of the RIN measurement facility was an HP 71400 Lightwave Signal Analyzer. This was used to measure the noise power spectral density of the system $\{P_N\}$ as described by equation (4.1.1). The dc current source used to drive the laser was an ILX LDX-3207B precision current source. The temperature of the semiconductor laser was controlled using a thermoelectric (TE) cooler mount, which used a TE cooler with surface dimensions of 11 mm x 11 mm and a heat pump capability of 6.67 Watts, and was monitored using a thermistor, both of which were controlled by an ILX LDT-5910B temperature controller. An IBM 386 was interfaced with these three devices using a National Instruments AT-GPIB IEEE computer interface card, controlled by customized NI-488 software in a QBASIC environment. The optical output of the laser was coupled into a tapered fiber. This tapered fiber was held in position by an XYZ piezoelectric positioner. The optical signal in the fiber was then passed through a 1310 nm Isowave Optical Isolator before being coupled into the lightwave signal analyzer (see Fig. 4.1). The optical isolator is an important component of the experimental setup since optical feedback can greatly affect the intrinsic noise of the laser. The optical isolator used had an extinction ratio of 65 dB which should minimize any effect back reflection could have on the RIN results. Reflection-induced noise shows up in the noise power spectrum as a ripple having a period of f=c/2nL [33]. These ripples where not observed in the electrical spectrum taken with the experimental apparatus once the optical isolator was put into place. Also near-field reflections within the laser's coherence length, such as from the tapered fiber interface, tend to enhance the low-frequency intensity noise of the laser. However, the frequency range effected extends only up to several kilohertz, which is far below the frequencies of interest to this study [34].

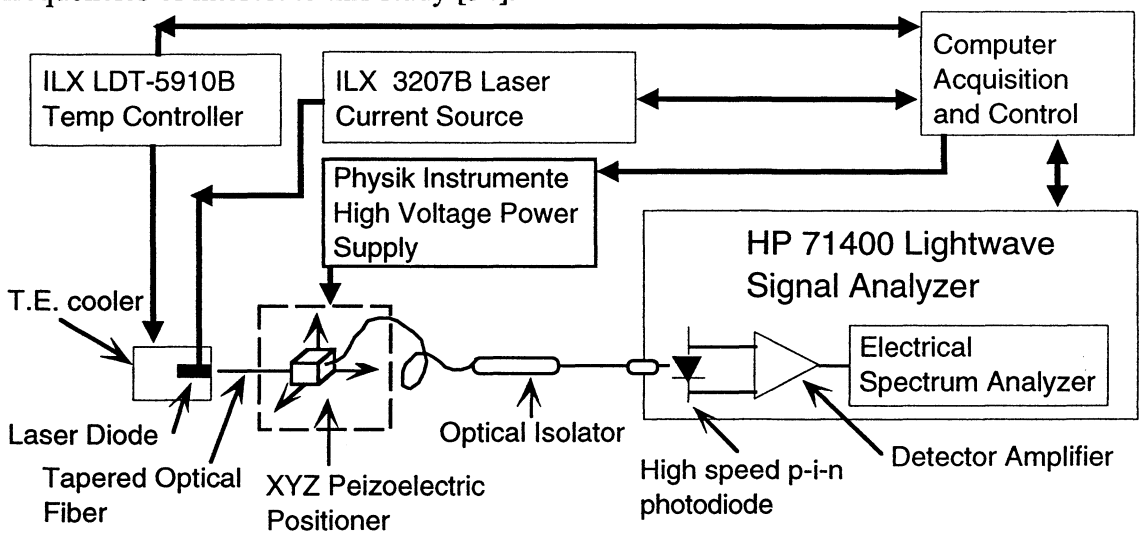

Figure 4.1: Schematic diagram of the experimental set-up used to measure the relative intensity noise (RIN) characteristics of the ridge waveguide MQW lasers.

For the automation of this experimental setup, the controlling software required several special features. A program module was included for controlling the temperature of the laser sample, ensuring that the temperature of the stage was stable to within +/- 0.05 °C before the measurements were made. According to the specifications of the lightwave signal analyzer, the photodetector of the analyzer could have been damaged if the average optical power coupled into the detector exceeded 3 dBm. Therefore a program module was included that continually monitored the average optical power and adjusted the attenuation of the analyzer accordingly, thus ensuring that the maximum dynamic range of the analyzer was always utilized.

The quality of the RIN spectrum data was very sensitive to the average power coupled into the fiber. It was found that the position of the fiber tip into which the output of the semiconductor lasers was coupled drifted as a function of time, necessitating continuous optimization of this coupling. This problem was overcome by automating the alignment of the fiber coupling apparatus which was controlled by a Physik Instrumente XYZ piezoelectric positioner. The Physik Instrumente high-voltage power supply controlling the XYZ piezoelectric positioner had analog voltage inputs for remotely controlling the positioner in all three directions. It was decided that the X and Y directions in the plane perpendicular to the fiber would be controlled by the automation software, by correlating fiber position with the maximum optical power monitored by the lightwave signal analyzer, so that the coupling of laser light into the fiber could be optimized before each RIN measurement. A National Instruments Lab-PC+ I/O board was added to the IBM 386. Two of the analog outputs from the I/O board were connected to the power supply controlling the XYZ piezoelectric positioner. The Z direction was left to be controlled manually since the lateral position of the fiber from the laser did not seem to be suffering from any drift problem, and the possibility of butting the fiber into the laser facet was also a concern. The additional software developed for the control of the fiber position had several special features. Using the average optical power detected at the initial position of the fiber as a lower limit, the XY plane of the fiber position was scanned within this power limit, and a fitting routine was used to optimize the fiber position. If an unusual drop in power was detected between RIN measurements, which occasionally occurred due to a sudden shift in the piezoelectric positioner, an emergency alignment sub program was initiated which scanned the laser facet to recover the laser signal. With the fiber position controlled by the automation software, consistent RIN spectral data were obtained.

With the setup successfully automated, attention was then focused on directly determining the RIN spectrum of the laser. As mentioned earlier, the lightwave signal analyzer was only capable of acquiring the noise power spectral density of the system, which included the laser intensity noise, thermal noise, and photonic shot noise. A downloadable program (RIN DLP) was available with the lightwave signal analyzer which measured the noise power spectral density of the system, attenuated the laser signal and measured the noise floor, and then calculated the RIN of the laser using equation (4.2.1) at a frequency preset by the user. However, the RIN DLP could not be activated remotely, and it was not possible to obtain the RIN of the laser over the entire frequency span. Hewlett-Packard was contacted to ascertain whether the RIN DLP could be modified to produce the entire RIN spectrum of the laser. A reply was received indicating that this was not possible using the RIN DLP. However information was sent which detailed the existence of an undocumented command, <|RIN|>, which could be activated remotely, that initiated a single measurement of the noise power spectral density of the system, and the noise floor, on two separate traces, similar in action to the RIN DLP. By accessing the data of these two traces the RIN spectrum of the laser was calculated by subtracting the analyzed noise floor and photonic shot noise contributions from the noise power spectral density of the system, to give the spectral distribution of the laser RIN.

4.1.3 Calibration Of RIN Spectrum Results

A regular perturbation of a non-periodic nature was observed in the noise floor response of the lightwave analyzer. This perturbation also appeared in the RIN spectra obtained using the experimental apparatus. Based on these observations it was decided that the response of the lightwave analyzer needed to be calibrated. One method of correcting the detection system response is to use a 'white' shot noise spectrum [15]. A semiconductor laser can be considered a good approximation of a 'white' shot noise source if the laser RIN contribution to the noise power spectrum is much lower than its shot noise contribution. For example, a high power semiconductor laser operated at high power would be such a source, since the peak of the RIN spectrum has an approximate $1/P^3$ dependence giving a relatively flat contribution over a wide frequency range easily dominated by shot noise [15]. However, such a laser was not available, so a viable alternative was to use an Erbium doped fiber pumped with a 980 nm source. The noise power spectral response of a fiber amplifier is flat since its dominant noise terms have a weak frequency dependence which are also easily dominated by shot noise at higher power operation. Measurements of the noise power spectra corresponding to ten differently coupled power values, ranging from -11.0 dBm to -1.0 dBm, were obtained using the fiber amplifier for the measurement frequency range of 0.13 GHz to 20 GHz. All ten spectra were normalized to a reference value at the same frequency. The resulting normalized curves all agreed in relative amplitude with frequency to within experimental error. Their agreement also confirmed that the optical output of the fiber amplifier was acting as a 'white' shot noise source since only the relative positions of the spectra changed with power and not the spectral shape. An average of the ten normalized 'white' noise spectra was the used to correct the response of the lightwave analyzer. The resulting correction curve varied non-periodically over the frequency range 0.13 GHz to 20 GHz by +/-2dBm. Applying the correction curve to the noise floor of the lightwave analyzer resulted in a very flat response to within +/-0.2 dBm consistently. As well, the resulting RIN spectra consistently corresponded to the theoretical shape predicted by equation (2.2.3), which dramatically improved the correlation with the experimentally obtained spectra.

4.2 LIGHT-CURRENT MEASUREMENTS

A schematic diagram of the experimental setup for the L-I measurements is shown in Fig. 4.2 [40]. The purpose of the vacuum chamber is to prevent condensation from forming on the devices at the lower temperatures. The vacuum chamber is capable of maintaining a pressure of about 15 millitorr which is monitored with a vacuum gauge. A two-stage thermoelectric cooling/heating stage inside the vacuum chamber controlled the temperature of the lasers. The primary stage consists of two thermoelectric coolers mounted in series. One side of this TE stack is contacted to the vacuum chamber base and the other side is contacted to a copper plate. The function of the primary cooling/heating stage is to assist in obtaining low temperature measurements without having the delay times associated with changing the temperature of a large thermal mass. The current to the primary stage is supplied by a Xantrex HPD 15-20 power supply which was remotely controlled. The secondary cooling/heating stage, which is mounted on top of the copper plate in contact with the primary cooling stage, consists of a smaller (11 mm x 11 mm) thermoelectric cooler on top of which was mounted a copper block and the laser diode. The power to this device is controlled by an ILX 3722 laser driver temperature controller. The temperature of the laser diode heat sink is monitored using thermistors situated beneath the position of the laser diode. The controller is connected to the data acquisition computer using an IEEE 488 interface.

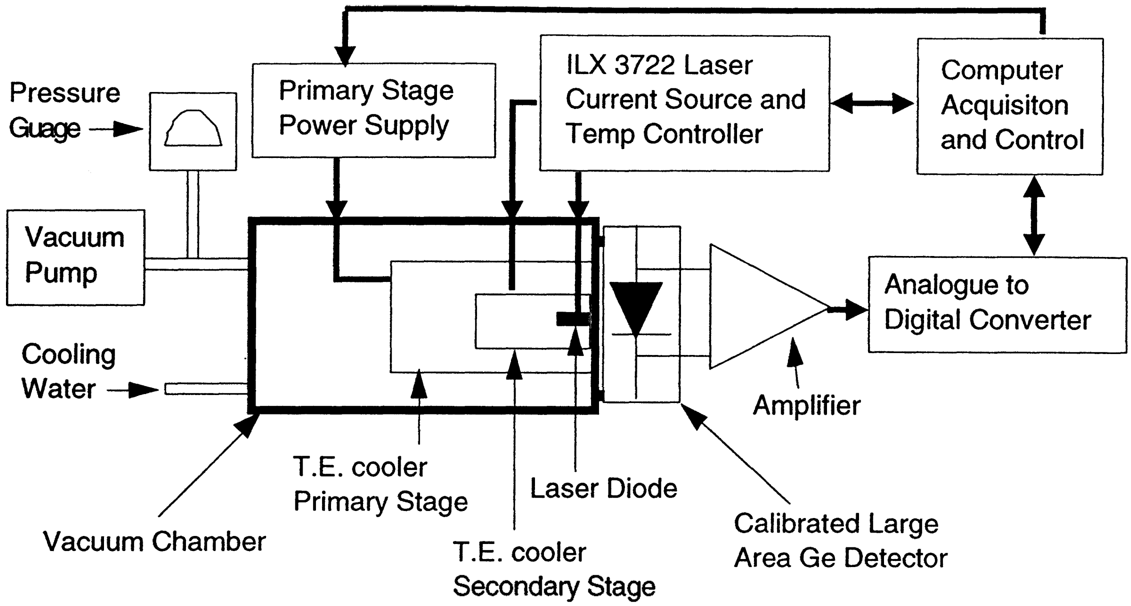

Figure 4.2: Schematic diagram of the experimental set-up used to measure the CW light-current characteristics of the ridge waveguide MQW lasers [40].

The light output from the laser diode is collected by a large area (1 cm^2), calibrated, germanium detector (Germanium Power Devices Corp. GM10HS08) which is situated within 3 mm of the laser diode facet. The detector has a responsivity of 0.55 A/W at a wavelength of 1300 nm. The photocurrent of the detector is amplified using a detector circuit consisting of an LF357 OP amp configured to have a gain which is variable from 1×10^2 to 2×10^6 V/A. The output voltage from the detector circuit is digitized using the analog-to-digital (ADC) converter of an SR510 lock-in amplifier with a resolution of 2.5 mV, which is then read by the IEEE 488 computer interface.

4.3 EXPERIMENTAL SET-UP FOR SPECTRAL MEASUREMENTS

The experimental setup for measuring the spectral characteristics of the lasers is used to study the temperature trends of two important spectral properties; the dominant emission wavelength of the laser, and the optical spectra as a function of sub-threshold injection current [40]. A schematic diagram of the experimental setup that was used is shown in Fig. 4.3 and is fundamentally similar to that shown in Fig. 4.2 save for the following differences. The light output from the laser diode, instead of being directly detected by a Ge detector, was collimated using a laser diode collimating lens and focused onto the entrance slit of an Jarrell-Ash Monospec 50 scanning monochromator. The monochromator had a 0.5 meter path length, with an f/8.6 aperture, and a linear dispersion of 3.2 mm/nm. The light at the output slit of the monochromator was then detected using an InGaAs photodiode. The InGaAs detector had a responsivity of 0.84 A/W at 1310 nm, and the gain in the detector circuit could be adjusted from 1×10^2 to 2×10^7 V/A. In order to obtain a good signal-to-noise ratio, the light output from the laser diode was chopped for phase sensitive detection by a SR510 lock-in amplifier. The setup is also fully automated with monochromator control carried out using an RS-232 interface connected to an SX Series Compumotor stepping-motor. This stepping motor had a resolution of 25000 steps/revolution, or 2500 steps/nm, which allowed for fine wavelength control.

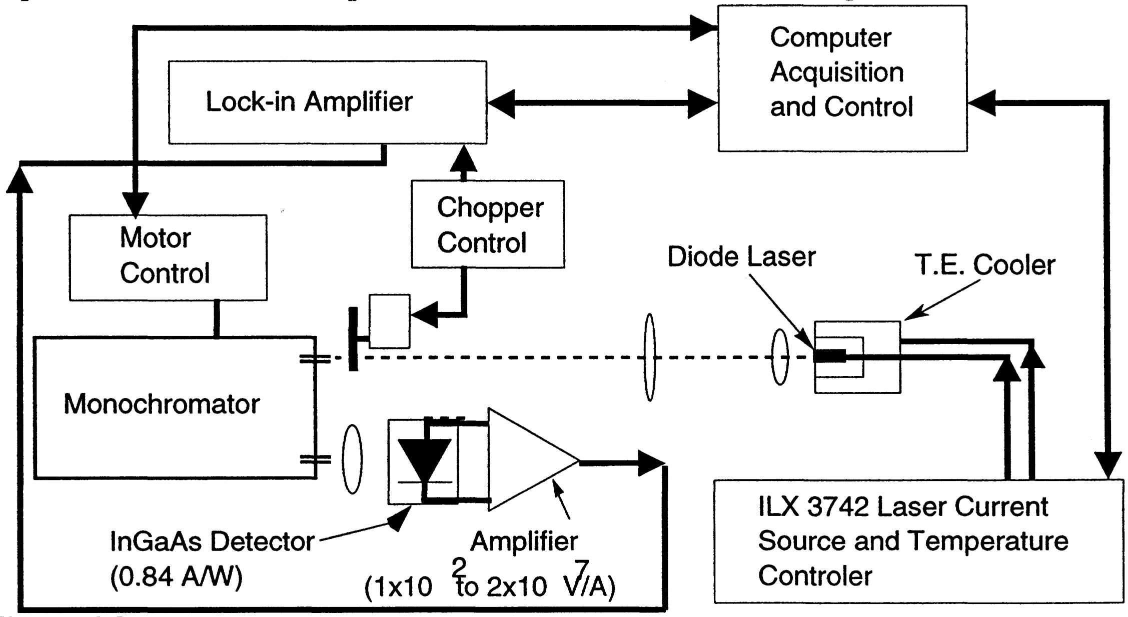

Figure 4.3: Schematic diagram of experimental set-up used to perform spectral measurements [40].

4.4 SUMMARY

In summary, this chapter described the experimental apparatus and configurations used to test the relative intensity noise (RIN), continuous wave (CW), and spectral characteristics of devices for the laser structures studied. Some explanation of how RIN measurements provide a parasitic-free means of observing the dynamic operation of a laser is given.

CHAPTER 5: DEVICE CHARACTERIZATION

5.0 INTRODUCTION

The experimental work of this thesis focused on characterizing the intrinsic modulation performance of the structures studied by extracting parameter values from RIN spectra taken as a function of injected current. The fitting routine that was developed using equation (2.2.3) to extract the resonance frequency and damping factor values from the RIN data will be discussed and the quality of the fits to the RIN data obtained will be presented. Also, the validity of the resonance frequency and damping factor values extracted will also be considered based on a comparison of these results to those obtained on an identical device using small-signal analysis.

The light output of the laser structures as a function of injected current was measured to characterize the single facet output power, as well as the threshold current. The calibration of this L-I data will be discussed in this chapter. Comparing the results of the RIN and L-I characterizations allowed for an examination of how the resonance frequency behaved as a function of injected current above threshold as well as the optical power. The fitting routine used to extract D' and D coefficient values using equations (2.3.13) and (2.3.16) from the comparison of the RIN and L-I characterizations will also be discussed in this chapter. The problems encountered fitting to the resonance frequency versus injected current above threshold and optical power data due to the inadequacy of the single mode rate equation model, and internal device heating will also be examined. As well, results on how D' and D were found to change as a function of device structure and device length will be presented.

Further information was obtained from the RIN data by examining how the damping factor values varied with the square of the resonance frequency as predicted by equation (2.3.5). The fitting routine used to characterize the K factor based on equation (2.3.5) will be presented, as well, the observation of non linearity in the damping factor-resonance frequency behavior will be discussed.

In order to calculate the differential gain, g_n, from the D' and D coefficient values for the group velocity, v_g, average photon energy, $h\nu$, internal quantum efficiency, η_{int}, and the internal loss, α_{int}, had to be determined. Using equation (2.5.1) the group velocity can be calculated given values for the longitudinal mode spacing as well as the cavity length of the laser. The method used to characterize the average longitudinal mode spacing, as well as the average optical wavelength, from optical spectra obtained for each of the laser structures will be presented. Values for η_{int} and α_{int} were determined from the length dependence of the external differential efficiency, η_{ext}, using equation (2.5.4). The fitting routine used to extract η_{ext} using equation (2.5.2) from the calibrated L-I data mentioned above will be discussed. Using the v_g values the modal reflectivity for each structure was determined with Fresnel's formulae which was used to calculate the mirror losses, α_m. The photon lifetimes could then be calculated using equation (2.3.8) and how the resulting values varied as a function of device structure and length will be discussed as a follow up to §3.2 and §3.3.

Finally based on the resulting calculations, the trends observed in g_n and ε as a function of barrier height, QW number, and cavity length will be presented.

5.1 RESONANCE FREQUENCY AND DAMPING FACTOR CHARACTERIZATION

5.1.1 Characterization of RIN spectrum

The fitting routine developed to fit equation (2.2.3) to the RIN spectra obtained as a function of current for each of the diode lasers as described in §4.1.2 used the Marquardt-Levenberg nonlinear least-squares method [46]. This method is well-suited to fitting to complex function like (2.2.3) since it involves the combination of two fitting strategies, the gradient search, and linearizing the fitting function. The gradient search does well to approach a minimum from far away but is slow to converge when in the immediate area. Conversely, the method of linearizing the fitting function converges on the minimum quite rapidly where the Chi Square surface is approximately parabolic but outside of this area it cannot be relied upon to approach the minimum. It can be analytically shown that the hyper surface directions the gradient and analytical searches take are perpendicular to each other, and that the optimum direction lies vectorally between these two. The changes in the fitting parameters suggested by the two approaches are combined vectorally by the fitting algorithm to give the best iteration towards the solution. A C program using this routine was modified from a Borland Turbo C program found in Numerical Recipes in C . The best fits maximizing number of points used and quality of fit were obtained when a 6 GHz range chosen relative to the peak of the RIN spectrum was used. A typical fit used 240 data points as shown in Fig 5.1. The fitting routine supplied values, and corresponding relative errors, for the resonance frequency, f_0, the damping constant, Γ_0, and coefficients A and B as a function of current.

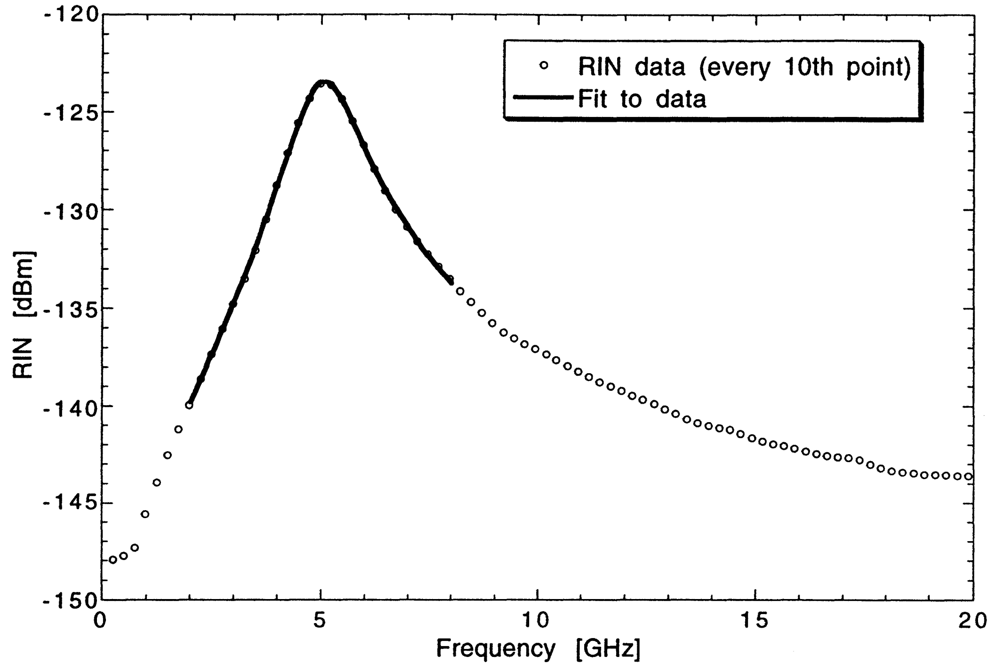

Fig. 5.1: Fit to RIN data obtained for device #32, with 10 mil (254 μm) cavity length, from sample S1-588. At 20 °C the device had a threshold current of 20.0 mA and when biased at 30 mA produced this RIN spectrum. The fit gave a resonance frequency (f_0) of 5.071 +/- 0.001 GHz and a damping constant (Γ_0) of 9.77 +/- 0.02 Grad/s. The values of the constants from equation (2.2.3) where A=9.4 +/- 0.5 x10^{-10} $Grad^4/s^4$ and B=4.23 +/- 0.01 x10^{-11} $Grad^2/s^2$.

5.1.2 Confirmation of validity of f_0 and Γ_0 results obtained from RIN spectrum through comparison with small-signal analysis

To confirm the validity of the resonance frequency and damping constant values obtained from the RIN characterization, the results from this approach were compared to those obtained from a small signal technique on identical devices. The small-signal technique employed a frequency subtraction approach to extract the intrinsic device response [47]. Using this approach all parasitic elements from the response are eliminated by taking the ratio, through subtraction on a log scale, in the extrinsic device response measured under two different bias conditions. The resulting ω_0 and Γ_0 values obtained from fitting this difference to a modified form of equation (2.3.1) represent their intrinsic values, in theory, for that particular bias condition. The parameters ω_0 and Γ_0 in equation (2.3.1) represent the same physical quantity as those found in the RIN spectrum described by equation (2.2.3). A study compared results obtained using the RIN measurement setup used in this study with results obtained by the small signal frequency subtraction technique and found the values to be in good agreement [48].

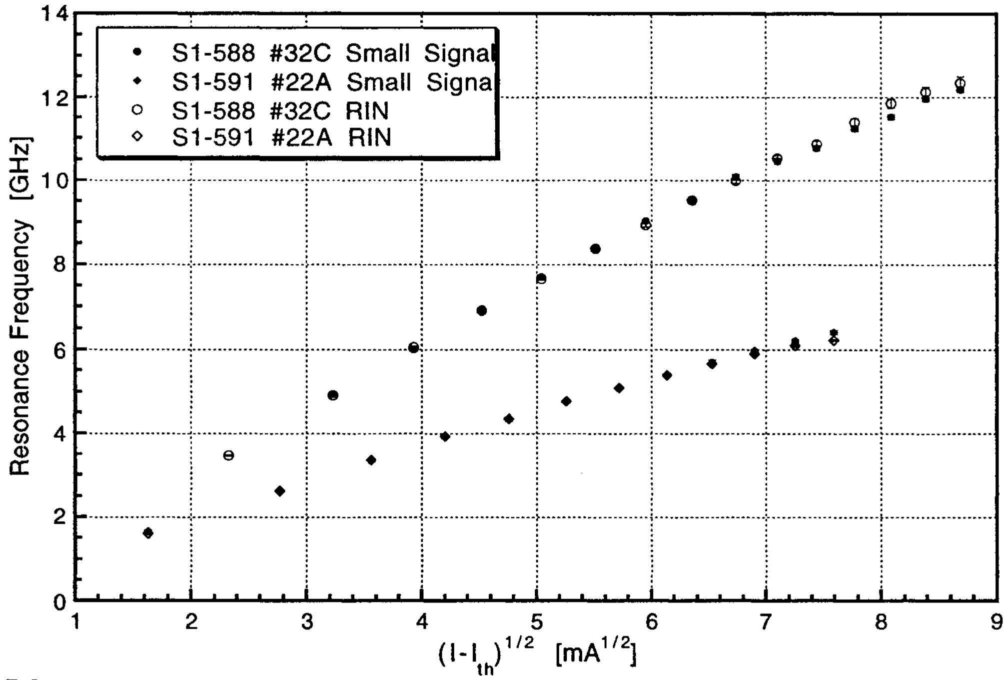

Fig. 5.2: Comparison of the resonance frequency data from fits to data obtained using the small signal frequency subtraction technique and the RIN measurements for device #32, with 30 mil (762 μm) cavity length, from structure S1-588 and device #22, with 10 mil (254 μm) cavity length, from structure S1-591 at an operating temperature of 20 °C.

In all cases, the values found for resonance frequency agreed well within experimental error, under all bias and temperature conditions (see Fig 5.2). For lower values of damping factor, there was good agreement. However, for larger values, the values were consistently lower than the RIN determined values. This trend was independent of device structure or chip carrier (see Fig 5.3). An acceptable explanation for this observed difference was not found, however, given its magnitude (~5%) the agreement is still excellent given the experimental conditions. As well the damping levels for which this discrepancy exists were not in the range of values examined in this study.

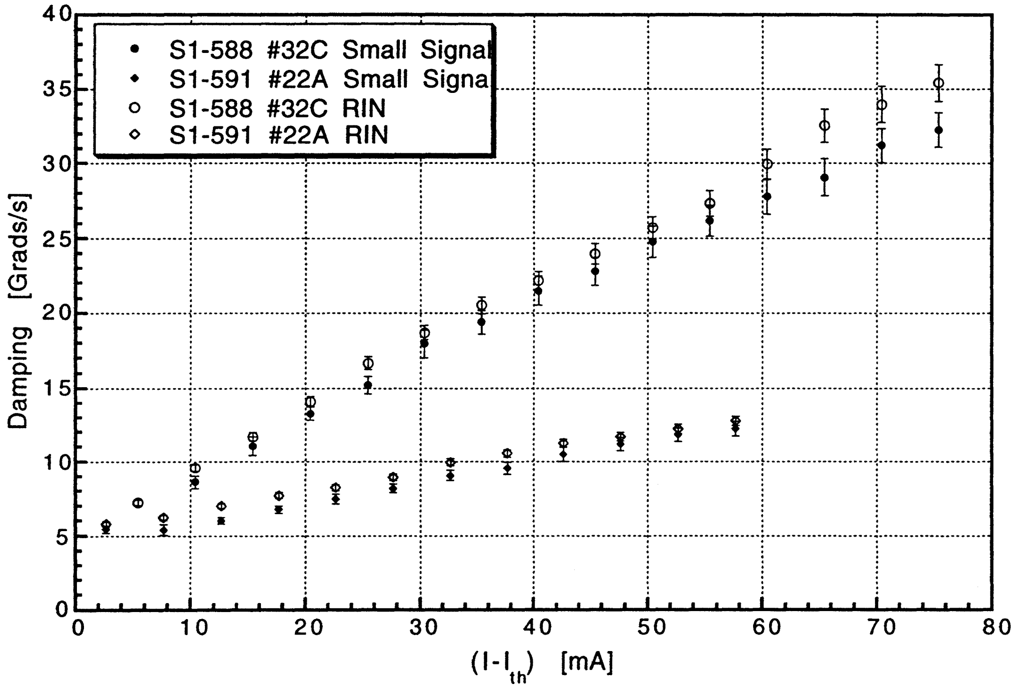

Fig. 5.3: Comparison of the damping data from fits to data obtained using the small signal frequency subtraction technique and the RIN measurements for device #32, with 30 mil (762 μm) cavity length, from structure S1-588 and device #22, with 10 mil (254 μm) cavity length, from structure S1-591 at an operating temperature of 20 °C.

5.2 D' and D COEFFICIENT CHARACTERIZATION

5.2.1 Characterization of power versus current

The power versus current characteristics for each diode laser were calculated using the L-I data acquired with the experimental setup described in §4.2 and the optical spectral data obtained using the experimental setup described in §4.3. The detector circuit voltage measured with the L-I experimental setup for a given diode laser bias current was converted to laser output optical power using the relationship

$$P_{out} = \frac{\eta \, V_{det}}{R(\lambda) \, G_{amp}} \tag{5.2.1}$$

where η is the collection efficiency, $R(\lambda)$ is the responsivity of the germanium detector as a function of wavelength, G_{amp} is the amplification of the detector circuit, and V_{det} is the detector circuit voltage. The typical optical divergence of InGaAsP/InP MQW RWG diode lasers studied in this work, is <90° full angle [49]. With the laser facet situated approximately 3 mm from the germanium detector the spot diameter would be < 6 mm. Since the detector active area is 1 cm^2 a collection efficiency, η, of near 100% is assumed. The responsivity, $R(\lambda)$, of the germanium detector as a function of wavelength was supplied by the detector manufacturer. The wavelength used corresponded to the dominant emission wavelength of the laser diode as measured using the spectral setup with the laser biased just above threshold.

5.2.2 Characterization of D' and D coefficients

Having determined the threshold current and the optical emission power as a function of current for each of the diode lasers, the resonance frequency as a function of current injected above threshold and optical emission power could be determined using the resonance frequency data as a function of current as described in §5.1.1. By fitting to this data using equations (2.3.13) and (2.3.16) the response coefficients D' and D introduced in §2.5.1 were extracted for each laser diode at an operating temperature of 20 °C. An example of the quality of fits obtained is shown in Figs 5.4 and 5.5.

Resonance frequency as a function of current injected above threshold, and optical emission power, were explored for operating temperatures above 20 °C but the trends observed revealed some potential limitations with the single-mode rate equation model used in this study. As shown in Fig 5.6 the resonance frequencies at lower levels of current injected above threshold for higher operating temperatures were lower than would be expected by theory according to the linear nature of equation (2.3.13).

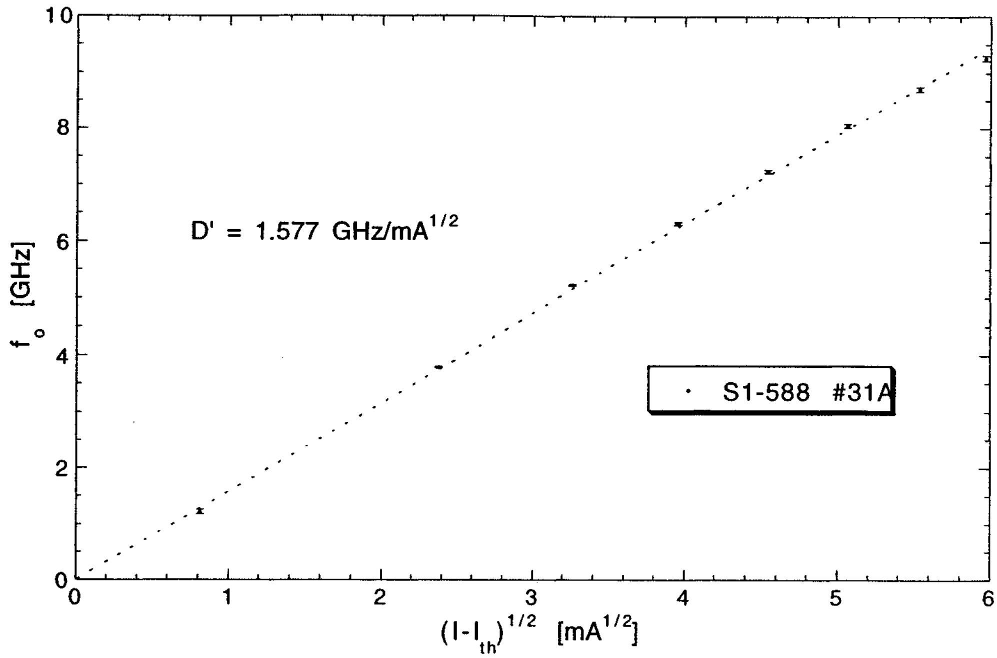

Fig. 5.4: Fit to equation (2.3.13) of resonance frequency versus square root of current injected above threshold for device #31, with 10 mil (254 μm) cavity length, from structure S1-588 at an operating temperature of 20 °C.

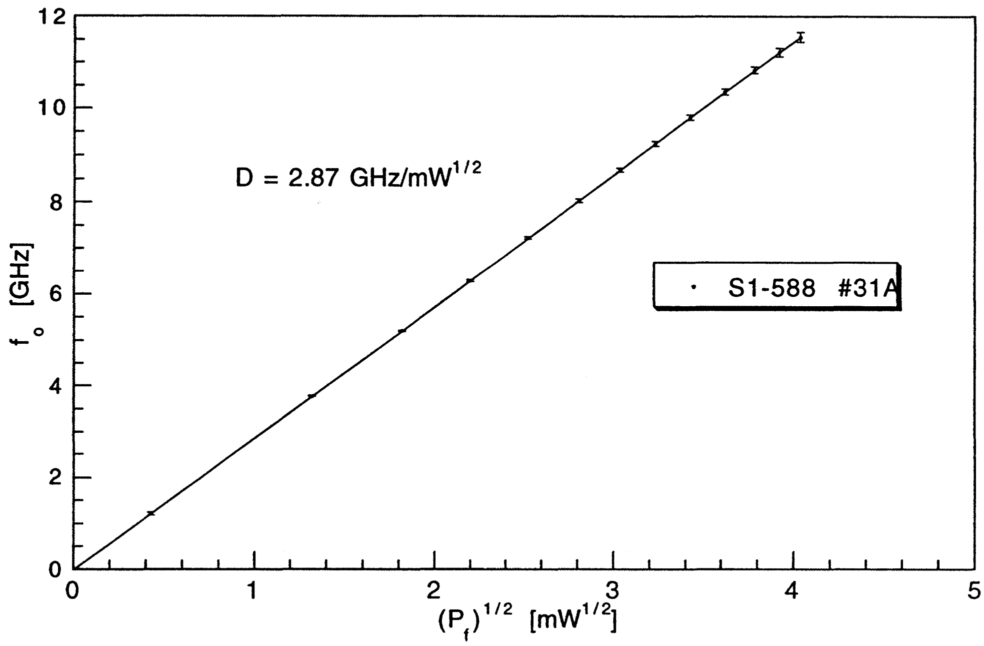

Fig. 5.5: Fit to equation (2.3.16) of resonance frequency versus square root of single facet optical emission power for device #31, with 10 mil (254 μm) cavity length, from structure S1-588 at an operating temperature of 20 °C.

This would naturally lead one to question whether the wrong value for the threshold current had been used. However, when the same resonance frequencies were plotted as a function of optical emission power the same phenomenon was observed at low levels of optical emission power. This trend in resonance frequency versus optical power with increasing operating temperature also runs counter to the linear trend predicted by equation (2.3.16). These phenomena were observed with all of the laser structures in this study.

Lower than expected resonance frequency values near threshold above room temperature may be a result of the predominately multimode operation observed in semiconductor lasers just above threshold resulting from spontaneous emission.[36] [50] It is possible that multimode operation near threshold persists to higher levels of optical power before the gain in one mode dominates over all of the initial lasing modes as the operating temperature of the laser increases. A characterization of the spontaneous emission rate as a function of temperature will be presented and discussed in §6.1. Proper modeling of this phenomena to allow for an accurate characterization of D at higher operating temperatures would have been beyond the scope of this thesis, so the characterization of these lasers was restricted to room temperature.

A deviation from the linear trend predicted by equations (2.3.13) and (2.3.16) was also observed at higher levels of current injection as shown in Fig 5.6. This is best explained by internal heating of the semiconductor laser resulting from contact resistance with increased current flow, and non-radiative recombination processes. This internal heating results in an increase of the operating temperature of the laser since the laser structure is incapable of dissipating the heat from the active region faster than it is being generated. As the operating temperature of the laser increases, the resonance frequency for a given output power drops causing a deviation from the linear trend of equations (2.3.13) and (2.3.16). Therefore, the data used for fitting to equations (2.3.13) and (2.3.16) was restricted to a current level below the point at which the trend observed began deviating from the linear one described by theory. This was typically associated with a power level of between 15 - 20 mW of single facet output power.

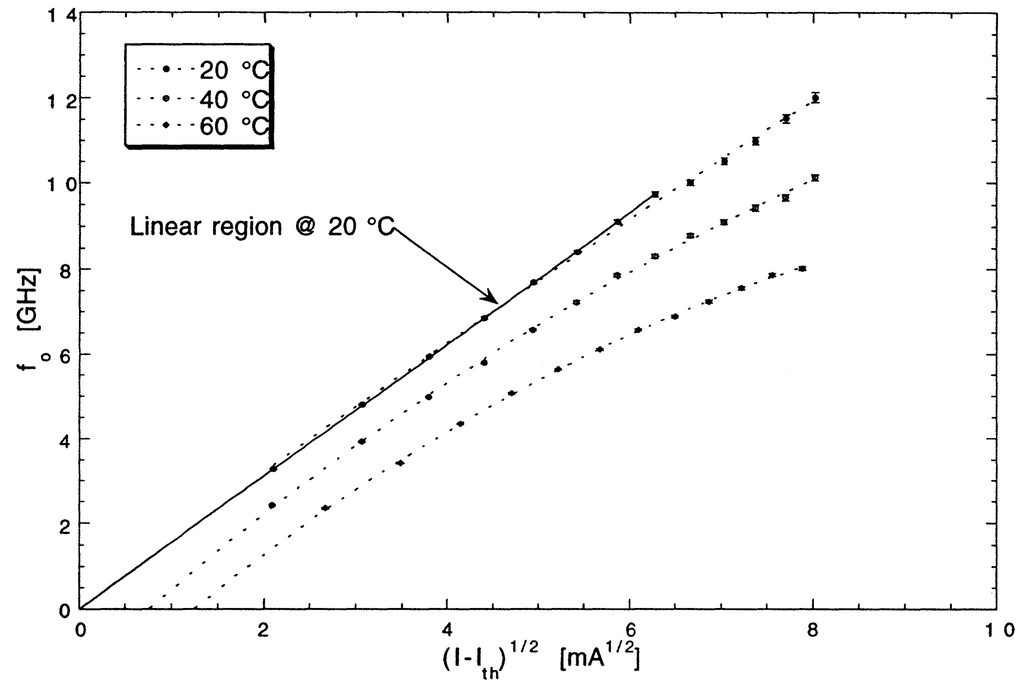

Fig. 5.6: Plot of resonance frequency versus square root of current injected above threshold at 20 °C, 40 °C, and 60 °C operating temperatures of for device #25, with 10 mil (254 μm) cavity length, from structure S1-590.

Since the values D' and D describe the rate at which the resonance frequency increases with current injected above threshold and output power, respectively, they are parameters that are of potential design interest. The parameters D' and D versus quantum well barrier height are shown in Fig 5.7. From the observed trend a barrier height between 1.1 and 1.15 Q gives the most efficient frequency response with current injected above threshold, or with output power, for the 10 quantum well design.

The change in D' and D parameters with quantum well number for the 1.1 Q barrier height design is shown in Fig 5.8. Here a slight improvement in the efficiency of the frequency response with current injected above threshold, or output power, for increasing quantum well number for 250 μm cavity length lasers is observed.

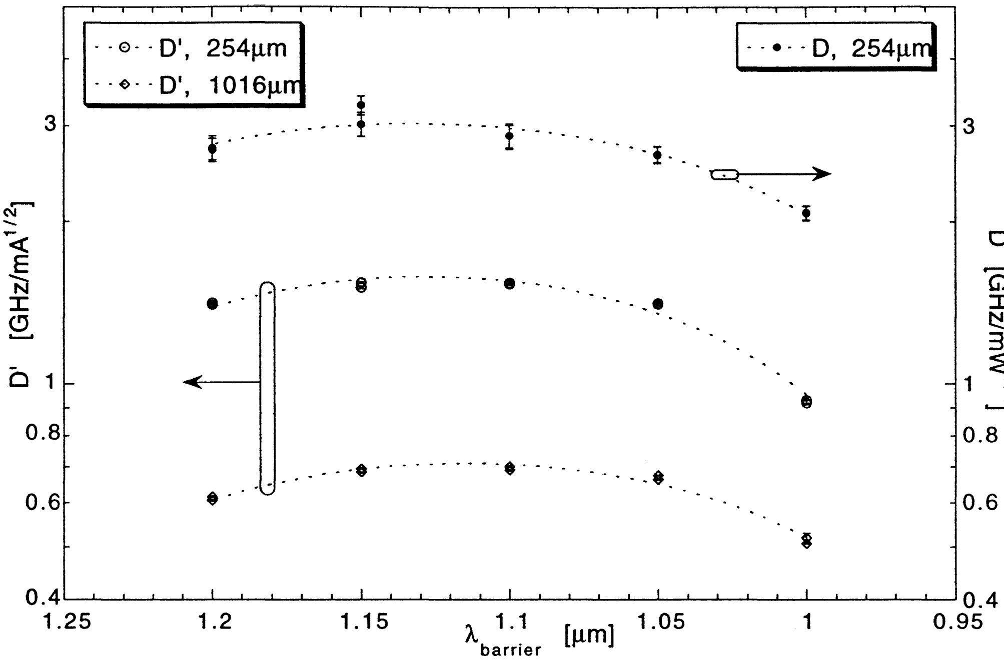

Fig. 5.7: D' and D parameter versus quantum well barrier height for 10 mil (254 μm) cavity length, and D' for 40 mil (1016 μm) cavity length, for a 10 quantum well design, at an operating temperature of 20 °C.

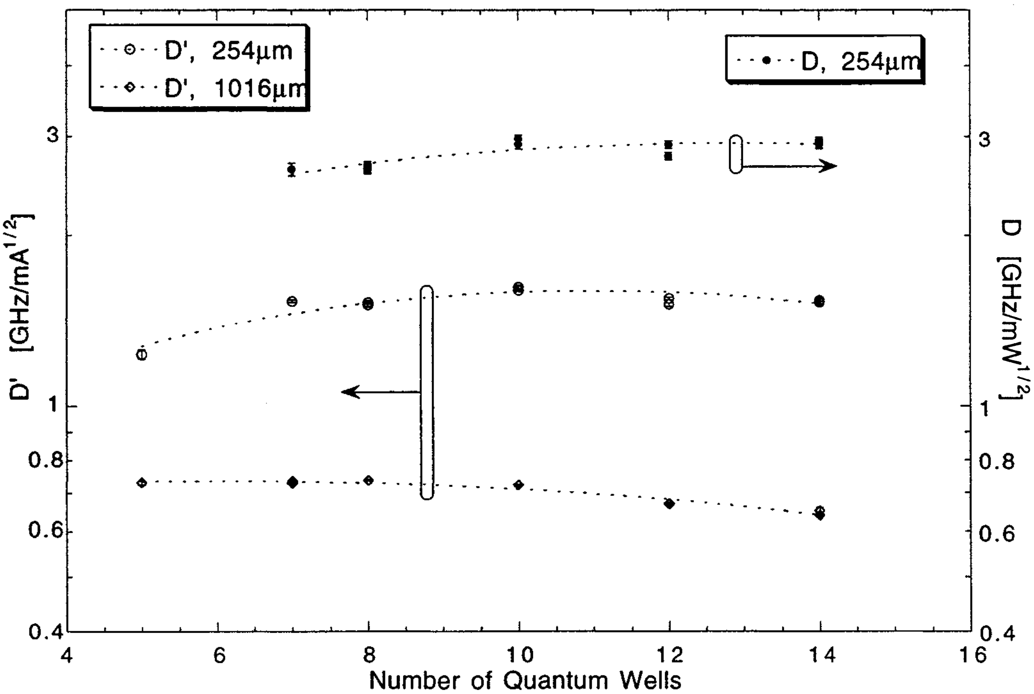

Fig. 5.8: D' and D parameter versus quantum well number for 10 mil (254 μm) cavity length, and D' for 40 mil (1016 μm) cavity length, for 1.1 Q well height design, at an operating temperature of 20 °C.

However the trend appears to reverse itself for 1016 μm cavity lengths lasers. An optimum frequency response with current injected above threshold, or output power for a given quantum well number with the 1.1 Q barrier height design would appear to correspond to 10 to 14 quantum wells or greater for 254 μm cavity lengths, where as for 1016 μm cavity lengths the optimum quantum well number would appear to be 5 or less. Given the trends shown the frequency response at these optimum quantum well numbers would not be significantly greater than the values shown in Fig 5.8.

The change in D' and D parameters with cavity length for the 1.1 Q barrier height, 10 quantum well design is shown on Fig 5.9. An improvement in the efficiency of the frequency response with current injected above threshold, or output power, for decreasing cavity length is observed. An optimum frequency response with output power for a given cavity length with the 1.1 Q barrier height, 10 quantum well design is not shown in the range of cavity lengths studied here.

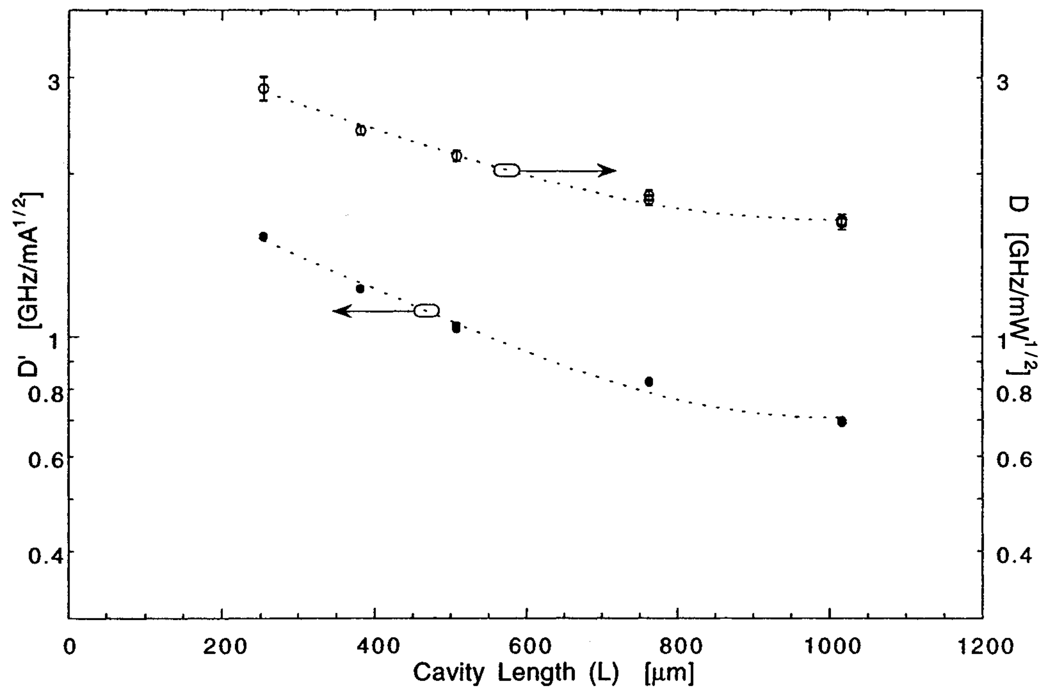

Fig. 5.9: D' and D parameters versus cavity length for 1.1 Q well height, 10 quantum well design, at an operating temperature of 20 °C.

5.3 K FACTOR CHARACTERIZATION

The resonance frequency and damping data as a function of current obtained in §5.1.1 was plotted according to equation (2.3.5), in order to characterize the K factor for each of the diode lasers at an operating temperature of 20 °C. In Fig. 5.10 the linear relationship described by equation (2.3.5) is demonstrated. As discussed in §2.3 this linear relationship does not hold for values obtained near threshold, shown here by the first data point.

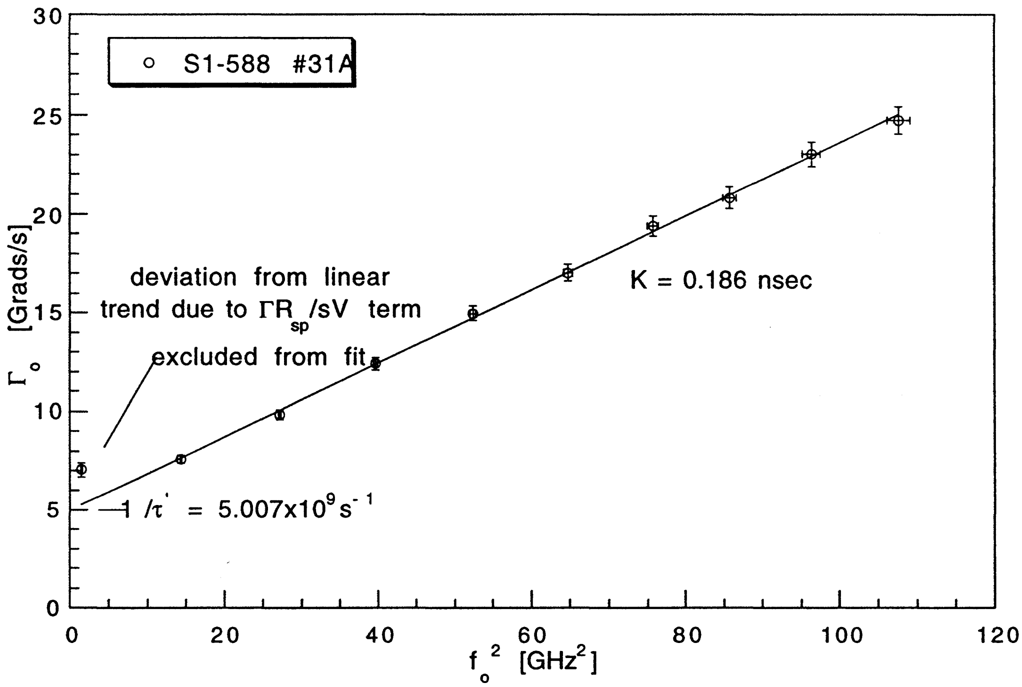

Fig. 5.10: Fit to equation (2.3.5) of damping versus resonance frequency squared for device #32, with 10 mil (254 μm) cavity length, from structure S1-588 at an operating temperature of 20 °C showing deviation of data from the linear terms of (2.3.5) due to spontaneous emission term.

Any of the initial data points for the diode lasers that did not follow the linear relationship described by equation (2.3.5) were assumed to be influenced by the spontaneous emission term and thus excluded from the fit. The resulting fits were in very good agreement with the experimental data as seen in Fig. 5.10 with a slope corresponding to the K factor and an intercept corresponding to the differential carrier lifetime at threshold, $1/\tau'$.

5.4 GROUP VELOCITY AND PEAK WAVELENGTH CHARACTERIZATION

The group velocity was determined for each of the laser structures using equation (2.5.1) as discussed in §2.5.3. Data of the optical emission spectra for a given laser structure was measured just below threshold using the experimental setup discussed in §4.3 as shown in Fig. 5.11. The optical emission spectra of the lasers was characterized at a bias just below their lasing threshold since at this point there is still spontaneous emission occurring such that there are multiple modes experiencing gain in the laser cavity which allows for a statistical determination of the mode spacing. At the same time there is enough stimulated emission beginning to occur such that the signal to noise ratio for each mode is good, and yet not so much that any one mode is monopolizing the cavity gain.

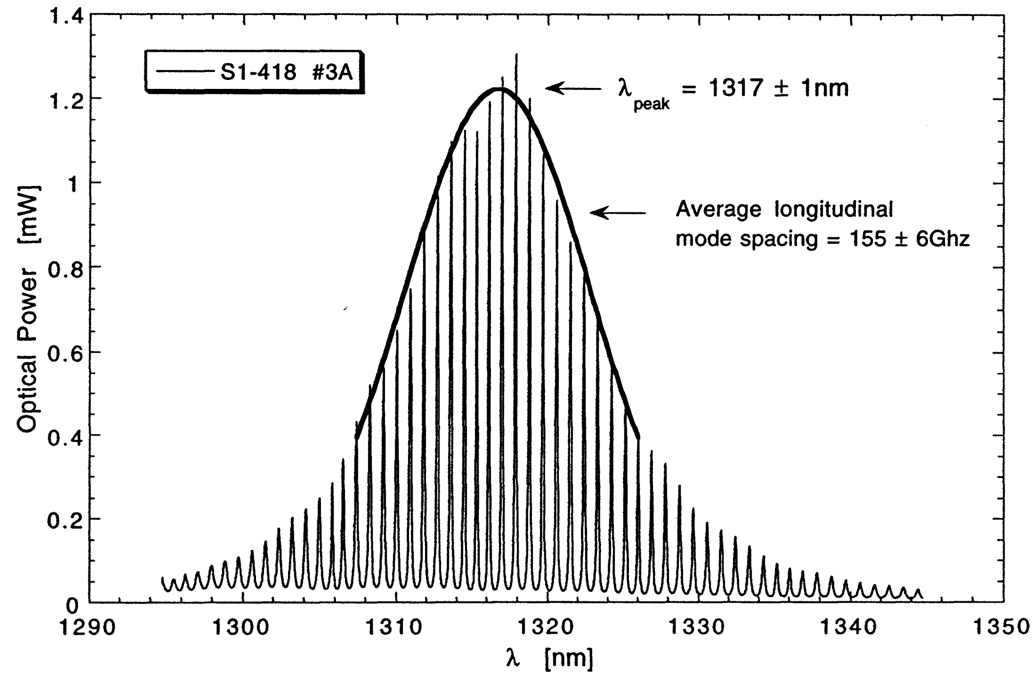

Fig. 5.11: Measured optical emission spectra for device #3, with 10 mil (254 μm) cavity length, from structure S1-418 at an operating temperature of 20 °C.

The longitudinal mode structure for each laser structure is visible when this spectral data, in the form of optical power is plotted versus wavelength as shown in Fig. 5.11. This data was converted to the frequency domain so that the frequency spacing between each mode could be determined to calculate the average longitudinal mode spacing. The accuracy of the longitudinal mode spacing was limited by the 0.02 nm resolution used to measure the optical power versus wavelength to a frequency resolution of approximately 3.5 GHz in the wavelength range of the structures characterized in this study. The average longitudinal mode spacing was taken to be the median of approximately 40 mode spacing with the standard deviation as the uncertainty. The group velocity was then calculated using equation (2.5.1). The lasers used in the study were cleaved into 10 mil, 15 mil, 20 mil, 30 mil, and 40 mil cavity lengths which is equivalent in metric units to 254 μm, 381 μm, 508 μm, 762 μm, and 1016 μm lengths. The maximum expected variation in the cleaving was about 1 mil so the uncertainty associated with the cavity lengths was assumed to be 10 μm.

The peak wavelength for each laser structure was determined from the same below threshold optical emission spectra used to determine the longitudinal mode spacing as demonstrated by Fig. 5.11. A gaussian distribution was fitted to the peak optical power values associated with each longitudinal mode in the higher power range of wavelengths of the optical spectra. The peak wavelength was taken to be the mean of the distribution with an estimated error of 1 nm.

5.5 OPTICAL CONFINEMENT CALCULATION

As was mentioned in §2.5.4, an algorithm based on an approach to calculating the optical confinement factor of a multilayer structure developed by L.M. Walpita [56] was used to calculate values representative of the structures studied in this work. This algorithm was programed by Dave Adams in the mainframe computer at Nortel Technologies.

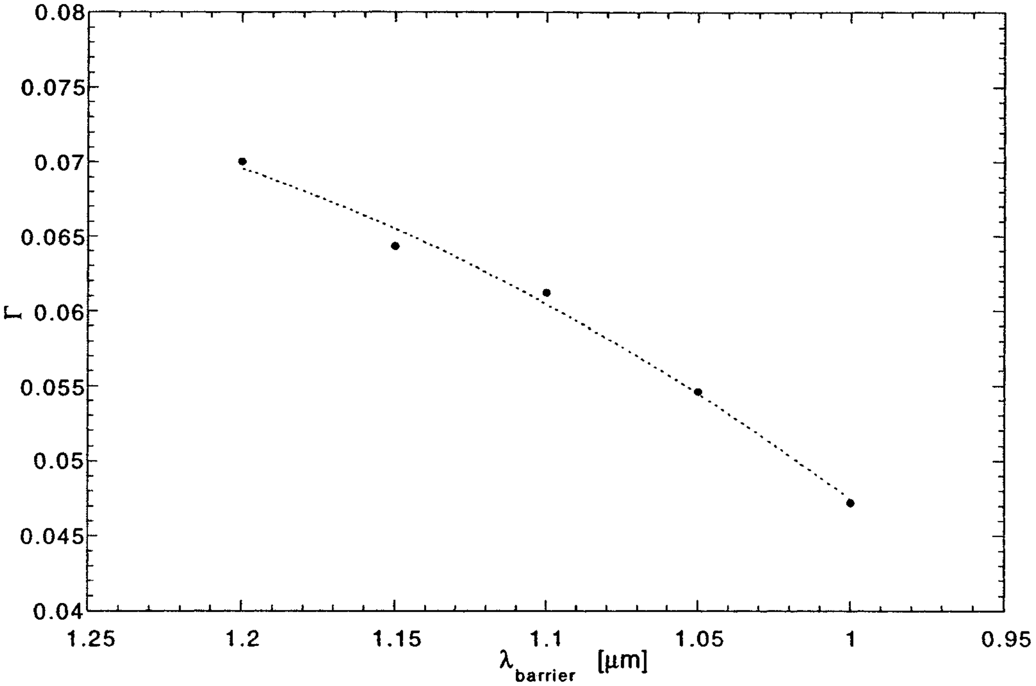

Fig. 5.12: Optical confinement factor versus quantum well barrier height for 10 quantum well design.

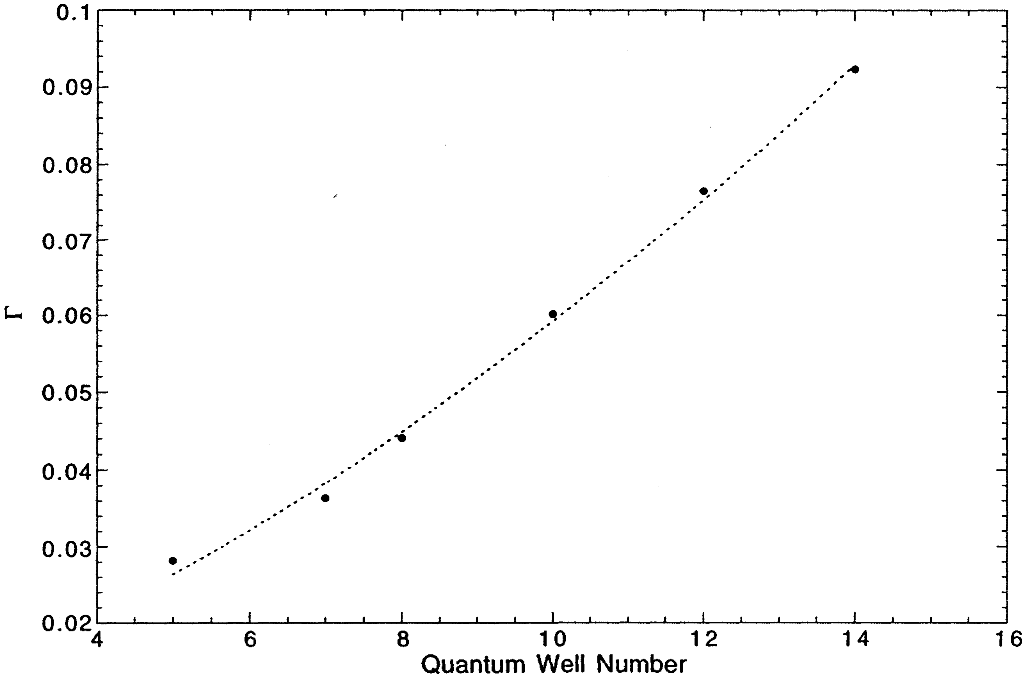

Fig. 5.13: Optical confinement factor versus quantum well number for 1.1 Q quantum well barrier design.

Values for the optical confinement factor for the structures where quantum well barrier height was varied are shown in Fig 5.12. A clear decrease in the optical confinement factor is observed in Fig 5.12 with increasing barrier height. Values for the optical confinement factor for the structures where quantum well number was varied are shown in Fig 5.13. A clear increase in the optical confinement factor is observed in Fig 5.13 with increasing quantum well number.

5.6 INTERNAL ABSORPTION, MIRROR LOSS, AND PHOTON LIFETIME CHARACTERIZATION

In §5.2.1 optical power versus current (P-I) characterization was described to correlate the resonance frequency measured at a given current level to output power. This P-I data was also used to determine the differential quantum efficiency for each laser structure. Using equation (2.5.2) the differential quantum efficiency was obtained from an optimized linear fit to the P-I data starting above the threshold current as shown in Fig 5.14. The resulting differential quantum efficiencies for devices with the same active region design were then plotted for varying cavity lengths as shown in Fig. 5.15. A fitting routine was used to extract the internal quantum efficiency, and internal absorption values from the external efficiency data according to its dependence on device cavity length in equation (2.5.5).

The calculated internal quantum efficiency versus quantum well barrier height is shown in Fig 5.16. From the observed trend internal quantum efficiency increases with decreasing barrier height for the 10 quantum well design. The calculated internal quantum efficiency versus quantum well number is shown in Fig 5.17. There is not much change in the internal quantum efficiency with increasing quantum well number for the 1.1 Q quantum well barrier design, the exception to this being the 5 well structure which showed a dramatically lower value.

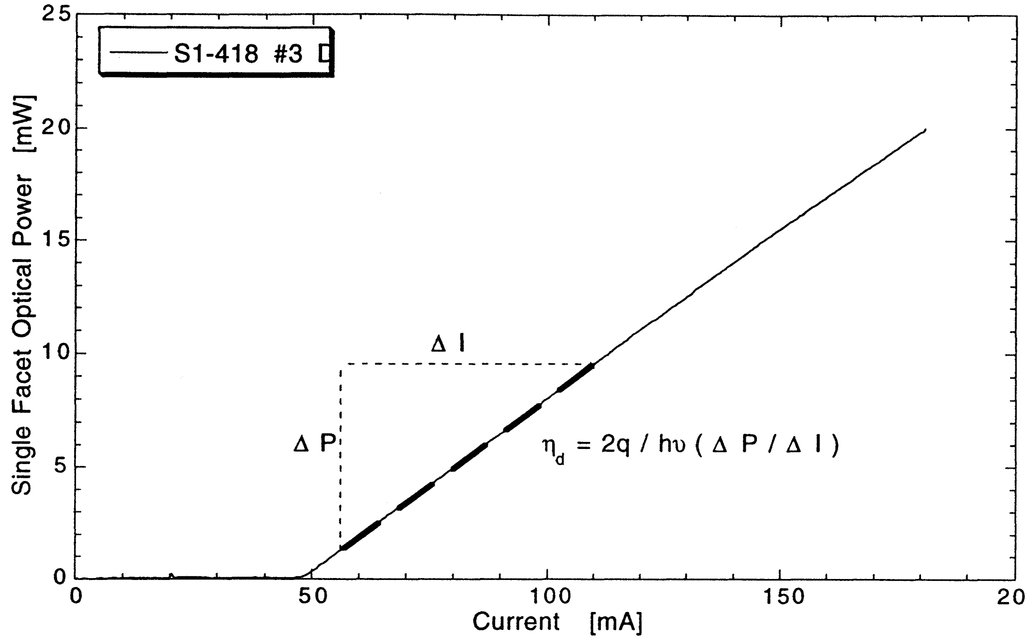

Fig. 5.14: Single facet optical power versus current for device #3, with 40 mil (1016 μm) cavity length, from structure S1-418 at an operating temperature of 20 °C, demonstrating the calculation of the external quantum efficiency from the slope of the plot above threshold.

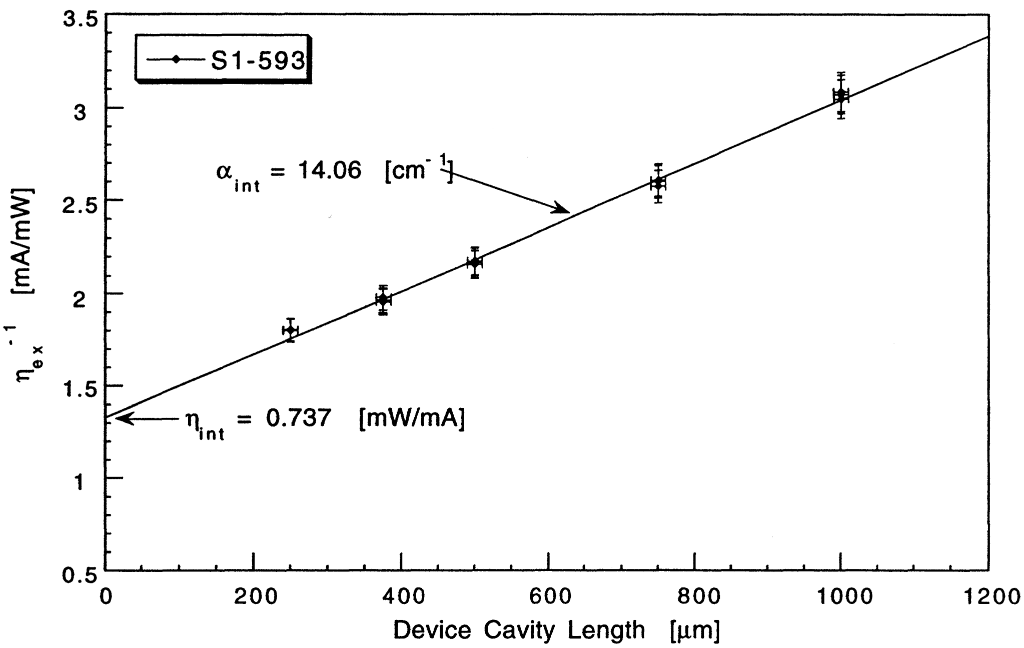

Fig. 5.15: Fit to equation (2.5.5) of inverse external differential quantum efficiency versus cavity length for structure S1-593 at an operating temperature of 20 °C showing the internal quantum efficiency calculated from the resulting intercept and the internal absorption calculated from the slope.

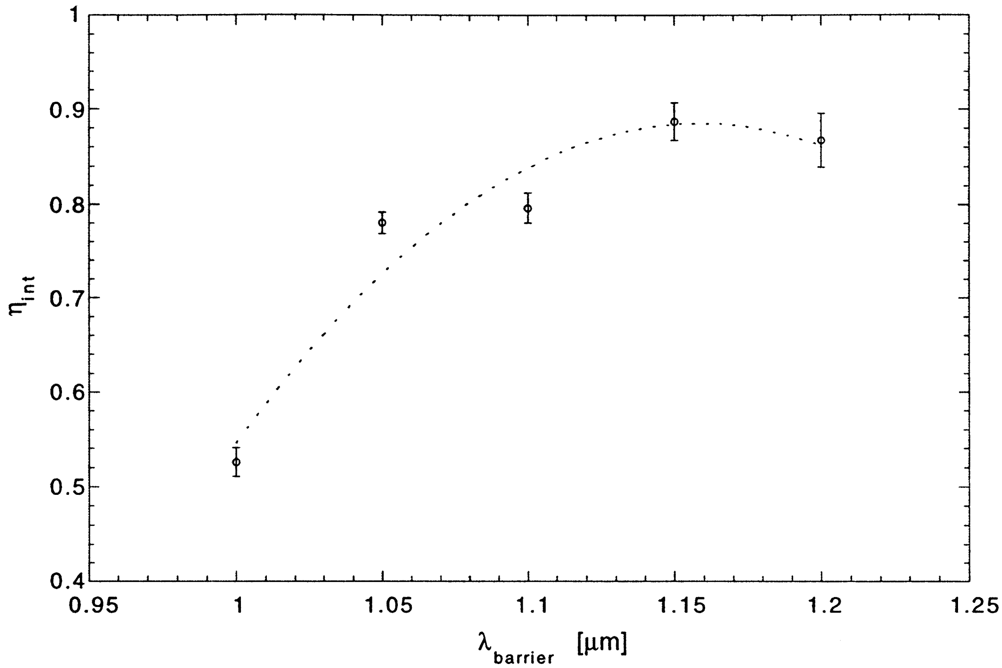

Fig. 5.16: Internal quantum efficiency versus quantum well barrier height for 10 quantum well design, with 10 mil (254 μm) cavity length, at an operating temperature of 20 °C.

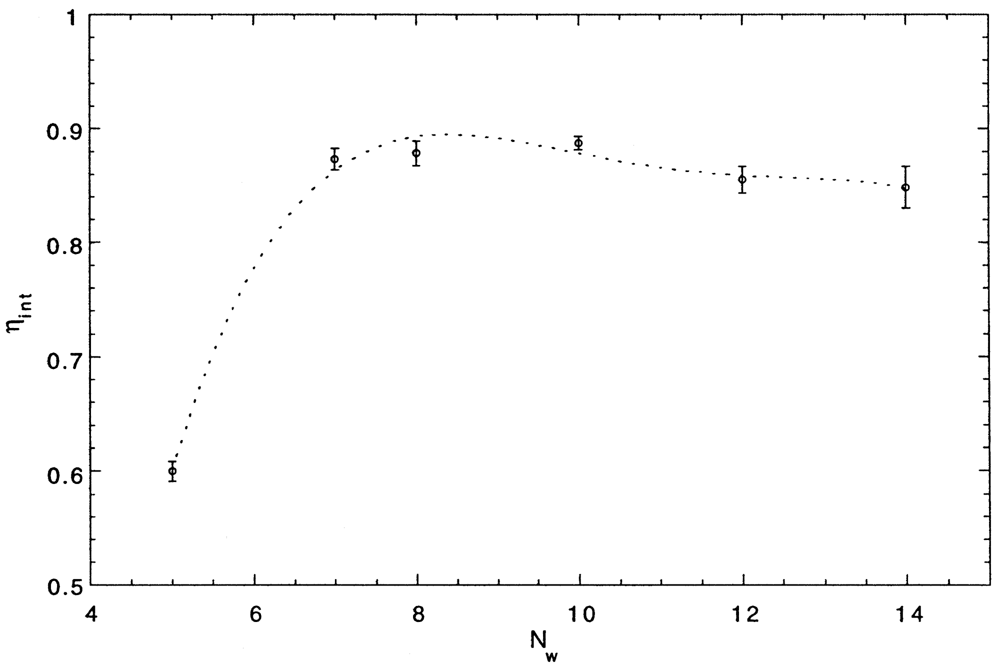

Fig. 5.17: Internal quantum efficiency versus quantum well number for 1.1 Q quantum well barrier design, with 10 mil (254 μm) cavity length, at an operating temperature of 20 °C.

Of greater importance to frequency response design is how the internal absorption changes with active region parameter since this directly influences photon lifetime. The calculated internal absorption versus quantum well barrier height is shown in Fig 5.18. An unexpected trend is observed where the internal absorption decreases with increasing barrier height. As was mentioned in §3.2.1, the band edge of the barriers are energetically far enough from the emission wavelength of the quantum wells that you would not expect to see any change in the internal efficiency with barrier height. The calculated internal absorption versus quantum well number is shown in Fig 5.19. As predicted in §3.2.2 a trend is observed were the internal absorption increases with increasing quantum well number.

Having determined values for the group velocity and internal absorption, calculating the mirror losses will allow for a determination of the photon lifetimes. The mirror loss is determined from the facet reflectivity and cavity length using equation (2.5.4). The facet reflectivity is calculated from the group velocity values determined earlier using equation (2.5.7) and (2.5.8). The resulting photon lifetimes versus quantum well barrier height are shown in Fig 5.20.

As predicted in §3.2.1 a trend is observed where the photon lifetime increases with increasing barrier height. The calculated photon lifetime versus quantum well number is shown in Fig 5.21. As predicted in §3.2.2 a trend is observed where the photon lifetime decreases with increasing quantum well number. The calculated photon lifetime versus laser cavity length is shown in Fig 5.22.

As was predicted in §3.3 a trend is observed where the photon lifetime increases with increasing cavity length. The change in the mirror losses, α_m, with cavity length clearly overpowered any change that could have been occurring in the group velocity with cavity length due to changes in the refractive index with carrier concentration and optical wavelength dependencies on cavity length.

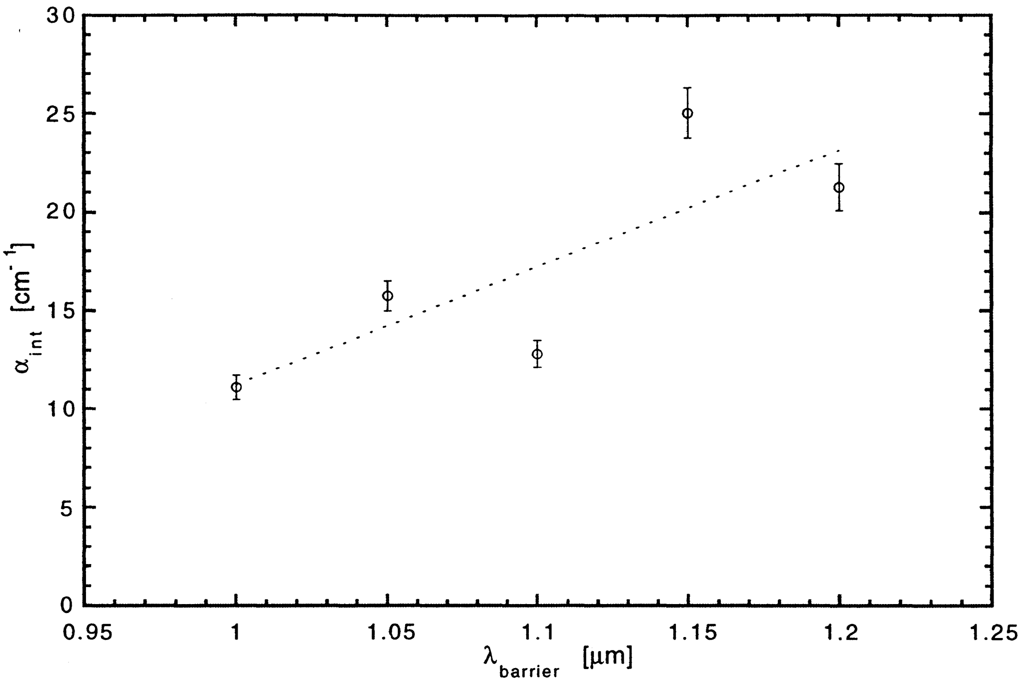

Fig. 5.18: Internal absorption versus quantum well barrier height for 10 quantum well design, with 10 mil (254 μm) cavity length, at an operating temperature of 20 °C.

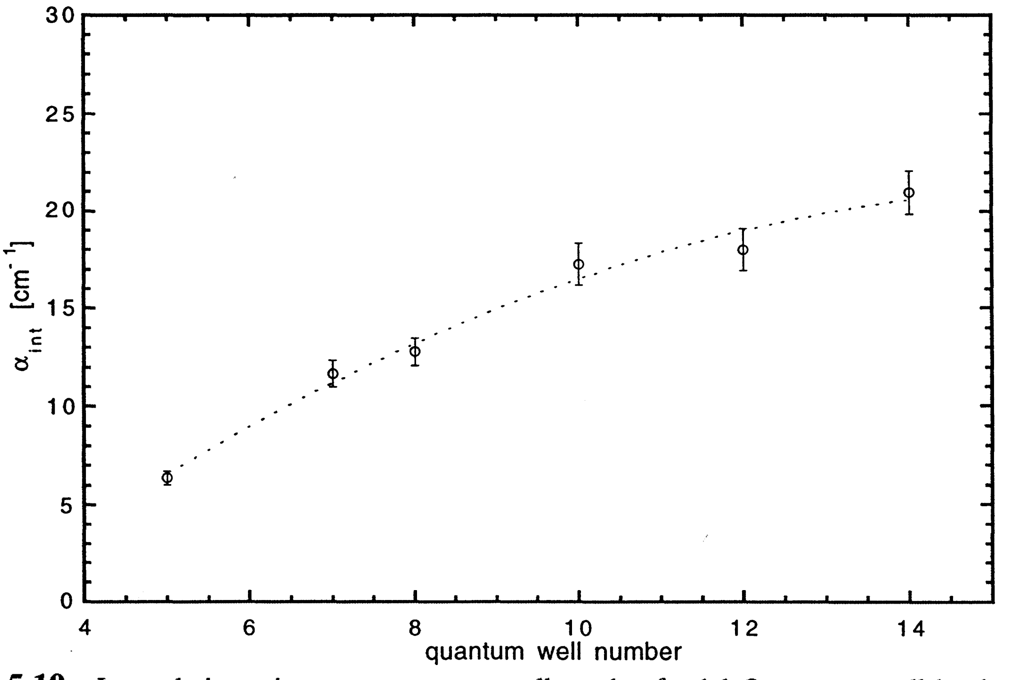

Fig. 5.19: Internal absorption versus quantum well number for 1.1 Q quantum well barrier design, with 10 mil (254 μm) cavity length, at an operating temperature of 20 °C.

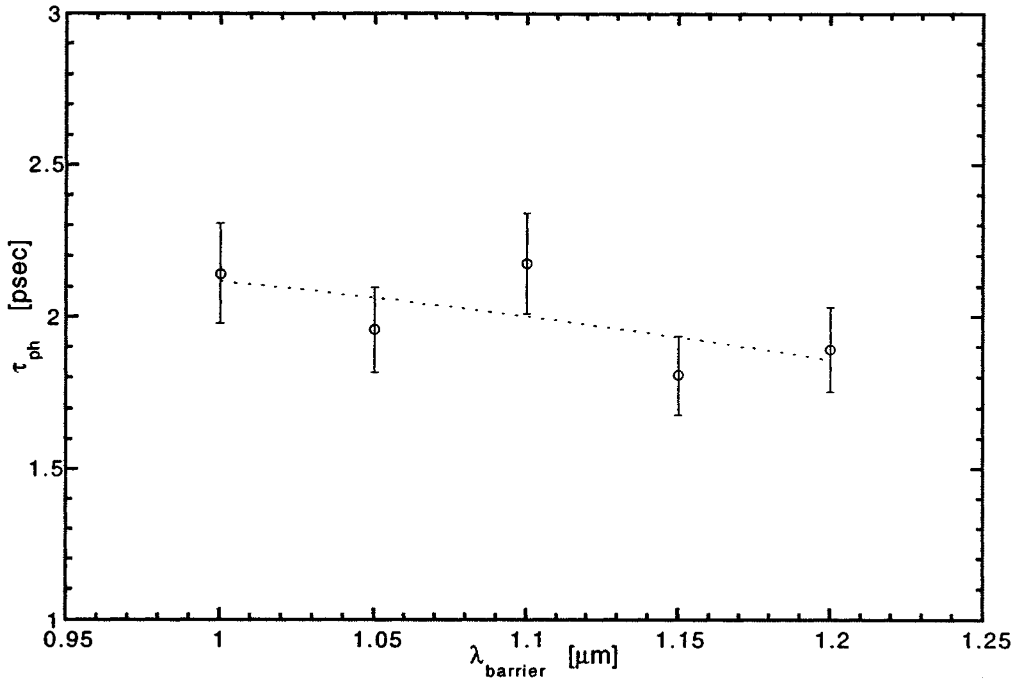

Fig. 5.20: Photon lifetime versus quantum well barrier height for 10 quantum well design, with 10 mil (254 μm) cavity length, at an operating temperature of 20 °C.

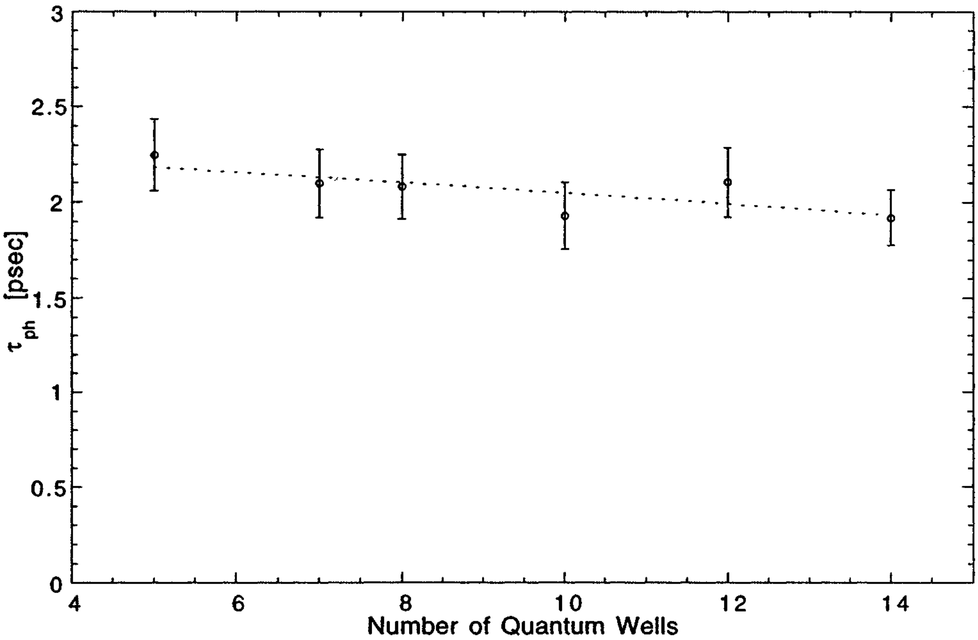

Fig. 5.21: Photon lifetime versus quantum well number for 1.1 Q quantum well barrier design, with 10 mil (254 μm) cavity length, at an operating temperature of 20 °C.

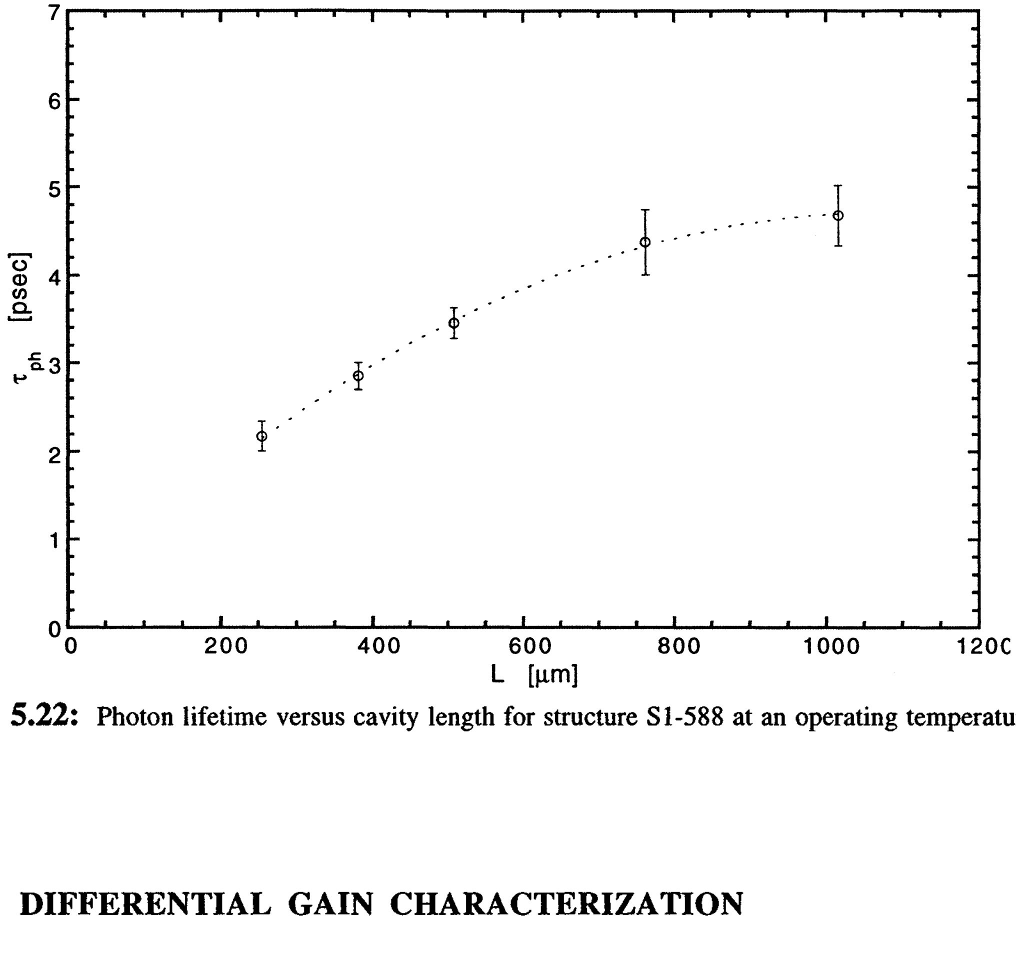

Fig. 5.22: Photon lifetime versus cavity length for structure S1-588 at an operating temperature of 20 °C.

5.7 DIFFERENTIAL GAIN CHARACTERIZATION

The characterization of differential gain using equations (2.3.14) and (2.3.17) relies on the accuracy of many of the previously determined parameters in this work. Some of these parameters have large degrees of uncertainty associated with them simply because assumptions had to be made as to the physical meaning of the parameters value. For example the active region cross sectional area, A, had a resulting average relative error of 33%. This is because the cross sectional area is given by $A = n_W\ d_W\ w$, where n_W is the number of quantum wells, d_W is the quantum well width, and w is the width of the stripe contact. One potential source of uncertainty exists in the width of the stripe contact, since as an active area width, it should represent the width of the active area where carriers are involved in carrier-photon interactions. This cannot simply be the width of the stripe contact since carriers will begin to diffuse laterally once they have entered the structure. The degree of this lateral diffusion will also have some dependence on the carrier density at the stripe contact. The stripe contact has a width of 2 μm so a reasonable estimation of the active area width would seem to be 3±0.5 μm to account for lateral current spreading which is an error of 17%. The width of the quantum wells is also a value requiring some assumptions. Since the well barriers are of an energetically finite height the carriers are not completely confined to the width of the quantum wells. As well the thicknesses used for the wells are based upon the requested grown thicknesses which are not always the final product. For these structures the requested well widths were 35 μm and so the value used for d_w was 35±5 μm which is an error of 14%. These two major contributions of 17% and 14% helped to give a 33% relative error in just one of the parameters involved in the determination of the differential gain.

Another heavy contributor to the uncertainty in the differential gain was the group velocity. This is because the group velocity, as described in equation (2.5.1), is given by $v_g=2L(\Delta v)$, where L is the cavity length of the laser, and Δv the longitudinal mode spacing. As was mentioned in §5.4, the longitudinal mode spacing was determined from the below threshold spectral output data of the lasers. The errors determined from the statistical analysis of approximately 40 measured mode spacing were in the range of 2-7 GHz, or 3-7%. Given that the frequency domain resolution of the optical emission spectra of the lasers was 3.5 Ghz the errors for this parameter were optimized to within the limitations of this method of characterization. The cavity length of the laser had an error of 10 μm which is simply the accuracy to which the laser cavities are cleaved from the wafer bars. This amounted to an error contribution of 1-4% depending on the cavity length. These two contributions of 2-6% and 1-4% combined to give an additional 3-7% relative error in the determination of the differential gain.

The two contributions described above were the main factors resulting a the total relative error of 33-34% in the calculated differential gain values. Despite these large errors the results obtained still convey comprehensible parametric trends. This is because the largest of these error contributions were most likely systematic across all of the lasers examined.

Having determined values for all of the parameters appearing in the expressions for D' and D, equations (2.3.14) and (2.3.17) respectively, values for the differential gain could be isolated. The differential gain was determined using the D' and D values as a check of the effect of the relative errors and assumptions associated with both methods. The resulting trend seen in the differential gain versus quantum well barrier height for 254 μm cavity length lasers determined from both D' and D values is shown in Fig 5.23.

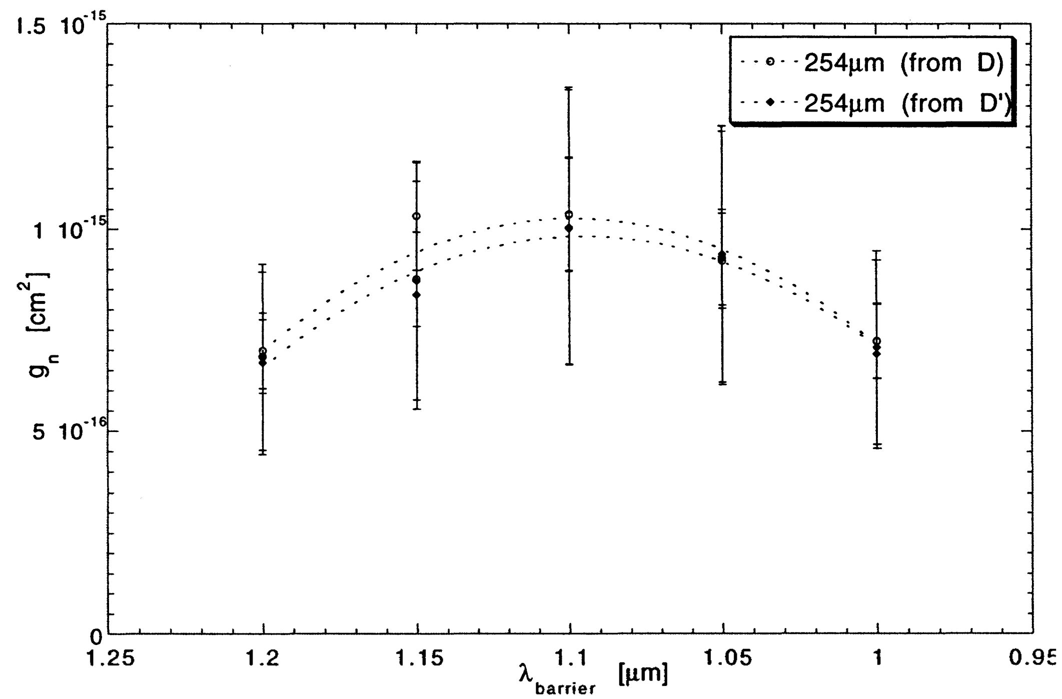

Fig. 5.23: Differential gain determined from both D' and D values versus quantum well barrier height for 10 quantum well design, with 10 mil (254 μm) cavity length, at an operating temperature of 20 °C.

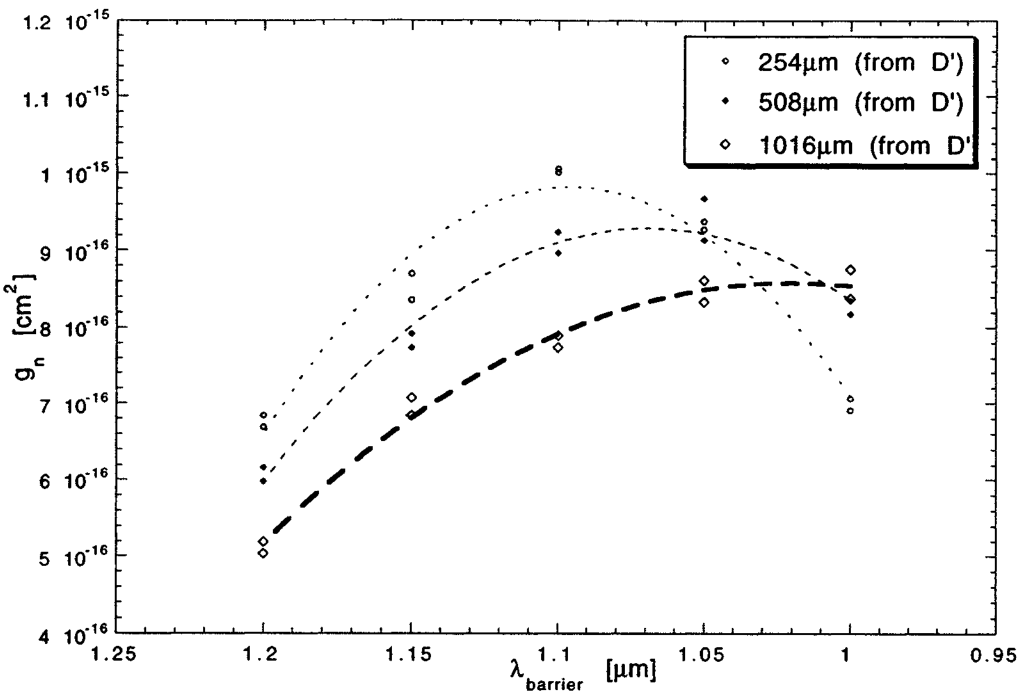

Fig. 5.24: Differential gain determined from D' values versus quantum well barrier height for 10 quantum well design, with 10 mil (254 μm), 20 mil (508 μm), and 40 mil (1016 μm) cavity lengths, at an operating temperature of 20 °C.

As can be seen in Fig 5.23 the two methods of determining the differential gain, from D' and D values, yield results that are in general very close to each other and well within experimental error. The plots in Fig 5.23 are also meant to demonstrate the magnitude of the error associated with these values. But rather than rely on the results from one laser cavity length the trend seen in the differential gain versus quantum well barrier height for 254 μm, 508 μm, and 1016 μm cavity length lasers determined from D' values is shown in Fig 5.24. As was predicted in §3.2.1 a trend is observed where the differential gain increases with increasing barrier height from 1.2 Q to 1.0 Q heights for the 1016 μm cavity lengths. However there is an increased deviation from this trend for the higher barrier heights for with decreasing cavity lengths as demonstrated by the 508 μm, and 254 μm cavity length results.

The resulting differential gain versus quantum well number for 254 μm cavity length lasers determined from both D' and D values is shown in Fig 5.25. Again, as can be seen in Fig 5.25 the two methods of determining the differential gain, from D' and D values, yield results that are in general very close to each other, well within experimental error. The plots in Fig 5.25 are also meant to demonstrate the magnitude of the error associated with these values. The trend seen in the differential gain versus quantum well barrier height for 254 μm, 508 μm, and 1016 μm cavity length lasers determined from D' values is shown in Fig 5.26. It was predicted in §3.2.2 that the differential gain should be observed to increase with increasing quantum well number. In Fig 5.26 the differential gain is observed to decrease with increasing quantum well number, except for 5-7 well 254 μm cavity length lasers, which runs contrary to that which has been demonstrated in other studies [15] [26] [42] [44]. This trend opposing that which is predicted by theory also appears to become stronger with increasing cavity length.

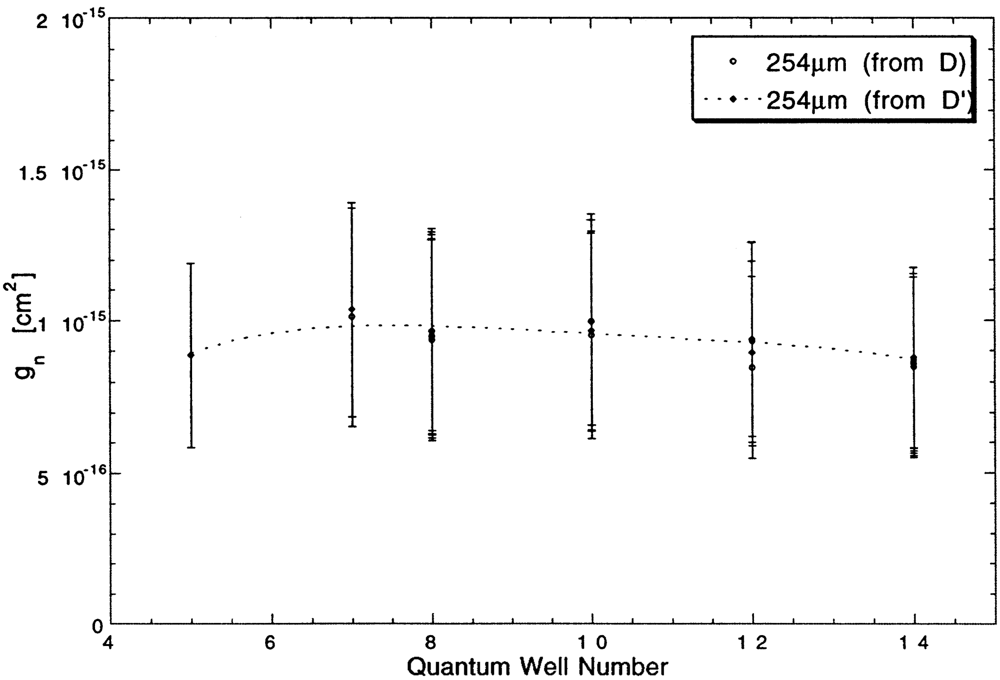

Fig. 5.25: Differential gain determined both from D' and D versus quantum well number for 1.1 Q quantum well barrier design, with 10 mil (254 μm) cavity length, at an operating temperature of 20 °C.

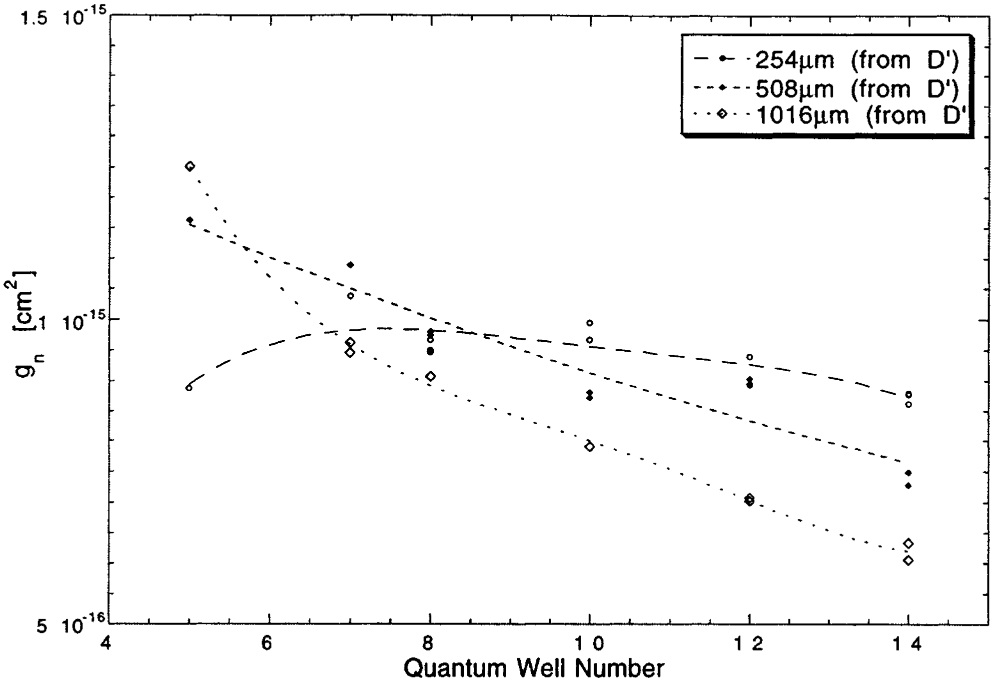

Fig. 5.26: Differential gain determined from D' versus quantum well number for 1.1 Q quantum well barrier design, with 10 mil (254 µm), 20 mil (508 µm), and 40 mil (1016 µm) cavity lengths, at an operating temperature of 20 °C.

Again, as can be seen in Fig 5.27 the two methods of determining the differential gain, from D' and D values, yield results that are in general very close to each other well within experimental error. The plots in Fig 5.27 of differential gain are also meant to demonstrate the magnitude of the error associated with these values. It was predicted in §3.3 that the differential gain should be observed to increase with increasing cavity length. This was based on the assumption that the modal threshold gain condition, Γg_{th}, representing the sum of the mirror losses, α_m, and the internal absorption, α_{int}, should be observed to decrease with increasing cavity length because of the expected decrease in the distributed mirror losses. However the differential gain was seen to decrease as shown in Fig 5.27.

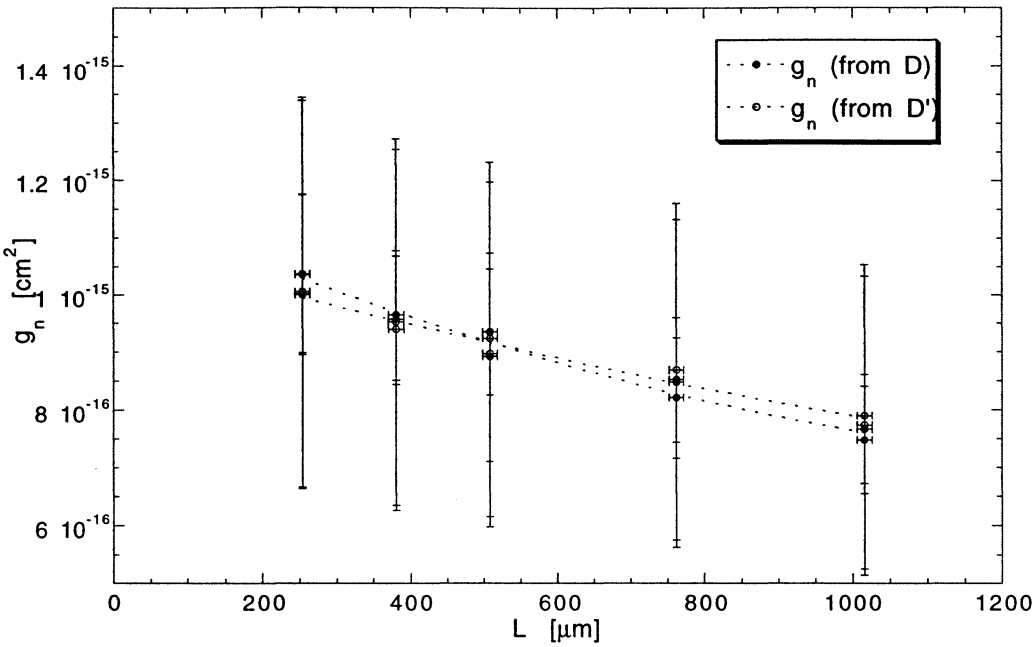

Fig. 5.27: Differential gain and modal threshold gain versus cavity length for structure S1-588, 1.10 Q barrier height, 10 quantum wells, at an operating temperature of 20 °C.

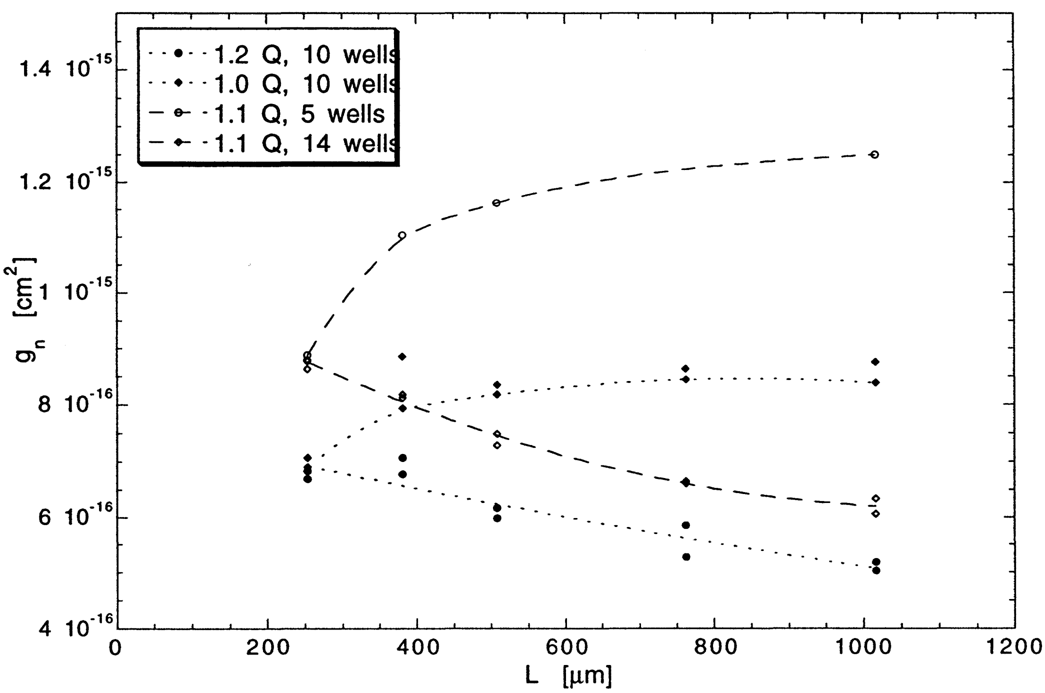

Fig. 5.28: Differential gain versus cavity length for structure S1-592 with 1.2 Q barriers and 10 quantum wells, S1-591 with 1.0 Q barriers and 10 quantum wells, S1-349 with 1.1 Q barriers and 5 quantum wells, and S1-422 with 1.1 Q barriers and 14 quantum wells, at an operating temperature of 20 °C.

This trend in the differential gain which contradicts theoretical predictions was not observed for all of the structures studied. In Fig 5.28 structure S1-591 with 1.0 Q barriers and 10 quantum wells follows the trend predicted by theory. As well structure S1-349 with 1.1 Q barriers and 7 quantum wells follows the trend predicted by theory. However structures S1-592 with 1.2 Q barriers and 10 quantum wells, and S1-422 with 1.1 Q barriers and 14 quantum wells show the same trend as each other contradicting theoretical predictions as with S1-588 in Fig 5.27.

The contradiction between this differential gain data and that which would be expected theoretically raises some concern about the validity of the data. The modal threshold gain as a function of cavity length was plotted in Fig 5.29 to check if any other gain parameters were in similar contradiction. As expected according to theory the modal threshold gain decreased with increasing cavity length in all cases. This result helps to restore some confidence in the data until suitable explainations for these observed contradictions can be found.

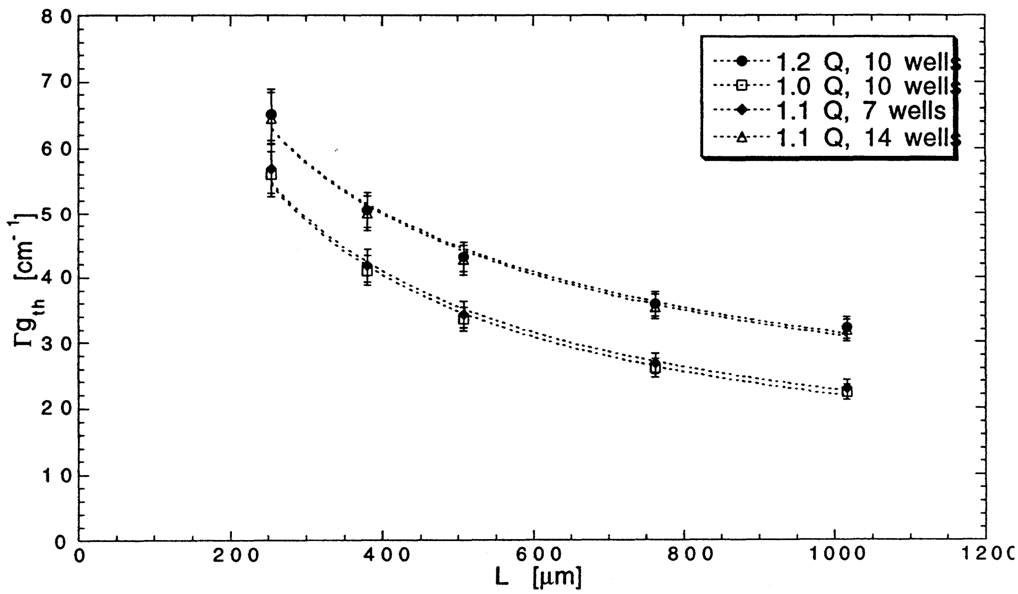

Fig. 5.29: Modal threshold gain condition versus cavity length for structure S1-592, S1-591, S1-341, and S1-422, at an operating temperature of 20 °C.

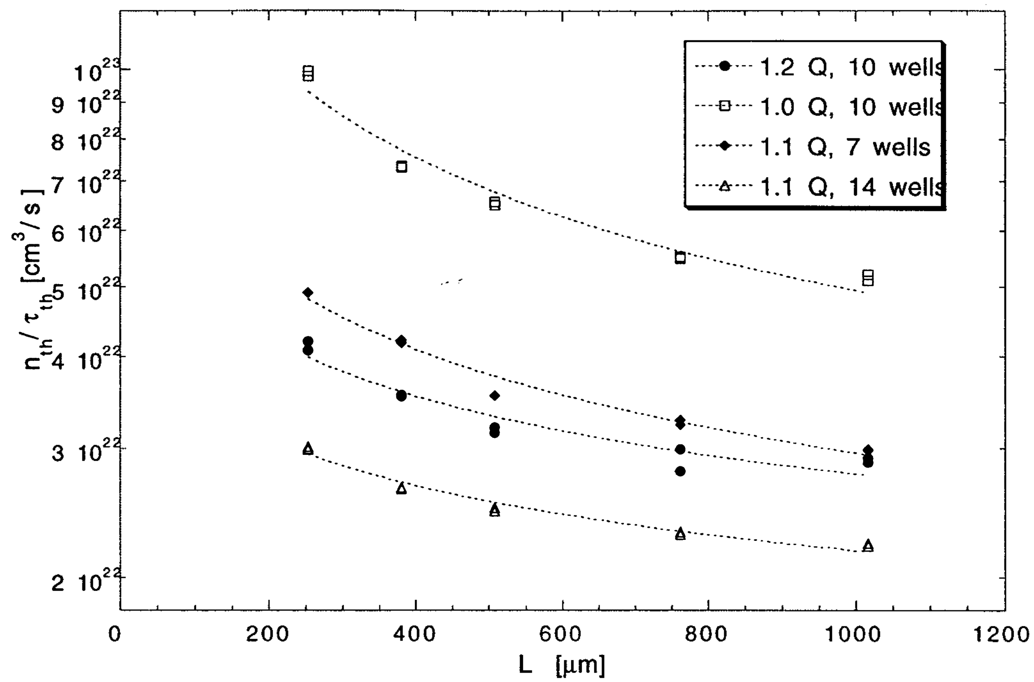

Fig. 5.30: Threshold carrier concentration divided by carrier lifetime versus cavity length for structure S1-592 with 1.2 Q barriers and 10 quantum wells, S1-591 with 1.0 Q barriers and 10 quantum wells, S1-341 with 1.1 Q barriers and 7 quantum wells, and S1-422 with 1.1 Q barriers and 14 quantum wells, at an operating temperature of 20 °C.

As a check of the validity of the results presented so far the threshold carrier concentration divided by the carrier lifetime was plotted versus cavity length in Fig 5.30. As expected it was found to decrease with increasing cavity length.

5.8 NONLINEAR GAIN COEFFICIENT CHARACTERIZATION

The characterization of the nonlinear gain coefficient, ε, using equation (2.3.10) relies on the accuracy of four previously determined parameters. As was explained in §5.7, the characterization of the differential gain relied on parameters which have large degrees of uncertainty associated with them. These uncertainties were a result of assumptions which had to be made as to the physical meaning of the parameter values. For this vary reason the main contribution of error to the nonlinear gain was from the differential gain with a total relative error of 33-34% as described above.

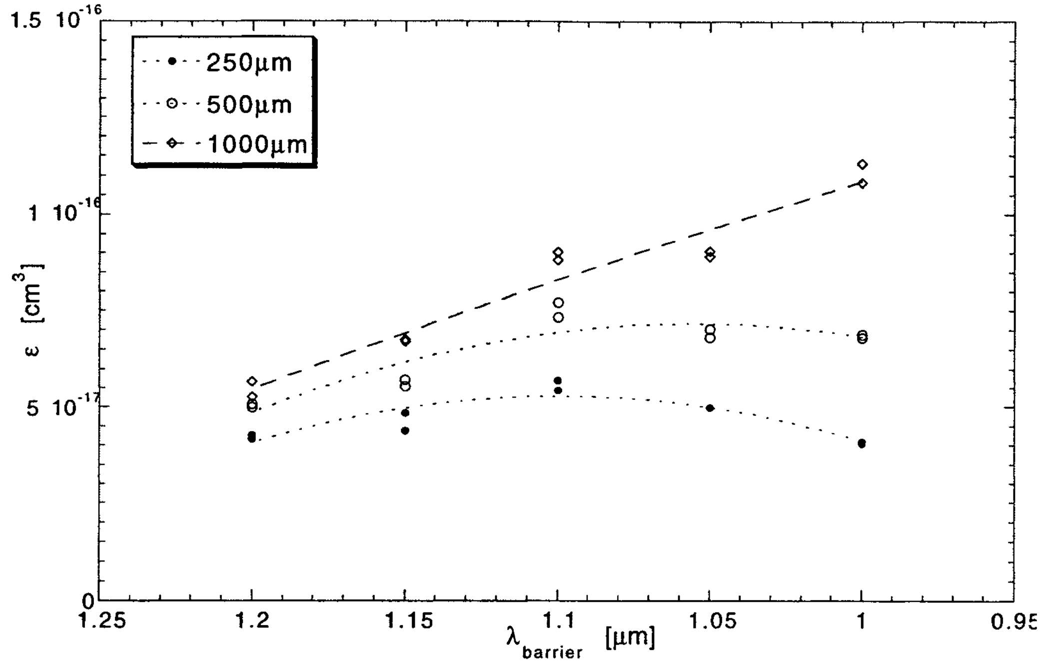

Fig. 5.31: Non-linear gain coefficient versus quantum well barrier height for 10 quantum well design, with 10 mil (254 μm) cavity length, 20 mil (508 μm) cavity length, and 40 mil (1016 μm) cavity length, at an operating temperature of 20 °C.

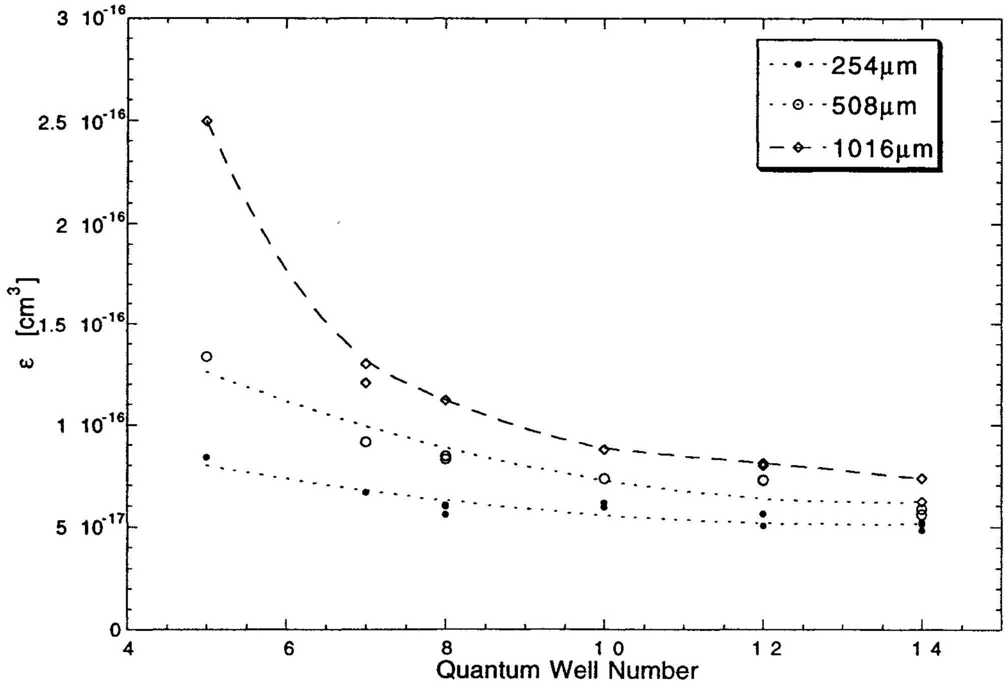

Fig. 5.32: Non-linear gain coefficient versus quantum well number for 1.1 Q quantum well barrier design, with 10 mil (254 μm) cavity length, 20 mil (508 μm) cavity length, and 40 mil (1016 μm) cavity length, at an operating temperature of 20 °C.

Further contributions to the error came from the value K with a relative error of 2-4%, the photon lifetime with a relative error of 5-9%, and the group velocity with a relative error of 3-7%. All of these errors combined to give a resulting total relative error of 34-37% in the non-linear gain coefficient values. Despite these large errors the results obtained still convey comprehensible parametric trends. This is because the largest of these error contributions were most likely systematic across all of the lasers examined as with the differential gain.

Once all of the parameters appearing in equation (2.3.10) had been characterized the non-linear gain coefficient was then isolated. The resulting trend seen in the non-linear gain coefficient versus quantum well barrier height is shown in Fig 5.31. It was mentioned in §3.2.1 that the non-linear gain coefficient has been seen to vary with the differential gain in other studies suggesting that similar mechanisms may be involved with both physical parameters. Comparing the trends observed in Fig 5.24 and 5.31 ε is observed to follow a similar trend to g_n for all of the cavity lengths shown. The resulting change in non-linear gain coefficient values with quantum well number is shown in Fig 5.32.

As was mentioned earlier, the non-linear gain coefficient is often seen to vary with the differential gain suggesting that similar mechanisms may be involved with both physical parameters. Comparing the trends observed in Fig 5.26 and 5.32 the non-linear gain coefficient is observed to follow a similar trend to the differential gain by decreasing with increasing quantum well number with a similar change in slope with each cavity length shown.

There have been no reports in the literature indicating how the non-linear gain coefficient is expected to change with increasing cavity length. The non-linear gain coefficient calculated in this study for four laser structures as a function of increasing cavity length is shown in Fig 5.33.

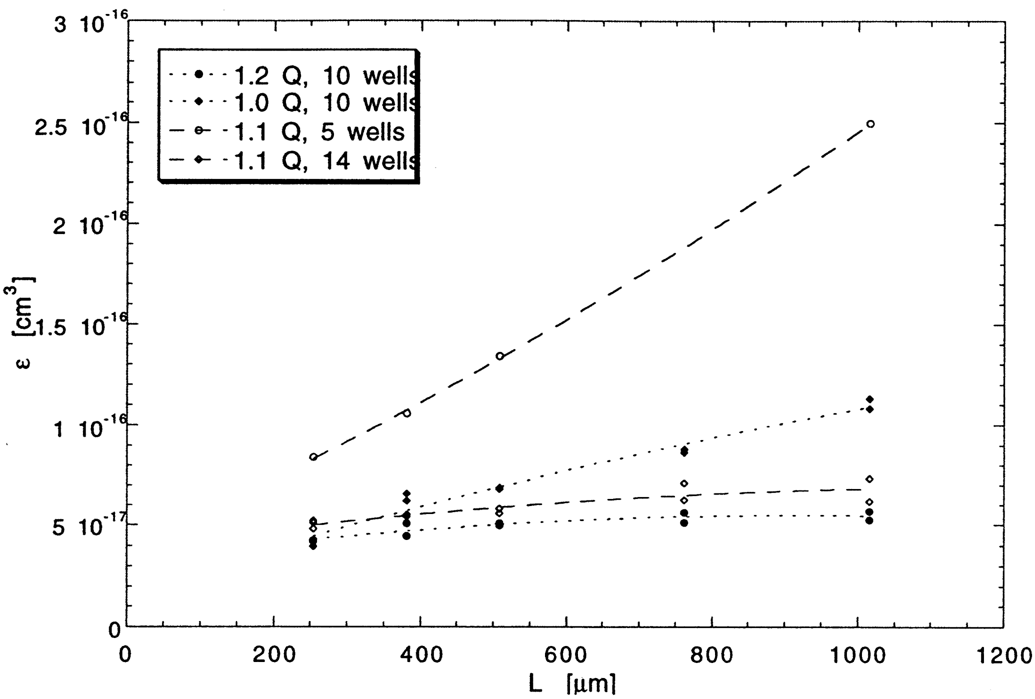

Fig. 5.33: Non-linear gain coefficient versus cavity length for structure S1-592 with 1.2 Q barriers and 10 quantum wells, S1-591 with 1.0 Q barriers and 10 quantum wells, S1-349 with 1.1 Q barriers and 5 quantum wells, and S1-422 with 1.1 Q barriers and 14 quantum wells, at an operating temperature of 20 °C.

In all cases the non-linear gain coefficient is shown to increase with increasing cavity length. However the rate of increase appears to be very structure dependent. Structure S1-592 with 1.2 Q barriers and 10 quantum wells, and S1-422 with 1.1 Q barriers and 14 quantum wells, which had differential gain values decreasing with increasing cavity length running counter to that expected by theory, showed a gradual increase in the non-linear gain coefficient values with increasing cavity length. Structure S1-349 with 1.1 Q barriers and 5 quantum wells, which showed differential gain values strongly increasing with increasing cavity length in agreement with that expected by theory, showed a rapid increase in non-linear gain coefficient values with increasing cavity length. Finally structure S1-591 with 1.0 Q barriers and 10 quantum wells showed a moderate increase in non-linear gain coefficient with increasing cavity length in comparison to a moderate increase in differential gain values with increasing cavity length in full agreement with that expect by theory.

5.9 MAXIMUM INTRINSIC BANDWIDTH CHARACTERIZATION

The K values characterized in §5.3 can be expressed as the maximum intrinsic bandwidth, f_{max}, using equation (2.4.3). As described in §2.4 the maximum intrinsic bandwidth is the damping limited modulation rate theoretically achievable ignoring RC parasitics, device heating, and maximum power of laser. It is also mentioned that the potential effects of carrier transport are not reflected in the intrinsic bandwidth as it is determined under dc conditions. The maximum intrinsic bandwidth demonstrates how changes in the differential gain, non-linear gain, and photon lifetimes resulting from variations in the design parameters of the semiconductor laser structures all combine together to give a resulting intrinsic bandwidth potential.

The resulting maximum intrinsic bandwidth versus quantum well barrier height is shown in Fig 5.34. In §3.2.1 it was suggested that with the expected increase in differential gain with barrier height, the maximum intrinsic bandwidth (f_{max}) should also increase. For the 254 μm cavity length lasers an increase in f_{max} with increasing barrier height is seen up to 1.05 Q which loosely follows the trend in differential gain for the same cavity length. The 508 μm cavity length lasers show the same trend as the 254 μm cavity length lasers, but there is a much closer correlation with the 508 μm cavity length differential gain trend. The most interesting result is with the 1016 μm cavity length results which show an almost constant trend in f_{max} with increasing barrier height. This was the only laser structure which had differential gain values exhibiting a clear increase with increasing barrier height.

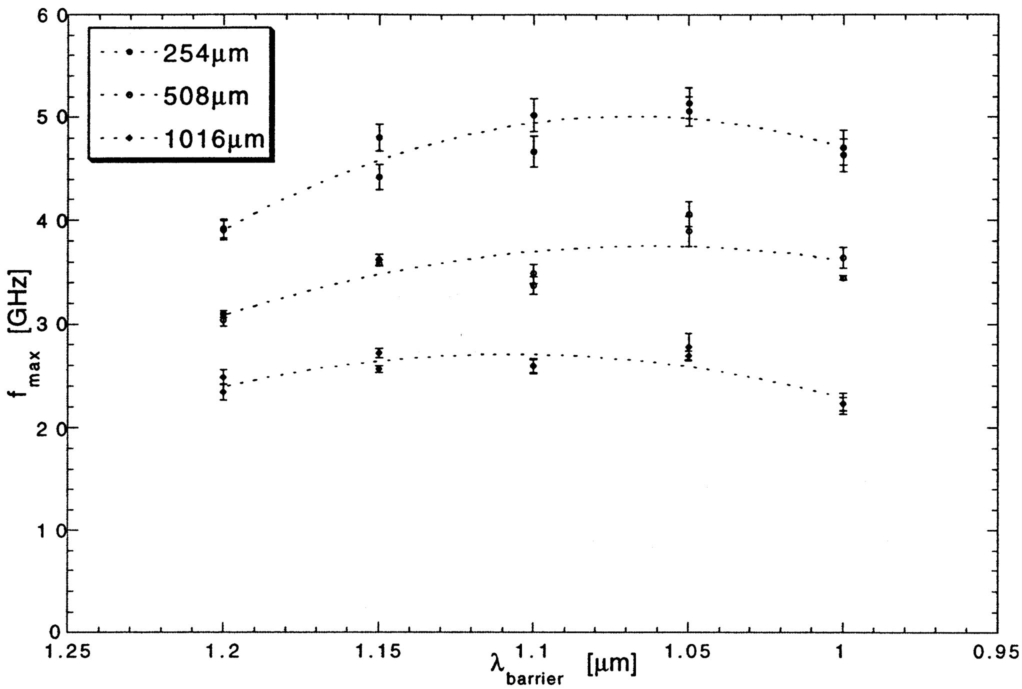

Fig. 5.34: Maximum intrinsic bandwidth versus quantum well barrier height for 10 quantum well design, with 10 mil (254 µm) cavity length, 20 mil (508 µm) cavity length, and 40 mil (1016 µm) cavity length, at an operating temperature of 20 °C.

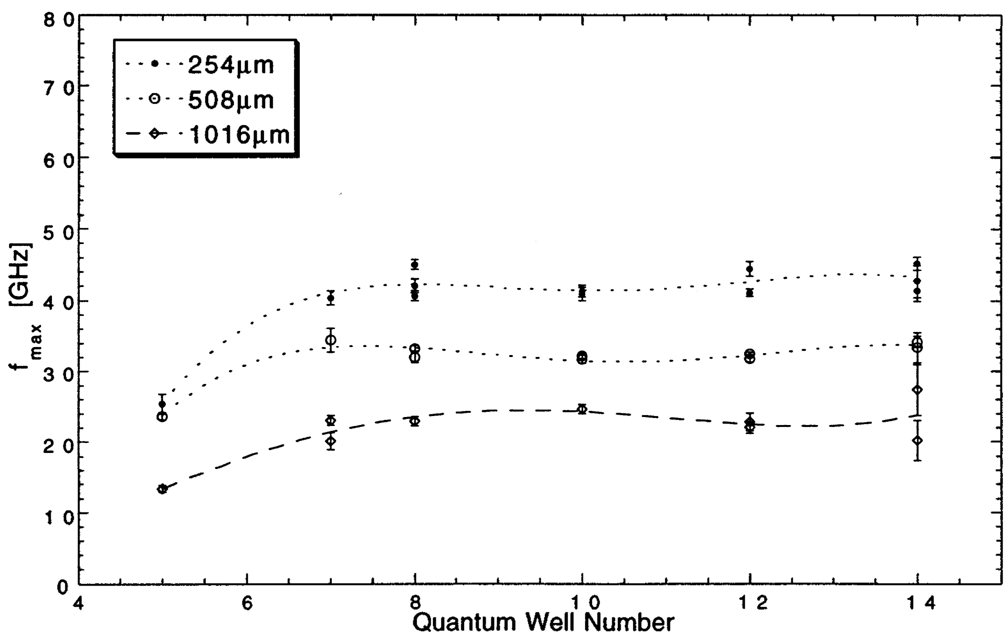

Fig. 5.35: Maximum intrinsic bandwidth versus quantum well number for 1.1 Q quantum well barrier design, with 10 mil (254 µm) cavity length, 20 mil (508 µm) cavity length, and 40 mil (1016 µm) cavity length, at an operating temperature of 20 °C.

The resulting f_{max} versus quantum well number is shown in Fig 5.35. In §3.2.2 an expected increase in the differential gain and decrease in the photon lifetime with quantum well number was predicted to result in an increase in the maximum intrinsic bandwidth. As well a further augmentation of the maximum intrinsic bandwidth was to result from a potential decrease in the non-linear gain coefficient with quantum well number. In fact, f_{max} is shown in Fig 5.35 to be fairly constant with increasing quantum well number for all cavity lengths, not including the results for the 5 quantum well structure S1-349. The trend of decreasing differential gain with increasing quantum well number observed in Fig 5.26, along with the trend towards an increase in the rate of this decrease with increasing cavity length, does not appear to be at all reflected in these maximum intrinsic bandwidth results.

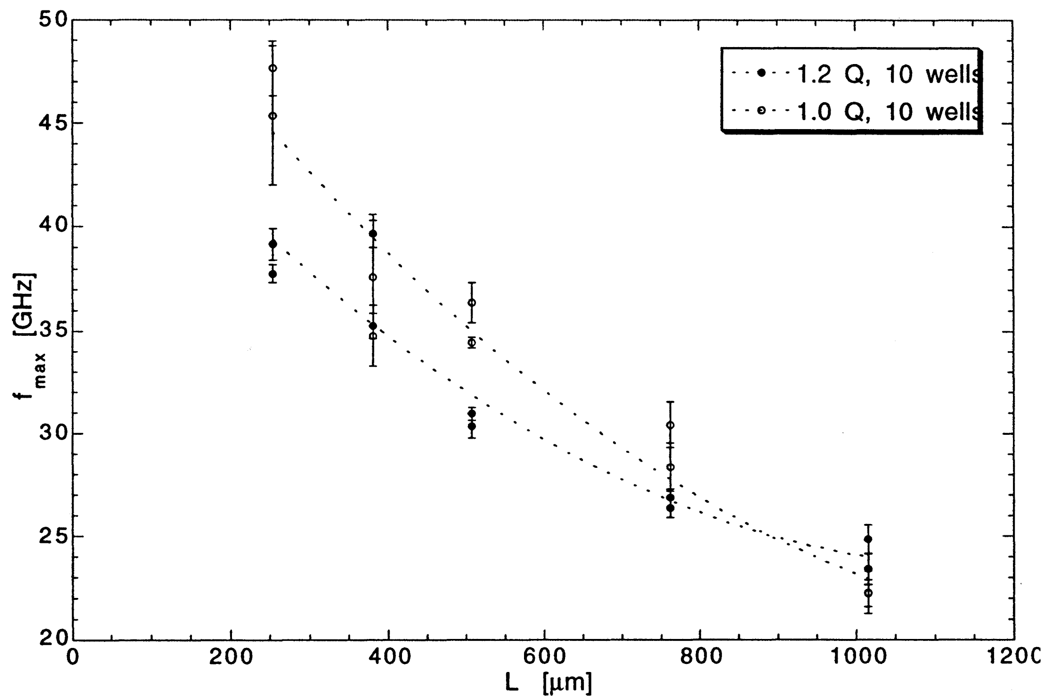

Fig. 5.36: Maximum intrinsic bandwidth versus cavity length for structure S1-592 with 1.2 Q barriers and 10 quantum wells, and S1-591 with 1.0 Q barriers and 10 quantum wells, at an operating temperature of 20 °C.

The resulting f_{max} versus semiconductor diode cavity length is shown in Fig 5.36. In §3.3 an expected increase in the differential gain and increase in the photon lifetime with laser cavity length were expected to have a competing influence on the maximum intrinsic bandwidth resulting in a potential optimum cavity length. However with an unexpected decrease in the differential gain and an increase in the photon lifetime with laser cavity length f_{max} was found to decrease rapidly over the range of cavity lengths studied for all of the structures. The rate of decrease changed from structure to structure as can be seen in Fig 5.36.

5.10 SUMMARY

In summary, resonance frequency and damping factor values were extracted from the RIN spectrum taken as a function of injected current for the structures studied. The resonance frequency and damping factor values extracted were compared to results obtained from identical device using small-signal analysis and found to be in good agreement to within experimental error.

The results of RIN and L-I characterizations were combined to allow for the examination of resonance frequency behavior as a function of injected current above threshold as well as versus optical power. From this data D' and D coefficient values were characterized. The problems encountered performing this analysis for data collected above room temperature were presented. Finally, results on how D' and D were found to change as a function of device structure and device length were presented.

The characterization of the K factor from damping factor versus square of the resonance frequency were presented with some discussion of the observation of non linearity in the damping factor-resonance frequency behavior. As well, the characterization of the group velocity, v_g, average photon energy, $h\nu$, internal quantum efficiency, η_{int}, and the internal loss, α_{int}, was presented.

Finally based on the resulting calculations, the trends observed in g_n and ε as a function of barrier height, QW number, and cavity length were presented.

CHAPTER 6: DISCUSSION

6.0 INTRODUCTION

It was found in §5.2.2 that for operating temperatures greater than 20 °C a deviation in the resonance frequency values measured near threshold from those expected by theory was observed. It was suggested that this may be an artifact of spontaneous emission above threshold resulting in a prolonged competition between lasing modes for gain in the laser cavity. Presented are values for the spontaneous emission rate, R_{sp}, showing that the amount of spontaneous emission occuring in the laser is likely to be increasing with temperature.

The characterized values for D represent the change in bandwidth with optical power, where as f_{max} represents the theoretical maximum intrinsic frequency response. Discussed is which parameter would be of more interest to a designer based on its physical relevance to the actual bandwidth performance expected from a laser.

Discussion of the differential gain values obtained for the structures studied in this thesis posed an interesting challenge. Not all of the differential gain results for the structures involving the variation of barrier height were found to agree with that expected by theory as discussed in §3.1.2. As well, the structures involving the variation of the number of quantum wells yielded differential gain values which contradicted that which was expected theoretically as discussed in §3.1.3. Some light is shed on these results when the dependence of the differential gain on threshold carrier concentration divided by the carrier lifetime is explored.

The wide range of differences between published values of ε for QW and bulk lasers suggests that ε has a dependence on QW design that is not well understood. Some studies suggest that similar mechanisms may be involved with both the differential gain and nonlinear gain. Initially this is shown to not be the case, but further exploration of the dependence of ε goes on to suggests that this linear approximation of the nonlinear gain with respect to photon density may not be well founded.

It is the maximum intrinsic bandwidth that ultimately demonstrates how the contributions from differential gain, nonlinear gain, and photon lifetime balance with each other. The influence of the photon lifetime on f_{max} is revisted followed by an investigation into the role that differential gain, g_n, and nonlinear gain, g_s, play in f_{max}.

Finally, now that some understanding of how the relative contributions of each parameter influence bandwidth performance has been developed, an investigation into how changing key design parameters can be used to improve on the overall design of the laser is presented.

6.1 LOWER THAN EXPECTED RESONANCE FREQUENCY VALUES NEAR THRESHOLD

It was demonstrated in Fig 5.6 that for operating temperatures greater than 20 °C a deviation in the resonance frequency values measured near threshold from those expected by theory with equations (2.3.13) and (2.3.16) was observed. This observed deviation actually applies to all of the measured resonance frequency values as a function of current injected above threshold, or optical output power. In §5.2.2 it was mentioned that this may be an artifact of spontaneous emission above threshold allowing for a prolonged competition between lasing modes for gain in the laser cavity. This effect has never been documented as a function of temperature but it has been correlated with FWHM spectral linewidth.[50] When this offset in the resonance frequency values is observed it is simply reflecting the fact that the optical output power just above threshold is resulting from multiple modes, each of which have a resonance frequency corresponding to the optical power in that mode. When one mode begins to dominate enough optical power is associated with that mode for the resonance frequency for that mode to begin to appreciably increase. This may not begin to occur until well above threshold depending on the spontaneous emission rate at threshold.

Using the third term of equation (2.3.6) it is possible to extract a value for the spontaneous emission rate, R_{sp}, by fitting to damping values plotted versus the square of the resonance frequency. Having fit a value for a coefficient to the $1/f_o^2$ factor in the third term of (2.3.6), R_{sp} can be calculated using already determined values of optical confinement factor, active area volume, group velocity, differential gain, and photon lifetime. The differential gain was calculated using D' values determined from a plot of resonance frequency versus root of current injected above threshold for operating temperatures of 20 °C, 50 °C, and 80 °C assuming a pseudo threshold current value associated with the x-axis intercept for each curve to take into account the resulting offset for the temperatures greater than 20 °C. This pseudo threshold current value could be thought of as the actual threshold current of the lasing mode which eventually dominates at higher current injection levels. Fits to equation (2.3.6) using the third term of the equation at 20 °C, 50 °C, and 80 °C operating temperatures for device #31 from structure S1-588 are shown in Fig 6.1. Included in the plots of Fig 6.1 are the values obtained for the m3 coefficient of the nonlinear term. Using these values the spontaneous emission rate was determined and plotted versus temperature as shown in Fig 6.2.

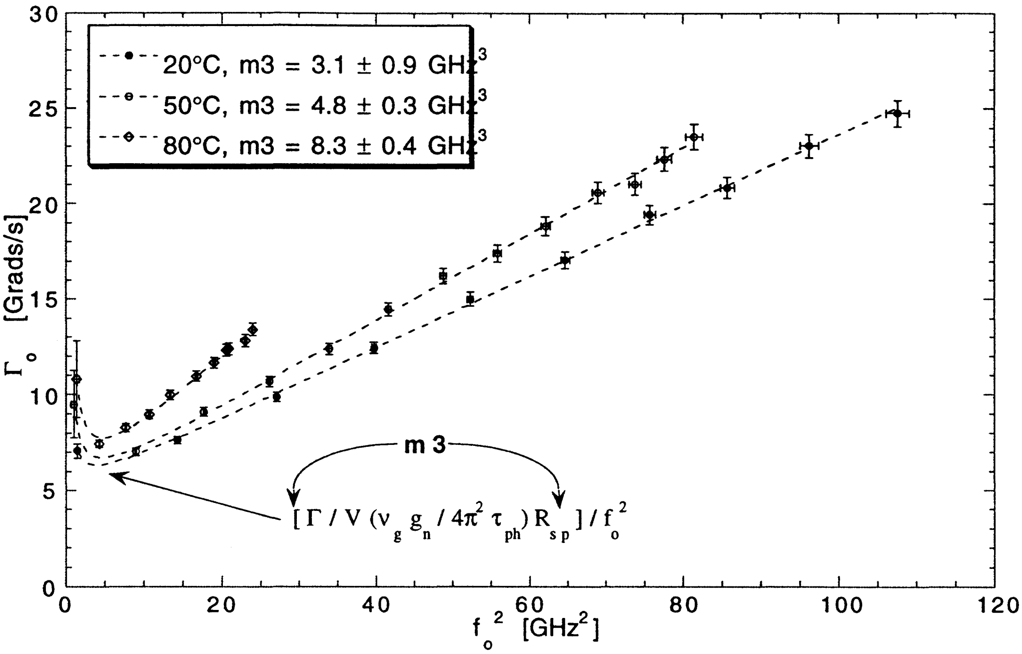

Fig. 6.1: Fit to equation (2.3.6) of damping versus resonance frequency squared for device #31, with 10 mil (254 μm) cavity length, from structure S1-588 at 20 °C, 50 °C, and 80 °C operating temperatures including a fit to the third term of (2.3.6) involving the spontaneous emission rate, R_{sp}.

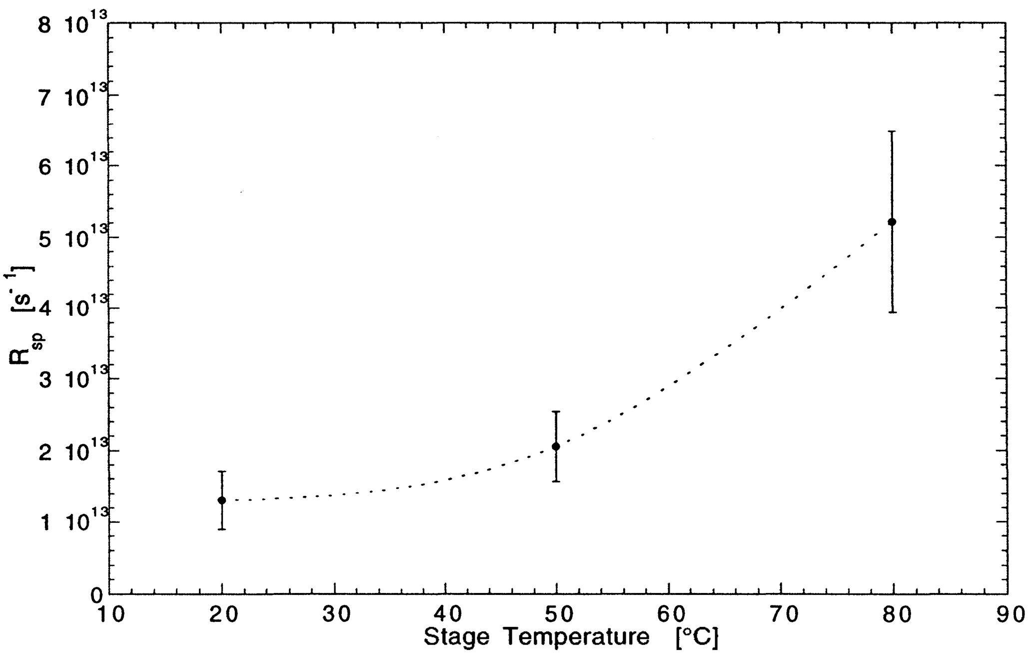

Fig. 6.2: Calculated spontaneous emission rate, R_{sp}, versus temperature for device #31, with 10 mil (254 μm) cavity length, from structure S1-588 at 20 °C, 50 °C, and 80 °C operating temperatures determined from the third term of equation (2.3.6).

The trend in the spontaneous emission rate, R_{sp}, plotted in Fig 6.2 would seem to correlate well with the observed increase in offset of resonance frequency values versus current injected above threshold, or optical output power, observed in Fig 5.6. The value R_{sp} appears to change very little up till around 40 °C and then begins to increase rapidly which correlates with the rate of increase in offset observed.

These results demonstrate a potential limitation with using the single mode rate equation model to analyze these results. While the room temperature results of resonance frequency versus the root of current injected above threshold, or optical power, demonstrate a zero crossing as predicted by theory, the results above room temperature do not. This could be due to the increase in spontaneous emission with temperature delaying the dominance of a single mode above threshold. This throws into question the assumed relationship between parameters like the internal quantum efficiency, internal absorption, and the correlation between the resonance frequency values and injected current for results above room temperature. Without confidence in these interrelationships the possible error in determined parameters such as differential gain, and the non-linear gain coefficient, become uncalculatable. Caution with respect to these potential inadequacies in the single mode rate equation model have been voiced in the past. [57]

6.2 D' AND D PARAMETER TRENDS VERSUS f_{max}

The characterized values for D' and D, based on equations (2.3.13) and (2.3.16), represent the most physically relevant parameters with respect to the intrinsic frequency response of the laser structures. Up to moderate optical output power levels the D' and D parameters describe the resonance frequency limited bandwidth of the lasers. In most applications these values would be of more interest to a designer than the values determined for the maximum intrinsic frequency response, f_{max}. In fact designers are sometimes not in agreement as to which structure will have the best modulation performance. For example the D' and D versus barrier height trends showed that the structures with 1.10 Q or 1.15 Q barrier heights should give the best frequency response out of all of the barrier height structures examined from Fig 5.7. However the f_{max} data shows that a higher barrier structure such as the 1.05 Q structure should achieve a higher maximum intrinsic modulation bandwidth for the 254 μm cavity lengths from Fig 5.34. As was mentioned in §2.4, the maximum intrinsic bandwidth does not take into account the device heating, and maximum achievable power of the laser. As a result the discrepancy between the highest performing structure according to D' and D versus f_{max} can be explained by the trend in the internal quantum efficiency for the different barrier height structures. According to the trend in Fig 5.16 the internal quantum efficiency drops dramatically for barrier heights greater than 1.15 Q.

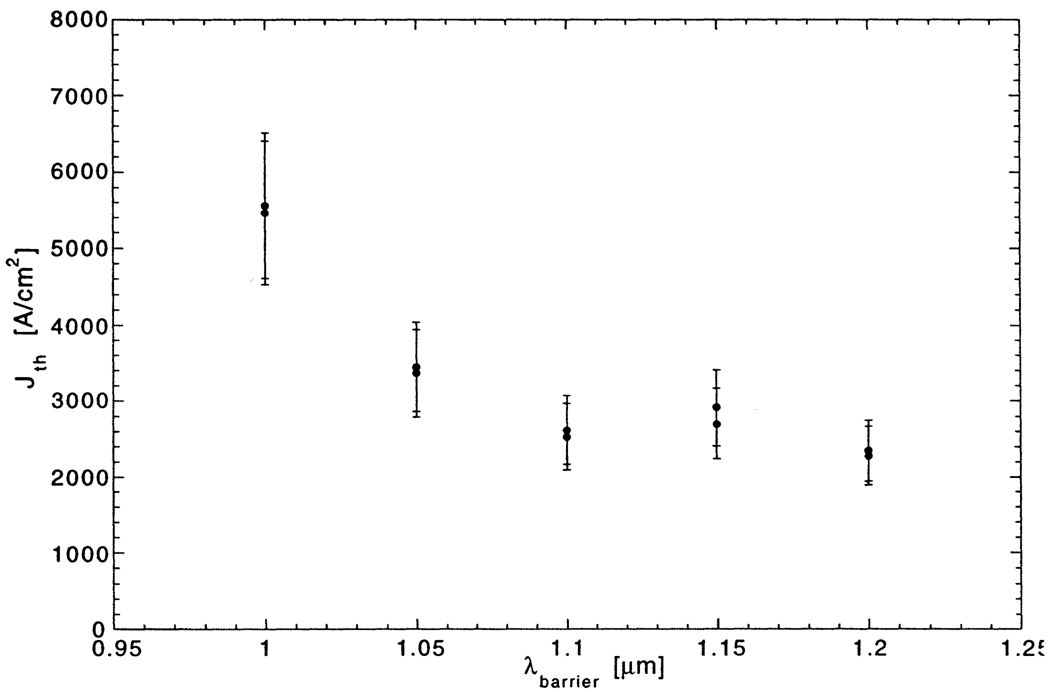

Fig. 6.3: Threshold carrier density versus barrier height with 10 quantum well structures, for 10 mil (254 μm) cavity lengths at a 20 °C operating temperature.

This would mean that the threshold carrier concentration will be much higher for the higher barrier structures which would cause them to be much more susceptible to internal heating and as a result have a lower maximum achievable optical power due to earlier onset of thermal runaway. This trend in the threshold carrier concentration is demonstrated in Fig 6.3 by plotting threshold carrier density versus barrier height. This is reflected in the D' and D values but not in the f_{max} values. For the structures where the number of quantum wells was varied from 5 wells to 14 wells there was no real change in D', D, or f_{max} values, excluding results for the 5 quantum well structure which were poorer than the others. When considering the results for the various cavity lengths the shortest cavity length, 254 μm, comes out the clear winner. In this case the decrease in the photon lifetime with decreasing cavity length due to the resulting increase in the distributed mirror losses dominates any other structural influence on the intrinsic frequency response of the lasers.

6.3 DIFFERENTIAL GAIN AND CARRIER TRANSPORT EFFECTS

Initially the discussion of the differential gain values obtained for the structures studied in this thesis posed an interesting challenge. When examining the differential gain results for the structures involving the variation of barrier height it was found that only the longer cavity length device results agreed with what was predicted by theory as discussed in §3.1.2. The structures involving the variation of the number of quantum wells yielded differential gain values which contradicted that which is expected theoretically as discussed in §3.1.3 despite the fact that the threshold carrier concentration was shown to clearly decrease with increasing quantum well number. As well this contradiction worsened as the cavity lengths of the structures were increased. But by far the most difficult results to understand were those of the differential gain resulting from the variation of cavity length. Out of the eleven structures studied only two of the structures yielded results where the differential gain increased with increasing cavity length in agreement with the theory in

§3.3 despite the fact that for all of the structures the modal threshold gain, and the threshold carrier density, decreased with increasing cavity length.

However some light is shed on these results when the differential gain is plotted versus the threshold carrier concentration divided by the carrier lifetime. The threshold carrier concentration divided by the carrier lifetime is simply the threshold current of the laser divided by the active area volume.

6.3.1 Differential gain versus cavity length

The results from Fig 5.28 are plotted versus threshold carrier concentration divided by the carrier lifetime, n_{th}/τ_{th}, in Fig 6.4. Given that it was confirmed with Fig 5.30 that the threshold carrier concentration decreases with increasing cavity length, the trends shown in Fig 6.4 correspond with increasing cavity length to the left.

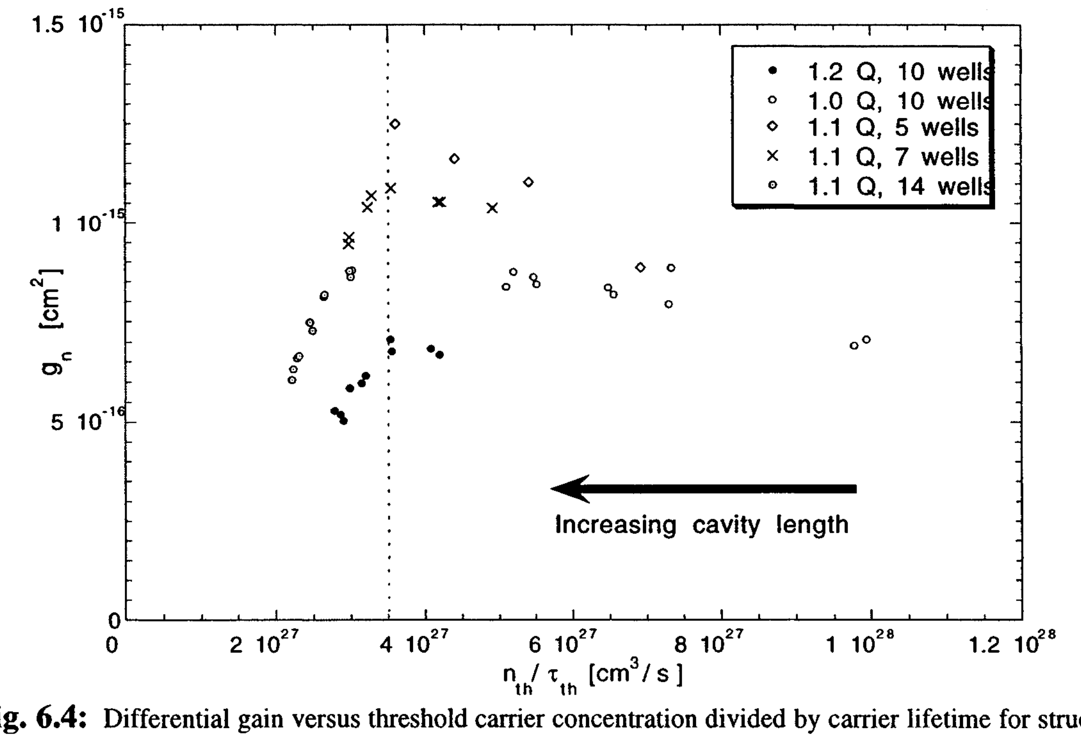

Fig. 6.4: Differential gain versus threshold carrier concentration divided by carrier lifetime for structure S1-592 with 1.2 Q barriers and 10 quantum wells, S1-591 with 1.0 Q barriers and 10 quantum wells, S1-349 with 1.1 Q barriers and 5 quantum wells, S1-341 with 1.1 Q barriers and 7 quantum wells, and S1-422 with 1.1 Q barriers and 14 quantum wells, at an operating temperature of 20 °C.

In Fig 6.4 it can be seen that the differential gain values plotted for the five structures shown follow a trend of increasing differential gain with decreasing carrier concentration up to a value of n_{th}/τ_{th} of 3.5 x 10^{27} cm^3/s. It is possible that these results suggest a certain carrier concentration threshold where the behavior of these laser structures no longer follows the single rate equation model. One possibility is that the electron and hole concentrations are not uniformly distributed in the active region of these laser structures and that this effect becomes more apparent as the carrier concentrations required to satisfy the conditions for lasing get smaller.

It has been theoretically demonstrated that the transport time of carriers across the separate confinement heterostructure region and the barriers in a semiconductor laser can have a significant impact on the modulation response of the laser.[51] [52] The limiting factor is the transport of holes which have an order of magnitude lower mobility than that of electrons. It has also been demonstrated theoretically that a nonuniform distribution of electrons and holes in the wells of an InGaAsP multiple quantum well structure are likely under certain structural conditions.[52]-[54] In the InGaAsP on InP system, the discontinuity of the valence band is much larger than that of the conduction band. This larger valence band discontinuity along with the lower mobility of holes can result in significantly slower transport of holes across the barrier layers in the multiple quantum well structure.

With the lower mobility of holes the wells in a multiple quantum well structure far away from the p-contact can receive less holes and therefore have smaller gain. Conversely the wells close to the p-contact can receiver more holes and therefore have larger gain. However, given that the differential gain increases with decreasing carrier concentration, the wells closer to the p-contact supplying most of the gain to satisfy the lasing condition of the cavity tend to reduce the differential gain from the value it would have if the carrier were distributed evenly throughout the wells.[52] [53] If the nonuniform distribution of carriers in the wells of the structures examined in this study is having an impact on the applicability of the single mode rate equation model to the analysis of this data then this should be even more apparent with the results involving the variation of quantum well number.

6.3.2 Differential gain versus quantum well number

For the structures involved with the variation of quantum well number, in all but two of the structures this was the only structural parameter changed. The five and seven well structure had 400 Å and 300 Å thick GRINCH regions respectively where as the remaining structures had 200 Å thick GRINCH regions. Varying only the quantum well number should not have any impact on gain performance characteristics of the material aside from any unforeseen variations in the processing of the material from wafer to wafer. Since the dimensions and composition of the quantum wells and barriers remain unchanged the band structure for the well region, and therefore its gain performance as a function of carrier concentration, should also behave similarly.

In Fig 6.5 all of the differential gain results for the structures where the quantum well number is varied are plotted versus threshold carrier concentration divided by the carrier lifetime, n_{th}/τ_{th}. Here we see that the carrier concentration at threshold barrier beyond which the data does not represent that behavior which would be expected by theory observed in Fig 6.5 appears to apply to all but one of the structures, that being the one with 12 wells. In the 12 well structure the same trend is observed, however the point at which the data no longer represents theoretical prediction possibly occurs at a lower concentration. Unfortunately the differential gain results for almost all of the structures correspond to a carrier concentration in the region where the assumptions of the model used in the analysis of these results breaks down.

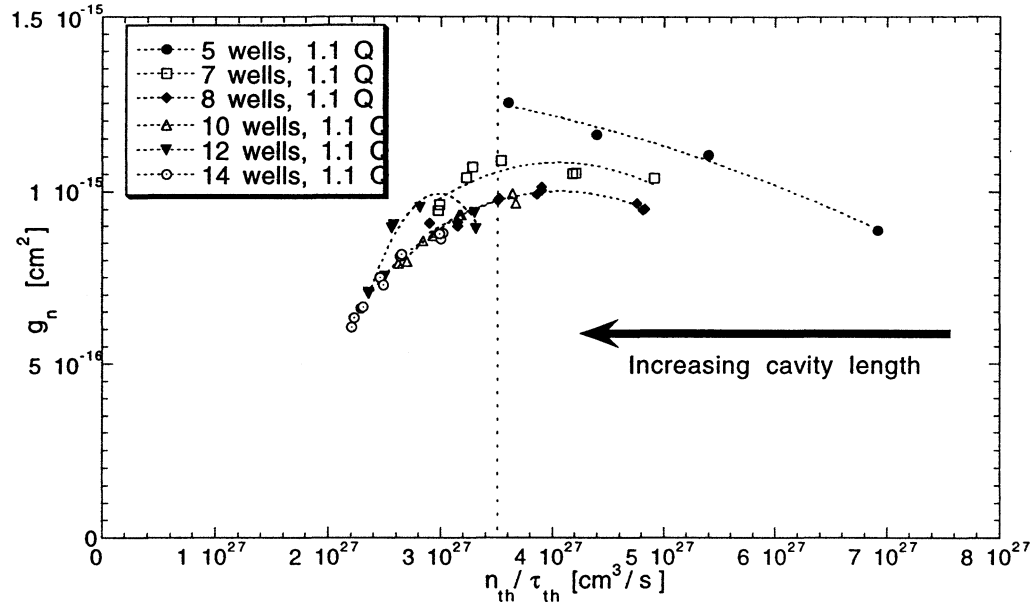

Fig. 6.5: Differential gain versus threshold carrier concentration divided by carrier lifetime for structures S1-349, S1-341, S1-340, S1-429, S1-418, and S1-422 with 1.1 Q barriers and 5, 7, 8, 10, 12, 14 quantum wells respectively, at an operating temperature of 20 °C.

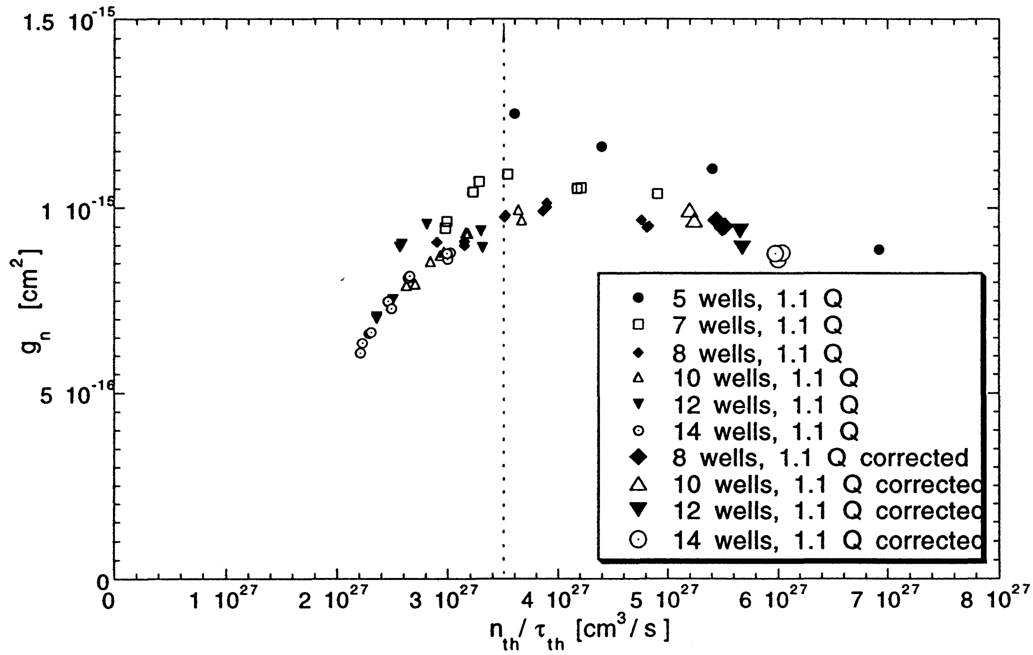

Fig. 6.6: Differential gain versus threshold carrier concentration divided by carrier lifetime for structures S1-349, S1-341, S1-340, S1-429, S1-418, and S1-422 with 1.1 Q barriers and 5-14 quantum wells respectively, at an operating temperature of 20 °C. Also included is the differential gain values for 254 μm cavity lengths for the 8, 10, 12, and 14 quantum well structures with threshold carrier concentrations corrected assuming only the first 7 wells are effectively being used.

However, the fact that the trends in the differential gain values for each structure represented here closely follow each other with carrier concentration would appear to support the statement made earlier suggesting that the gain performance of all the structures should follow a similar dependence with carrier concentration. This tight grouping of trends also supports the validity of the results in that there also appears to be a trend with respect to the number of quantum wells in the structure.

It is observed in the general trend shown in Fig 6.5 that the deviation in the trend of differential gain values from that which is expected by theory became worse with increasing number. This would seem to strongly support the postulation made earlier that there is a nonuniform distribution of carriers in the active region of these lasers at threshold. This results also seem to support that as a result of the nonuniform distribution of carriers in the active region, beyond a certain number of wells, additional wells are no longer significantly contributing to the lasing process. Plotted in Fig 6.6 are additional points representing the differential gain values for 254 μm cavity length lasers for the structures involving the variation of quantum well number shown in Fig 6.5. The threshold carrier concentrations corresponding to these values have been corrected assuming only the first seven wells are contributing gain to the lasing process. This simple demonstration of the potential impact of nonuniform carrier distribution in the active area of multiple quantum well structures shows that it is possible for the differential gain values found to be decreasing with increasing quantum well number as a result of higher concentrations of holes in the wells closer to the p-contact.

6.3.3 Differential gain versus quantum well barrier height

For the structures involved with the variation of quantum well barrier height this was the only structural parameter changed. Increasing the quantum well barrier height was expected to impact the gain performance characteristics of the material as a result of the increased parabolicity of the hh band caused by the increased heavy hole - light hole energy level separation experienced with the increased quantum confinement. With the increase in parabolicity, an increased change in gain with increasing carrier concentration should be observed, as explained in §3.2.1.

In Fig 6.7 all of the differential gain results for the structures where the quantum well barrier height is varied are plotted versus threshold carrier concentration divided by the carrier lifetime, n_{th}/τ_{th}. It was observed in Fig 5.24 of §5.7 that the differential gain was found to increase with increasing barrier height as predicted by theory in §3.2.1. Here in Fig 6.7 it can be seen that the grouping of results for all cavity lengths from each structure follow the same trend in general except for the devices from the 1.00 Q barrier height structure.

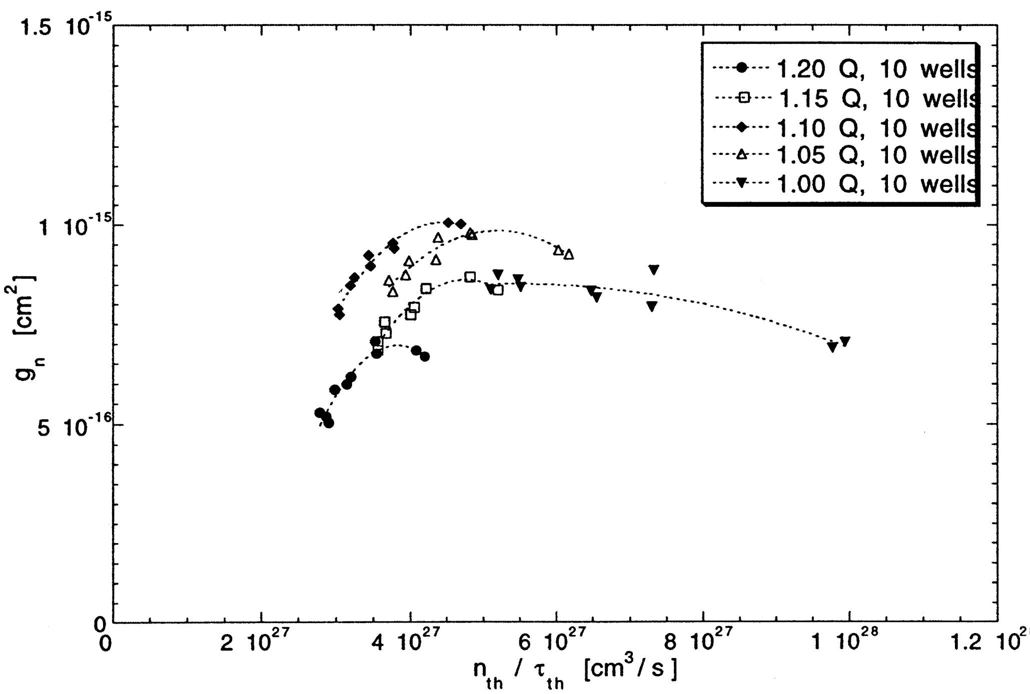

Fig. 6.7: Differential gain versus threshold carrier concentration divided by carrier lifetime for structures S1-591, S1-593, S1-588, S1-590, and S1-592 with 1.00, 1.05, 1.10, 1.15, and 1.20 Q barriers respectively and 10 quantum wells, at an operating temperature of 20 °C.

It is interesting to note at this point that the devices from the 1.00 Q barrier height structure had a substantially lower internal quantum efficiency as observed in Fig 5.16. A lower quantum efficiency may be symptomatic of a lower carrier capture rate thus resulting in a more even distribution of carriers throughout the ten wells of the active area. This would also explain why the results from the 1.00 Q barrier show a trend which rolls over more slowly near the carrier concentration at which the wells may not be optimally filled. With the other structures where barrier height is varied the differential gain rolls over at the carrier concentration where the wells may not be optimally filled more rapidly.

6.4 NONLINEAR GAIN COEFFICIENT, ε

As was mentioned in §3.2.1, the wide range of differences between published values of ε for QW and bulk lasers suggests that ε has a dependence on QW design that is not well understood. Theories have been put forward that suggest that nonlinear gain may depend strongly on QW structure parameters such as barrier height, well width, and well number [17]. The nonlinear gain coefficient was found to increase with increasing barrier height for 1016 μm cavity lengths in Fig 5.31, however this broke down with decreasing L in much the same way as the trend of increasing differential gain with increasing barrier height in Fig 5.24. This observation gave weight to some studies which suggested that similar mechanisms may be involved with both the differential gain and nonlinear gain [13] [15] [17] [18]. To test this potential interdependence the nonlinear gain coefficient was plotted versus the differential gain for the results obtained from structures where the barrier height is only changed, shown here in Fig 6.8.

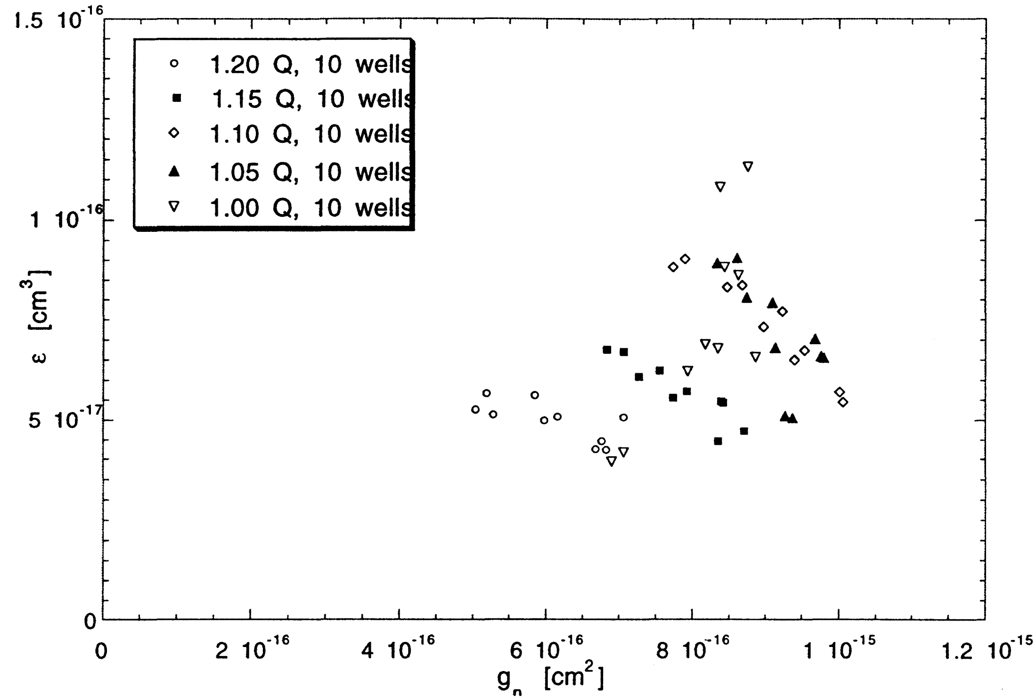

Fig. 6.8: Nonlinear gain coefficient versus differential gain for structures S1-591, S1-593, S1-588, S1-590, and S1-592 with 1.00, 1.05, 1.10, 1.15, and 1.20 Q barriers respectively and 10 quantum wells, at an operating temperature of 20 °C.

As can be seen in Fig 6.8 there does not appear to be any strong correlation between the changes in nonlinear gain coefficient and differential gain with changing barrier height indicating that very different mechanisms are probably influencing their values.

With quantum well number the nonlinear gain coefficient was found to consistently decrease with increasing well number in Fig 5.32, much different from the variability observed with differential gain as a function of well number in Fig 5.26. This supports the finding of an investigation reporting a regular decrease of ε as the number of wells is increased in InGaAs/InGaAsP MQW lasers [44]. It was concluded that this pointed towards a dependence of ε on carrier density since a lower carrier density is required to reach threshold as the number of QW's is increased. However the dependence of nonlinear gain on carrier density must be of a very different nature than that of differential gain based on the observations made from Fig 6.8 possibly supporting that very different mechanisms are probably influencing the values of the two parameters.

Some studies have assumed that ε remains constant with cavity length [15] [26] [41]. However nonlinear gain was observed to always be decreasing with increasing cavity length as shown previously by Fig 5.33. This could also be pointing towards nonlinear gain being dependent on carrier density since the carrier density at threshold decreases with increasing cavity length. Some light is shed on these results when the dependence of nonlinear gain on the threshold carrier concentration divided by the carrier lifetime is explored.

6.4.1 Nonlinear gain coefficient versus quantum well number

The nonlinear gain coefficient was first plotted versus the threshold carrier concentration divided by the carrier lifetime for the structures involving only the variation of quantum well number, as shown in Fig 6.9. As suggested before, Fig 6.9 demonstrates a dependence between nonlinear gain and carrier concentration with the nonlinear gain coefficient clearly decreasing with increasing carrier concentration. However the dependency of nonlinear gain on carrier density must be of a very different nature than that of differential gain which is based on the quantum confinement of carriers. Here, the shift in this trend with increasing quantum well number appeared suspiciously regular. This prompted the plotting of these nonlinear gain results with respect to threshold current density which normalizes the contribution of varying quantum well number, as shown in Fig 6.10. The trend observed in Fig 6.10 clearly demonstrates that the nonlinear gain coefficient is not dependent on the number of quantum wells directly so that an equivalent threshold current density in any of these structures regardless of the number of quantum well's would appear to result in the same nonlinear gain coefficient value to within experimental error.

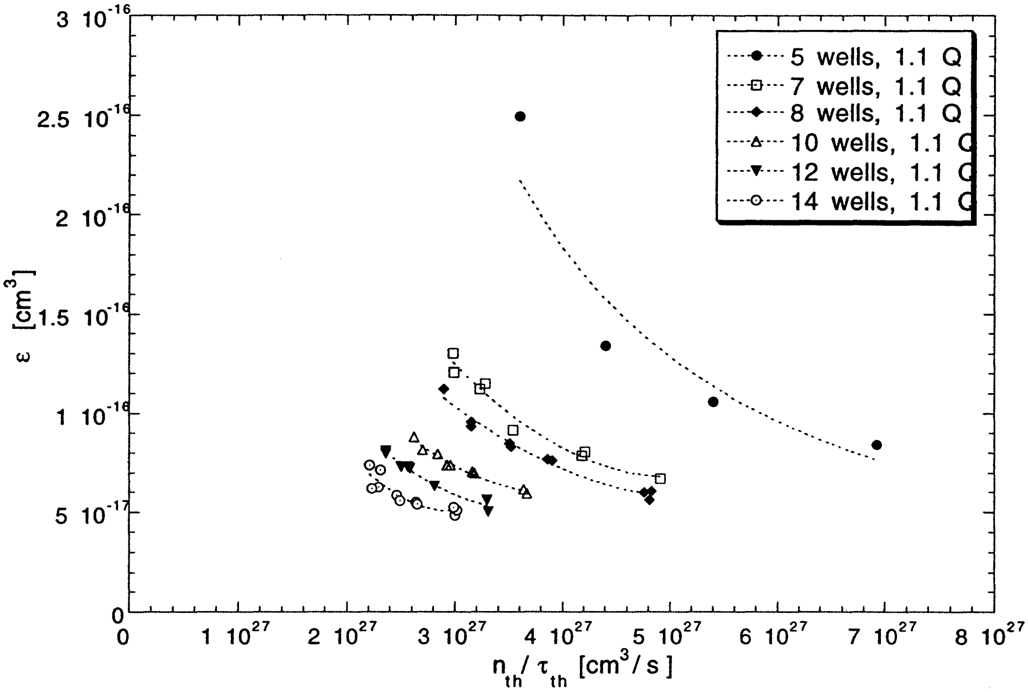

Fig. 6.9: Nonlinear gain versus threshold carrier concentration divided by carrier lifetime for structures S1-349, S1-341, S1-340, S1-429, S1-418, and S1-422 with 1.1 Q barriers and 5, 7, 8, 10, 12, 14 quantum wells respectively, at an operating temperature of 20 °C.

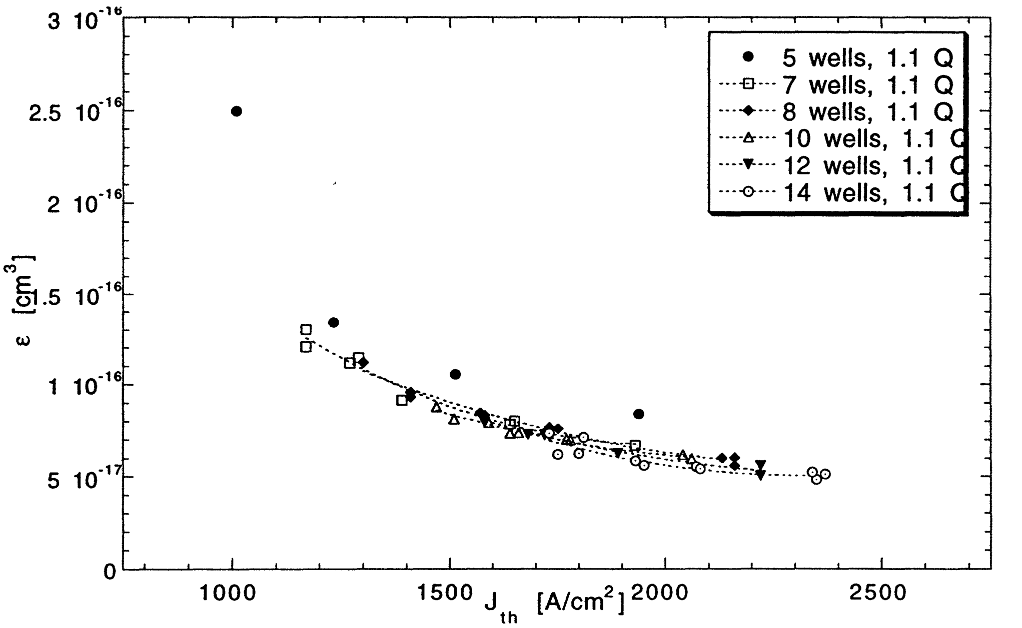

Fig. 6.10: Nonlinear gain coefficient versus threshold current density for structures S1-349, S1-341, S1-340, S1-429, S1-418, and S1-422 with 1.1 Q barriers and 5, 7, 8, 10, 12, 14 quantum wells respectively, at an operating temperature of 20 °C.

This suggests that the nonlinear gain coefficient is not influenced by the density of the carrier population. It would appear that the nonlinear gain coefficient is more dependent on a parameter whose value and influence is invariant for a given threshold condition independent of the active region structure. To explore this possibility further the influence of quantum well barrier height was examined next.

6.4.2 Nonlinear gain coefficient versus quantum well barrier height

The nonlinear gain coefficient was again plotted versus the threshold current density, but this time for the structures involving the variation of quantum well barrier height, as well as quantum well number, shown here in Fig 6.11.

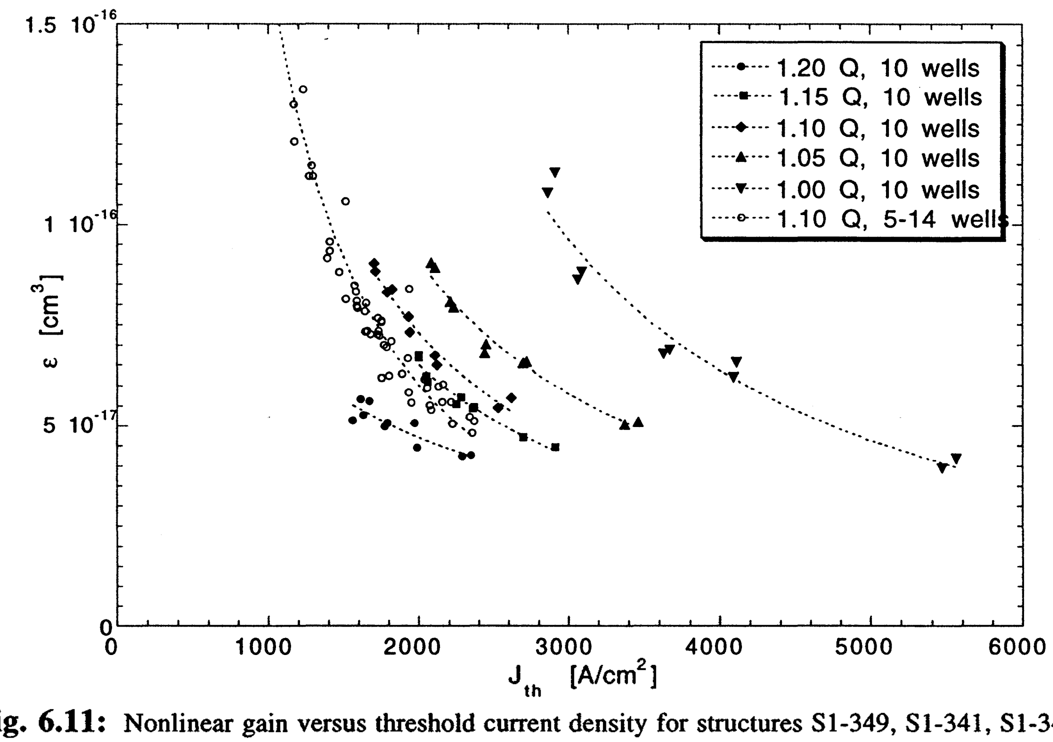

Fig. 6.11: Nonlinear gain versus threshold current density for structures S1-349, S1-341, S1-340, S1-429, S1-418, and S1-422 with 1.1 Q barriers and 5-14 quantum wells, and for structures S1-591, S1-593, S1-588, S1-590, and S1-592 with 1.00, 1.05, 1.10, 1.15, and 1.20 Q barriers respectively and 10 quantum wells, at an operating temperature of 20 °C.

In Fig 6.10 it was observed that the nonlinear gain coefficient was not dependent on the number of quantum wells directly in so that an equivalent threshold current density in any of these structures regardless of quantum well number appeared to result in the same nonlinear gain coefficient value to within experimental error. With the additional data showing the dependence of the nonlinear gain coefficient on quantum well barrier height in Fig 6.11 it is observed that varying quantum well barrier height has an impact on this dependency.

An interesting observation to make at this point is that when the number of quantum wells in the structure is changed the gain properties of the material itself are not expected to change because there has been no change in the carrier confinement properties of the wells, only the carrier densities are effected. However when the quantum well barrier height is changed the carrier confinement properties are changed thus changing the gain properties of the material. It was suggested in §6.4.1 that the nonlinear gain coefficient may be dependent on a parameter whose value and influence is invariant for a given threshold condition independent of the active region structure. Observations based on Fig 6.11 have shown this to not be true, however, based on the observation that the gain properties of the material are varying for the results in Fig 6.11, the nonlinear gain coefficient may be dependent on the material gain properties of the active region structure, which are the same for any structure at threshold for the same threshold gain condition. This observation is supported by the offset observed between the trends in Fig 6.11 for the 10 well structures with 1.1 Q barrier height from the varying quantum wells group, S1-429, and the varying barrier height group, S1-588. One might expect that two structures with the same number of quantum wells and quantum well barrier heights would behave the same. However, with these two structures there is an additional design difference in the doping concentration of the barriers which will obviously impact the carrier confinement properties of the wells and thus the material gain of the structures.

A problem arises as a result of there appearing to be a dependency of the nonlinear gain coefficient on the material gain properties of the active region structure. Recall that the nonlinear gain coefficient, ε, appearing in equation (2.3.10) for the damping constant K came from the approximation of the material gain represented by equation (2.3.9). In this equation the dependency of the material gain on photon density is represented by the linear coefficient ε which, if correct, should not have any further dependency on the material gain itself. The observation that the nonlinear gain coefficient has a dependency on the material gain properties of the active region structure suggests that representing that material gain dependency on photon density with the linear coefficient ε is inadequate.

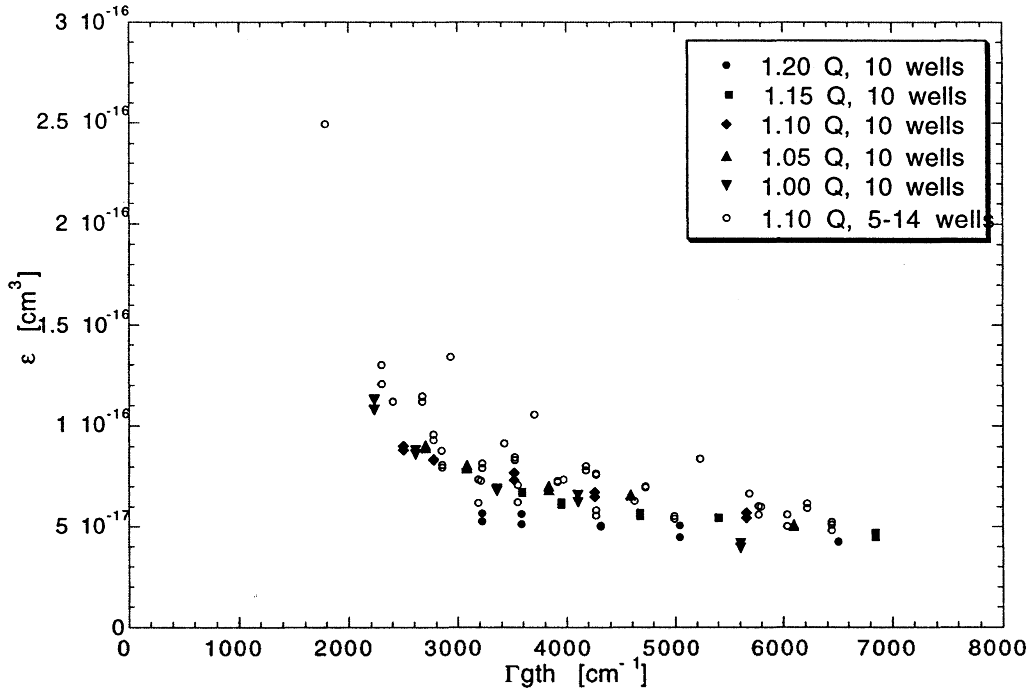

Fig. 6.12: Nonlinear gain coefficient versus modal threshold gain condition for structures S1-349, S1-341, S1-340, S1-429, S1-418, and S1-422 with 1.1 Q barriers and 5-14 quantum wells, and for structures S1-591, S1-593, S1-588, S1-590, and S1-592 with 1.00, 1.05, 1.10, 1.15, and 1.20 Q barriers respectively and 10 quantum wells, at an operating temperature of 20 °C.

To explore this possibility further the characterized value ε for all structures was plotted against the modal threshold gain which is directly related to the material gain properties of the active region structure, shown in Fig 6.12. Before commenting on the trend seen in Fig 6.12 it is helpful to review the role that the nonlinear gain coefficient, based on the linear coefficient approximation in (2.3.9), plays in the modal threshold gain.

Multiplying both sides of equation (2.3.9) by the optical confinement factor results in the following expression at threshold

$$\Gamma g_{th} = \Gamma g_o(n_{th})\,(1 - \varepsilon\, s_{th}) \tag{6.4.1}$$

where n_{th} and s_{th} are the carrier and photon densities at threshold. From (6.4.1) it is shown that the multiplication of the nonlinear gain coefficient with the photon density at threshold should describe the offset observed between the achieved material gain and an ideal value based on its carrier density dependence at threshold resulting from gain saturation effects. The photon density at threshold, s_{th}, is the photon population present in the laser cavity when optical gain has overcome the cavity losses, those being the internal and mirror losses. The state at which the internal losses of the laser are overcome by the material gain is referred to as the transparency condition where a balance has been achieved between the rate of photon generation and photon absorption. At the transparency condition the population of photons in the cavity is theoretically zero. The population of photons that exists between the transparency condition and threshold is a result of overcoming the mirror losses such that stimulated emission becomes the dominant process of photon generation in the active region of the laser. Since all of the laser structures studied here have similar facet reflectivity's, their photon densities at threshold should be similar. That would mean that the observed decrease in the nonlinear gain coefficient with increasing modal threshold gain actually confirms dependency of the nonlinear gain coefficient on the material gain. This supports the postulation made earlier, that representing that material gain dependency on photon density with the linear coefficient ε is inadequate.

The conclusion that material gain dependency on photon density with a linear coefficient is inadequate should not be a surprise. It is well accepted that the physical mechanisms that result in gain nonlinearity are not well understood [55]. The approximation of nonlinear gain, $\partial g(n,s)/\partial s$, using an equivalent gain scaling factor as used in equation (2.3.9) should be recognized as a phenomenological approach [55].

Rather than relying on the characterization of an approximation of the nonlinear gain, $\partial g(n,s)/\partial s$, or g_S, one can extract a value for g_S directly, recognizing that its value represents the value of the nonlinear gain as seen at the threshold condition, as was the case with the differential gain, g_n (see §2.5.6). A value for g_S can be characterized using equation (2.3.7) much the same way ε was characterized using equation (2.3.10). Shown in Fig 6.13, the value of the nonlinear gain at threshold is plotted versus the threshold gain condition. The relationship between these two parameter values for all of the laser structures more clearly demonstrates the dependency of nonlinear gain on the achieved material gain.

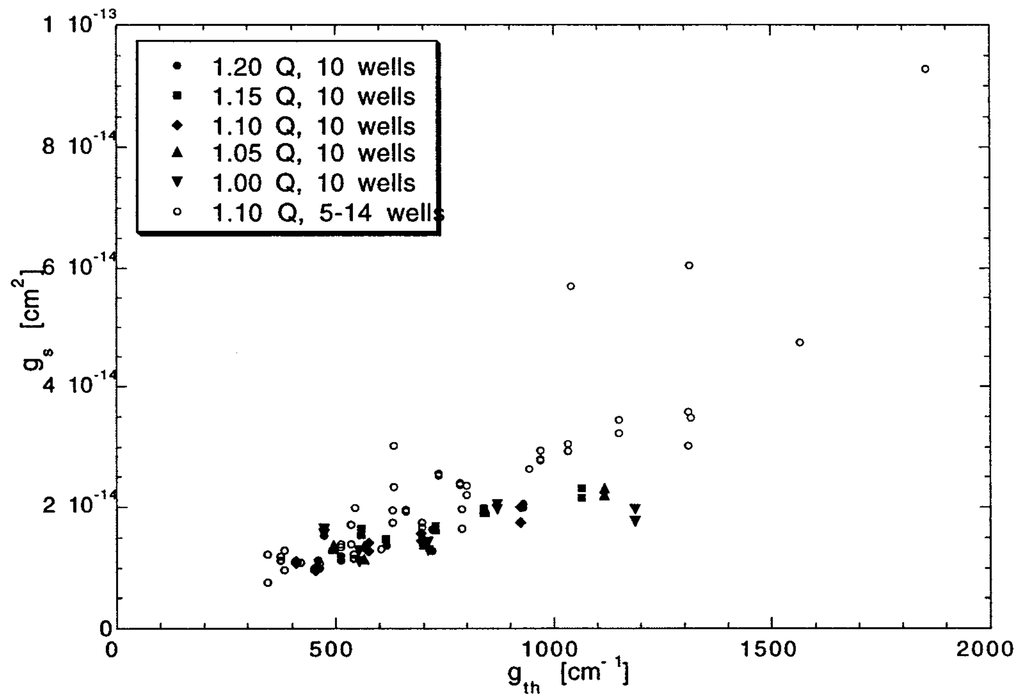

Fig. 6.13: Nonlinear gain versus threshold gain condition for structures S1-349, S1-341, S1-340, S1-429, S1-418, S1-422, S1-591, S1-593, S1-588, S1-590, and S1-592 at an operating temperature of 20 °C.

Further analysis of data like this could be used to establish a better understanding of the nature of nonlinear gain and its dependencies on device design, as opposed to trying to understand the dependencies of a poorly established linear approximation. Since the gain achieved is a reflection of the stimulated emission process of photon generation, the trend observed in Fig 6.13 shows that a fairly simple relationship between the amount of stimulated emission occurring in the laser structure and the degree to which the efficiency of the process is saturated by the increasing population of photons probably exists.

From the stand point of device performance optimization it is more useful as well to examine the relationship between the differential gain and an actual characterized value for the gain saturation observed at threshold, plotted in Fig 6.14.

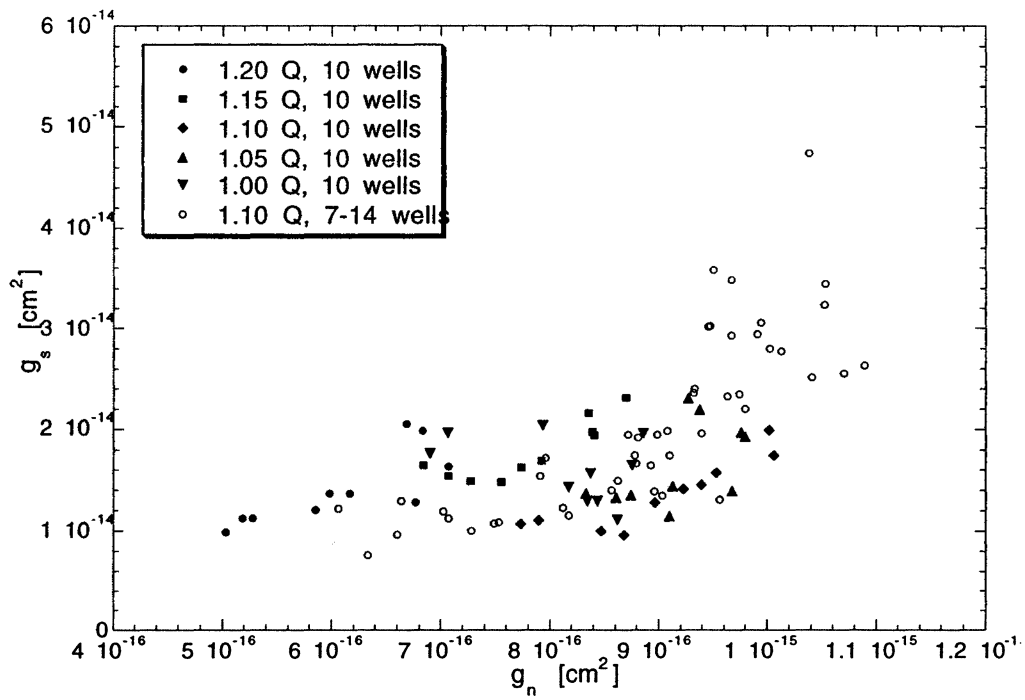

Fig. 6.14: Nonlinear gain versus differential gain for structures S1-349, S1-341, S1-340, S1-429, S1-418, and S1-422 with 1.1 Q barriers and 5-14 quantum wells, and for structures S1-591, S1-593, S1-588, S1-590, and S1-592 with 1.00, 1.05, 1.10, 1.15, and 1.20 Q barriers respectively and 10 quantum wells, at an operating temperature of 20 °C.

In Fig 6.14 a much stronger correlation between nonlinear gain and differential gain as characterized at threshold is demonstrated than was observed in Fig 6.8 with the linear approximation ε. The trend observed in Fig 6.14 clearly demonstrates why a higher modulation bandwidth has been difficult to achieve in moving from a bulk active region device design to multiple quantum well structures as discussed in §1.2. From the modeling of the high speed dynamics of semiconductor lasers it was initially felt that an improvement in the differential gain performance of a structure should result in a higher modulation bandwidth. However, it is clear from Fig 6.14 that any initial attempt to improve the differential gain performance of the basic design studied here would result in a more rapidly increasing nonlinear gain, which has also been shown to play an important role in the frequency response of semiconductor lasers. This clearly demonstrates the need to understand the design dependencies of both these performance parameters before any deliberate improvement in high speed performance of this basis design can be achieved.

Based on the understanding developed so far on the behavior of the differential gain and nonlinear gain for this basic multiple quantum well design a simple explanation may exist as to why the nonlinear gain is seen to increase more rapidly with increasing differential gain. It was postulated in §6.3 that the differential gain parameter for the lower carrier concentration threshold conditions may be considerably lower than expected from these designs because of nonuniform filling of the quantum wells. If this were not the case then we would have consistently observed higher differential gain values for designs that achieved lower threshold carrier concentrations. In addition these lower threshold carrier concentrations would correspond to lower threshold gain conditions and so, according to Fig 6.13, lower nonlinear gain. If the effect where by lower differential gain values were observed for lower carrier concentrations did not exist then clearly the trend between differential gain and nonlinear gain would be reversed with the nonlinear gain becoming smaller for increasing differential gain. In the case of this MQW design the difficulty of improving the bandwidth through design lies in overcoming the irregular behavior of differential gain with respect to carrier concentration at threshold.

6.5 MAXIMUM INTRINSIC BANDWIDTH

When considering the maximum intrinsic bandwidth of a semiconductor laser as defined by equation (2.4.4) an additional physical parameter, photon lifetime, shows an obviously important role in determining the frequency response of semiconductor lasers. It is the maximum intrinsic bandwidth that ultimately demonstrates how the contributions from differential gain, nonlinear gain, and photon lifetime balance with each other. Given that it was found more effective to examine the role that nonlinear gain, g_s, plays in the laser performance as opposed to ε, f_{max} as defined by equation (2.4.4) should be changed to reflect this. This can be achieved by substituting equation (2.3.7) for K into equation (2.4.3) for f_{max} resulting in

$$\frac{1}{f_{max}} = \sqrt{2}\,\pi\,\tau_{ph}\left(1 - \frac{\Gamma g_s}{g_n}\right) \qquad (6.5.1)$$

Before investigating the role that differential gain, g_n, and nonlinear gain, g_s, plays in f_{max}, as defined by equation (6.5.1) it is instructive to first look at the overall influence of the photon lifetime by plotting f_{max} versus τ_{ph} as shown in Fig 6.15.

The dependence of maximum intrinsic bandwidth on photon lifetime demonstrated in Fig 6.15 is understandable given the strong dependence of the photon lifetime on cavity length and the first order role photon lifetime plays in equation (6.4.1). Given that the photon lifetime has such a dominating effect on the maximum intrinsic bandwidth the additional dependence of the differential gain, g_n, and nonlinear gain, g_s, is only resolvable when cavity length is held constant. Shown in Fig 6.16 is the maximum intrinsic bandwidth versus differential gain for all of the structures for the same cavity lengths. A general trend of maximum intrinsic bandwidth increasing with differential gain is observed for the 254 μm and 508 μm cavity length devices.

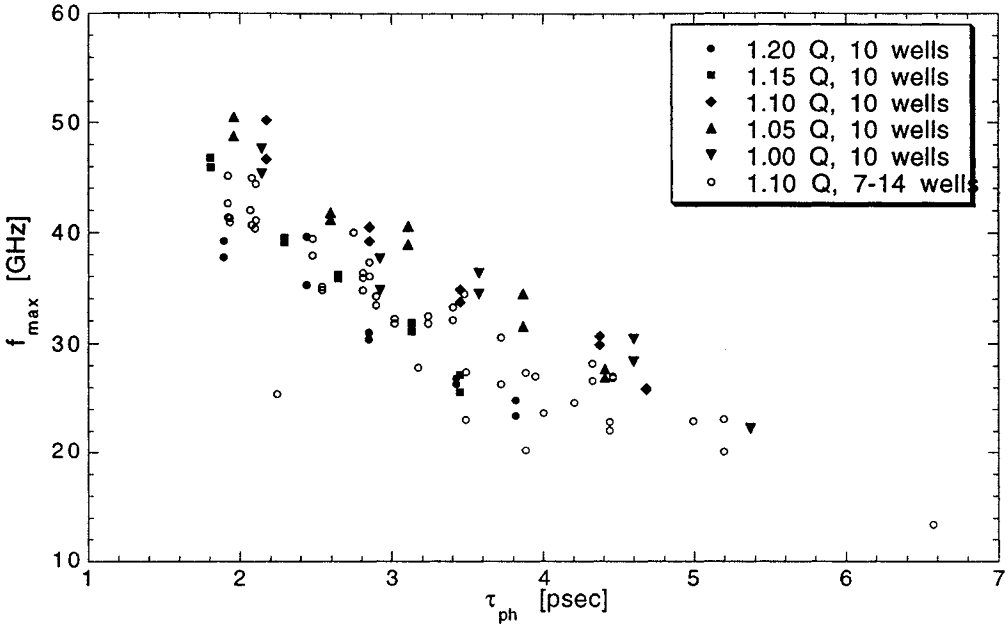

Fig. 6.15: Maximum intrinsic bandwidth versus photon lifetime for structures S1-349, S1-341, S1-340, S1-429, S1-418, S1-422, S1-591, S1-593, S1-588, S1-590, and S1-592 at an operating temperature of 20 °C.

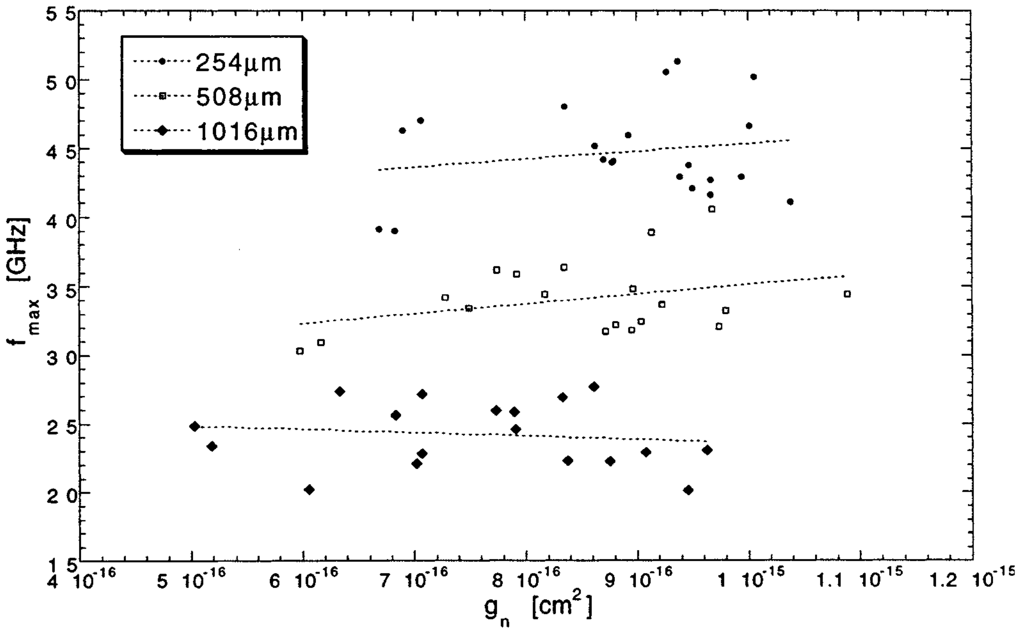

Fig. 6.16: Maximum intrinsic bandwidth versus differential gain for structures S1-349, S1-341, S1-340, S1-429, S1-418, and S1-422 with 1.1 Q barriers and 5-14 quantum wells, and for structures S1-591, S1-593, S1-588, S1-590, and S1-592 with 1.00-1.20 Q barriers and 10 quantum wells, with 254 μm, 508 μm, and 1016 μm cavity lengths, at an operating temperature of 20 °C.

As was mentioned in §1.2, and predicted by equation (6.5.1), an increase in the intrinsic bandwidth of the laser is expected with increasing differential gain. However, for the 1016 μm cavity length devices this does not appear to apply. As was discussed in §1.2, some studies have observed this as well as a result of the gain saturation increasing with the differential gain canceling out the benefits of its influence on intrinsic bandwidth, as is predictable by equation (6.5.1). Shown in Fig 6.17 is the maximum intrinsic bandwidth versus gain saturation for all of the structures for the same cavity length.

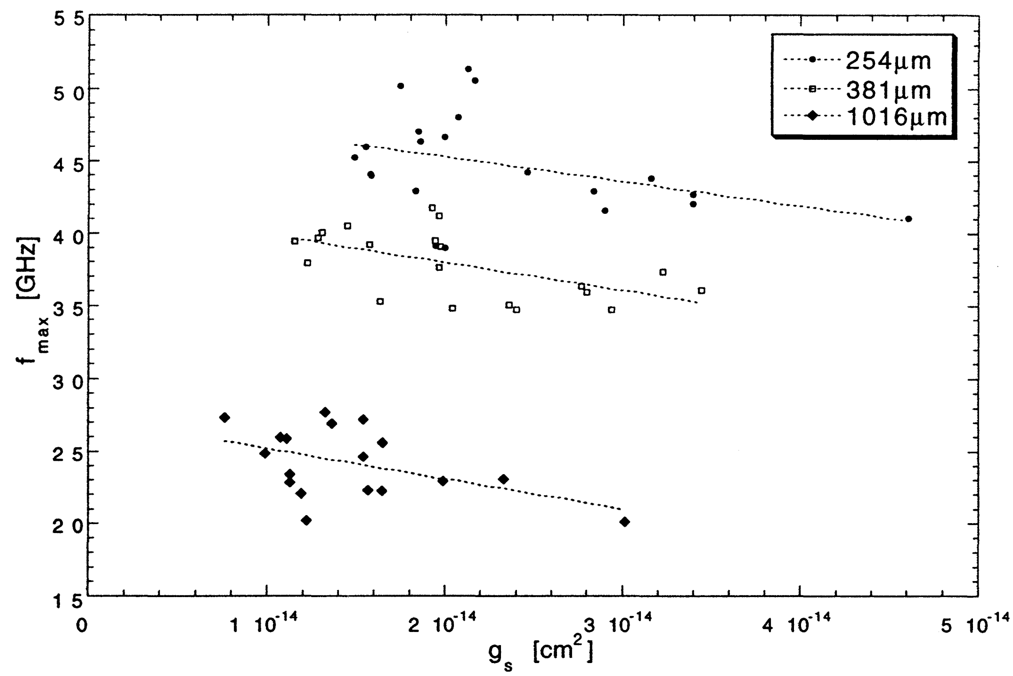

Fig. 6.17: Maximum intrinsic bandwidth versus gain saturation for structures S1-349, S1-341, S1-340, S1-429, S1-418, S1-422, S1-591, S1-593, S1-588, S1-590, and S1-592 with 254 μm, 381 μm, and 1016 μm cavity lengths, at an operating temperature of 20 °C.

A general trend of maximum intrinsic bandwidth decreasing with increasing gain saturation is observed for all cavity length devices. As was discussed in §1.2, and predictable by equation (6.5.1), an increase in gain saturation causes a decrease in the intrinsic bandwidth of the laser. Based on the two above observations, taking into account the influence that both differential gain and gain saturation have on the intrinsic bandwidth should therefore be a better guide for determining the true impact of a design variation on the modulation performance of a laser. As confirmation of this the maximum intrinsic bandwidth is plotted versus the differential gain divided by the gain saturation in Fig 6.18.

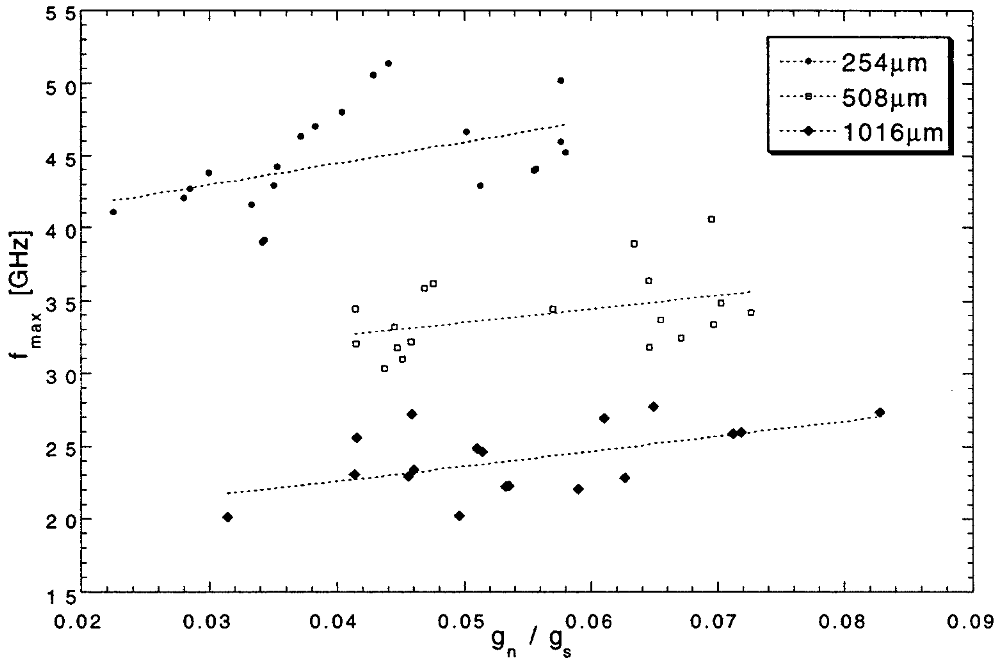

Fig. 6.18: Maximum intrinsic bandwidth versus differential gain divided by gain saturation for structures S1-349, S1-341, S1-340, S1-429, S1-418, and S1-422 with 1.1 Q barriers and 5-14 quantum wells, and for structures S1-591, S1-593, S1-588, S1-590, and S1-592 with 1.00-1.20 Q barriers and 10 quantum wells, with 254 μm, 508 μm, and 1016 μm cavity lengths, at an operating temperature of 20 °C.

As expected the general trend for all cavity lengths is for the maximum intrinsic bandwidth to increase with an increasing ratio of differential gain to gain saturation. However the trends do not appear to be strong enough to be convincing that the differential gain and gain saturation are all that need to be considered here. As it was not present in the original expression for the maximum intrinsic bandwidth in equation (2.4.4) the influence of the optical confinement factor was not initially examined. In equation (6.5.1), the optical confinement factor would also appear to play an important role in the bandwidth response of lasers when the linear approximation for gain saturation is removed. As was demonstrated in §5.5, the optical confinement factor steadily decreases with increasing quantum well barrier height, shown in Fig 5.12, and steadily increases with increasing quantum well number, shown in Fig 5.13. Including the influence of the optical confinement factor, the maximum intrinsic bandwidth is plotted versus the differential gain divided by the optical confinement factor and gain saturation, shown in Fig 6.19. As expected, a trend for all cavity lengths of the maximum intrinsic bandwidth increasing with an increasing ratio of differential gain to optical confinement and gain saturation is observed. However in this case the correlation appears to be stronger that those shown in Fig 6.18 indicating that better agreement is achieved when the optical confinement is included in consideration of influences on the maximum intrinsic bandwidth.

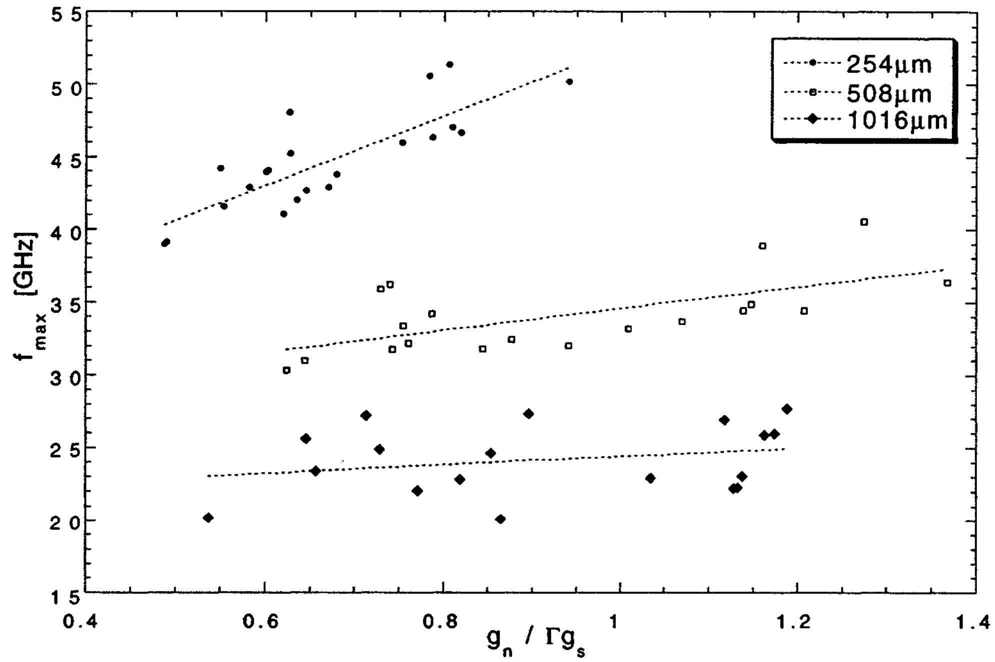

Fig. 6.19: Maximum intrinsic bandwidth versus differential gain divided by the optical confinement factor and gain saturation for structures S1-349, S1-341, S1-340, S1-429, S1-418, and S1-422 with 1.1 Q barriers and 5-14 quantum wells, and for structures S1-591, S1-593, S1-588, S1-590, and S1-592 with 1.00-1.20 Q barriers and 10 quantum wells, with 254 μm, 508 μm, and 1016 μm cavity lengths, at an operating temperature of 20 °C.

6.6 DESIGN OPTIMIZATION

Now that each parameter that contributes to the bandwidth performance of semiconductor lasers has been characterized, some understanding of how their relative contributions influence bandwidth performance has been developed. This information should now be useful in the investigation of how changing key design parameters can be used to improve on the overall design of the laser. As well, better insight into the limitations that arise with respect to the influence these design parameters can have on performance can be developed. Using the maximum intrinsic bandwidth of each laser as determined from the characterized damping coefficient, K, as an indicator of the overall bandwidth performance of the laser structures, optimization of the design by varying quantum well barrier height and quantum well number was explored.

6.6.1 Optimization by varying quantum well barrier height

It was observed in §5.9 with Fig 5.34 that f_{max} appeared to achieve a maximum value some where between a barrier height of 1.1 μm and 1.05 μm depending on the cavity length of the structure examined. Initially it was thought that the differential gain would be observed to consistently increase with increasing barrier height, and this was predicted to result in a corresponding increase in f_{max}. However this increase in differential gain was not observed in §5.7 with Fig 5.24 for all but the 1016 μm cavity lengths.

As discussed above, with what has been discovered with respect to the influence of other parameters, the impact of increasing quantum well barrier height and its limitations can be re-examined. Plotted in Fig 6.20 is the differential gain divided by optical confinement factor and gain saturation, and the inverse of the optical confinement factor versus quantum well barrier height.

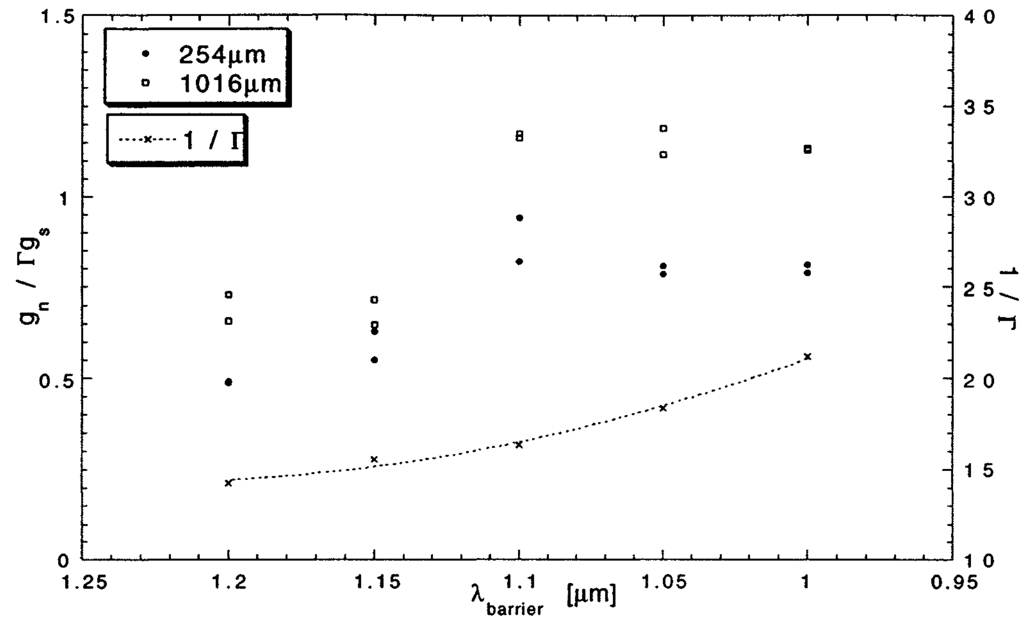

Fig. 6.20: Differential gain divided by optical confinement factor and gain saturation, and the inverse of the optical confinement factor versus quantum well barrier height for structures S1-591, S1-593, S1-588, S1-590, and S1-592 with 1.00-1.20 Q barriers and 10 quantum wells, for 254 μm, and 1016 μm cavity lengths, at an operating temperature of 20 °C.

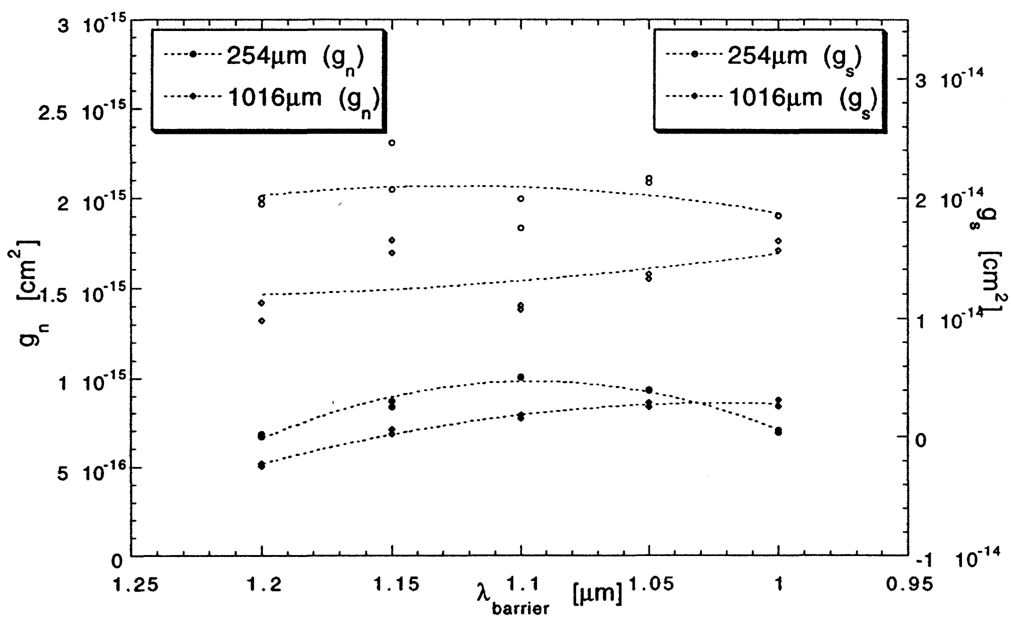

Fig. 6.21: Differential gain and gain saturation versus quantum well barrier height for structures S1-591, S1-593, S1-588, S1-590, and S1-592 with 1.00-1.20 Q barriers and 10 quantum wells, for 254 μm, and 1016 μm cavity lengths, at an operating temperature of 20 °C.

From the steady increase in the inverse of the optical confinement factor with quantum well barrier height it can be seen that the decrease in optical confinement with increasing barrier height will benefit the maximum intrinsic bandwidth of the laser design. However when examining the ratio of the differential gain to the optical confinement factor and gain saturation it is clear that the benefit of a decreasing optical confinement is overwhelmed by the influences of the differential gain and gain saturation.

In Fig 6.21 the differential gain and gain saturation are plotted versus quantum well barrier height. Looking at the differential gain trend with quantum well barrier height for the 254 μm cavity length lasers an initial increase is observed but a deviation from that expected by theory occurs above 1.1 μm barrier heights, as was noted in §5.7. Reviewing the analysis of the impact of carrier concentration on differential gain in §6.3, the deviation from that expected by theory above 1.1 μm barrier heights for 254 μm cavity lengths is accountable for by the increase in threshold carrier concentration with increasing barrier height. The increase in threshold carrier concentration with increasing barrier height is unavoidable because of the decrease in the internal quantum efficiency of the structure which occurs, as observed in Fig 5.16. With the 1016 μm cavity length devices the impact of a decreasing internal quantum efficiency on the threshold carrier concentration of the devices is much weaker because of the lower threshold gain conditions resulting from lower mirror losses. Therefore in this case an increase in the differential gain with increasing barrier height is observed. However, it is also observed that the gain saturation is increasing with barrier height at a faster rate than the differential gain, overtaking its influence above a 1.1 μm barrier height.

From these observations it would appear that several limitations exist with respect to taking advantage of increased differential gain with increasing barrier height. When designing a high modulation rate laser a shorter cavity length is preferred given the influence that photon lifetime has on achievable bandwidth. However as cavity length is reduced and mirror losses increase the threshold gain condition for the structure will increase resulting in an increase in the carrier concentration at threshold. At higher threshold gain conditions the impact of a decreasing internal quantum efficiency with increasing barrier height will result in a noticeable increase in the threshold carrier concentration. The decrease in differential gain resulting from this increase in threshold carrier concentration will overwhelm the expected increase in differential gain resulting from increasing the barrier height. Therefore this design is inherently limited to any benefit above 1.1 μm barrier heights by the internal quantum efficiency currently achievable by this design. As well, another inherent physical limitation exists as it has also been observed that the influence of the gain saturation overtakes that of the differential gain above 1.1 μm barrier heights possibly due to the increase in the threshold gain condition as well.

6.6.2 Optimization by varying quantum well number

It was observed in §5.9 with Fig 5.35 that varying the quantum well number had very little influence on f_{max}, not including the results for the 5 quantum well structure S1-349, regardless of the cavity length of the structure examined. Initially it was thought that an expected increase in the differential gain and decrease in the photon lifetime with quantum well number would result in an increase in the maximum intrinsic bandwidth. With what has been discovered with respect to the influence of other parameters, the impact of increasing quantum well number and its limitations can be re-examined.

The differential gain divided by optical confinement factor and gain saturation, and the inverse of the optical confinement factor versus quantum well number is shown in Fig 6.22. From the steady decrease in the inverse of the optical confinement factor with quantum well number it can be seen that the decrease in optical confinement with decreasing quantum well number will benefit the maximum intrinsic bandwidth of the laser design going against the original expected benefit of increasing differential gain with increasing quantum well number. When examining the ratio of the differential gain to the optical confinement factor and gain saturation it is unclear whether the change in the optical confinement with quantum well number is the dominant factor with respect to the bandwidth performance.

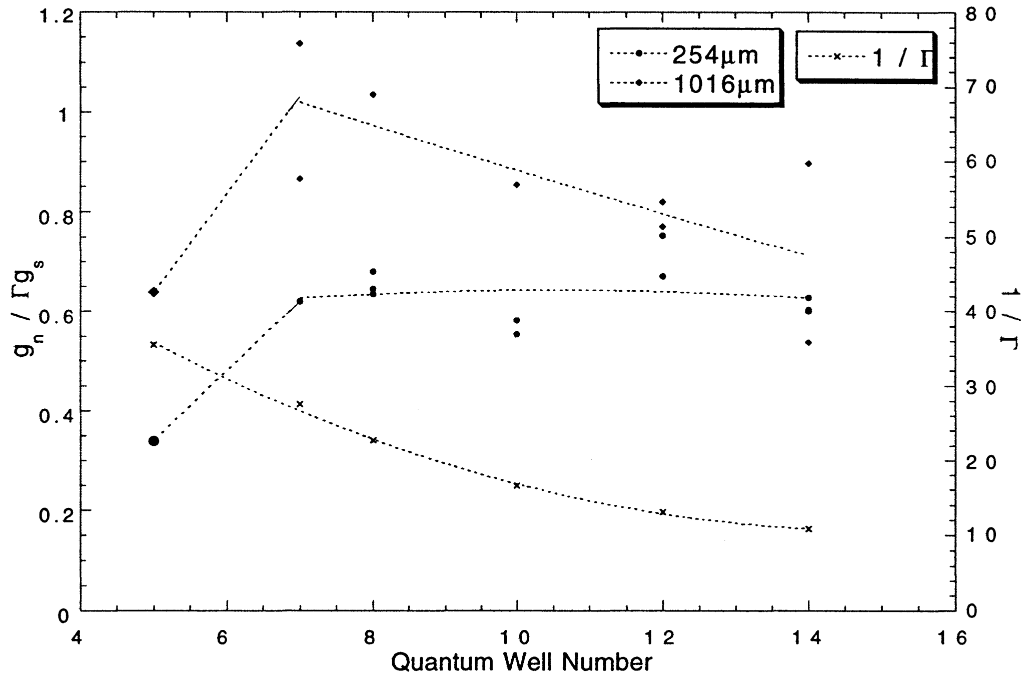

Fig. 6.22: Differential gain divided by optical confinement factor and gain saturation, and the inverse of the optical confinement factor versus quantum well number for structures S1-349, S1-341, S1-340, S1-429, S1-418, and S1-422 with 1.1 Q barriers and 5-14 quantum wells, for 254 μm, and 1016 μm cavity lengths, at an operating temperature of 20 °C.

In Fig 6.23 the differential gain and gain saturation are plotted versus quantum well number. Looking at the differential gain trend with quantum well number for the 254 μm cavity length lasers an initial increase is observed up to 7 wells. However the trend then deviates that expected by theory above 7 wells, as was noted in §5.7. Reviewing the analysis of the impact of carrier concentration on differential gain in §6.3, the deviation from that expected by theory above 7 wells for 254 μm cavity lengths may be accountable for by incomplete filling of the quantum wells resulting in higher carrier concentrations in some wells than others resulting in a lower differential gain.

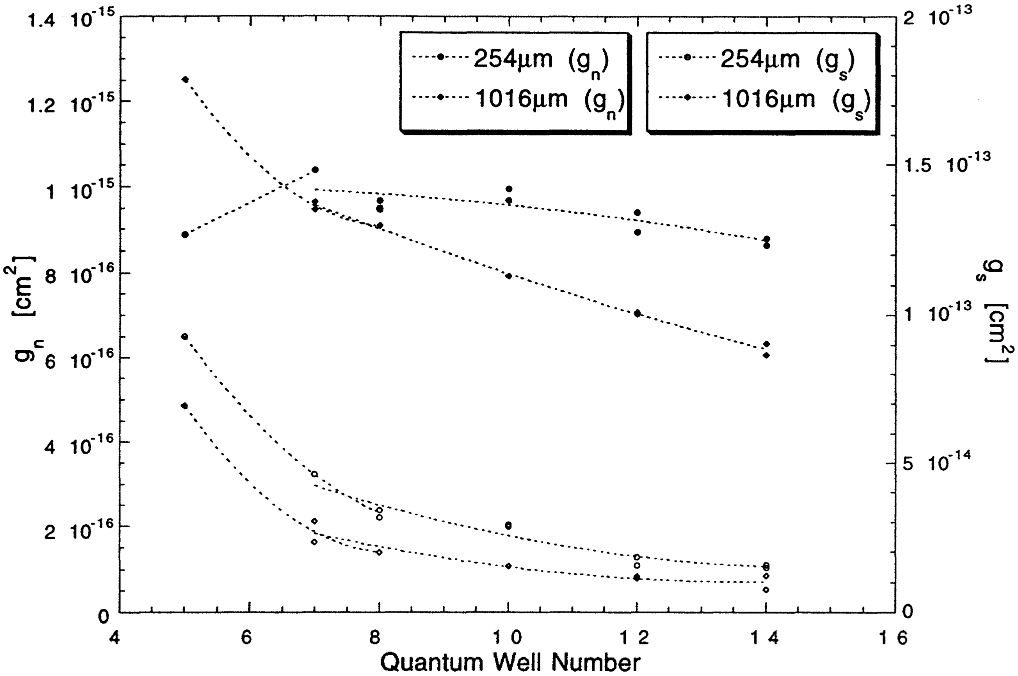

Fig. 6.23: Differential gain and gain saturation versus quantum well number for structures S1-349, S1-341, S1-340, S1-429, S1-418, and S1-422 with 1.1 Q barriers and 5-14 quantum wells, for 254 μm, and 1016 μm cavity lengths, at an operating temperature of 20 °C.

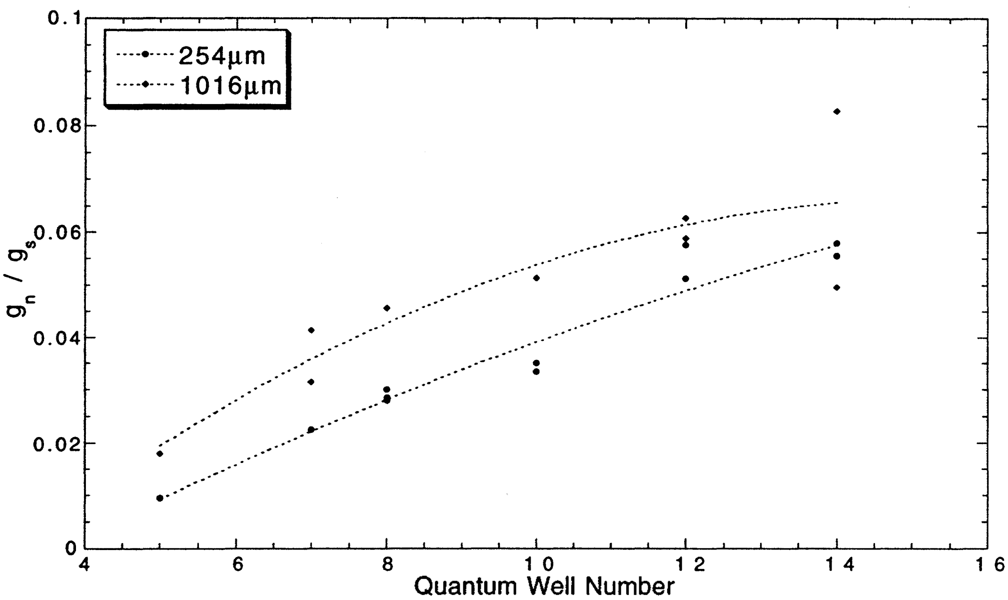

Fig. 6.24: Ratio of differential gain to gain saturation versus quantum well number for structures S1-349, S1-341, S1-340, S1-429, S1-418, and S1-422 with 1.1 Q barriers and 5-14 quantum wells, for 254 μm, and 1016 μm cavity lengths, at an operating temperature of 20 °C.

With increasing well number this effect would just become more pronounced. This explanation would also hold true for the 1016 μm cavity lengths with incomplete filling of the quantum wells beginning at lower well numbers because of the lower carrier concentrations involved with longer cavity length structures as postulated in §6.3. In Fig 6.23 it would appear that gain saturation behaves very similarly to differential gain with respect to how it is influenced by quantum well number. However it is unclear as to which is dominant until the ratio of differential gain to gain saturation is plotted versus quantum well number as in Fig 6.24. From Fig 6.24 it is clear that the rate of decrease of differential gain with increasing quantum well number is much lower than that of gain saturation. Therefore the decrease in the inverse of the optical confinement factor would appear to almost exactly compensate for the increase in the ratio of the differential gain to gain saturation for increasing quantum well number.

From these observations it would appear that several limitations exist with respect to taking advantage of increased differential gain with increasing quantum well number. With these current active region designs it is possible that the quantum wells are not being adequately filled with carriers thus eliminating the possible benefit of increased differential gain with increasing well number. Under these possibly non ideal operating conditions the change in differential gain with respect to gain saturation would appear to be of benefit to the maximum intrinsic bandwidth of the design. However this benefit is cancelled out by the increase in optical confinement. If the design were to be modified to allow for proper filling of the quantum wells it is possible that the increase in differential gain would over power the increase in optical confinement. However it is unclear at this point how the gain saturation would behave.

6.7 SUMMARY

In summary, it was suggested that the observed deviation in the resonance frequency values measured near threshold from those expected by theory may be an artifact of increasing spontaneous emission above threshold with temperature. In exploration of this possibility the spontaneous emission rate, R_{sp}, was characterized for dependence on temperature above threshold and was found to be increasing with temperature.

It was also discussed whether the parameter D or f_{max} would be of more interest to a designer based on its physical relevance to the actual bandwidth performance expected from a laser. It was found that the behavior of the D parameter more closely matched the changes in other key parameters such as the threshold carrier concentration with design variations and therefore would serve a more immediate purpose for design optimization. However, the parameter f_{max} ultimately reveals more about how the parameters that influence the bandwidth capability of each design modification interact.

The trends observed in the calculated differential gain with changing cavity length, quantum well number, and barrier height suggested that with the structures considered here non-uniform filling of the quantum wells may have been occurring. Despite the fact that the behavior of the calculated differential gain values with respect to carrier concentration did not agree with theory, there was good theoretical agreement with the differential gain for a given carrier concentration being the same irregardless of quantum well number, as well as the differential gain for a given carrier concentration increasing with increasing barrier height somewhat confirming the validity of the calculated differential gain values.

The values calculated for the nonlinear gain coefficient, ε, showed a dependency on the characterized modal threshold gain which was interpreted as having demonstrated a dependency on the material gain. It was suggested that the nonlinear gain coefficient, ε, as a gain scaling factor, was possibly inadequate. Attention was then turned to the characterization of the nonlinear gain at threshold, represented by g_S, which demonstrated a fairly linear trend with threshold gain.

It was found that the maximum intrinsic bandwidth is most influenced by the photon lifetime. The magnitude of the photon lifetime is most easily changed with decreasing cavity length indicating that the shorter cavity length designs would appear to always be preferred. Aside from the photon lifetime the combined influence of the optical confinement factor, the gain saturation, and the differential gain was found to have the most consistent influence on the modulation bandwidth performance of the structures.

Finally, examining the relative contributions of each of the parameters to the bandwidth performance it was found that no real change in the key design parameters noticeably improved on the overall speed of the laser other that the obvious benefits of reducing cavity length and marginal improvements from a barrier height of 1.1 μm.

CHAPTER 7: CONCLUSIONS

7.0 INTRINSIC FREQUENCY RESPONSE OF 1.3 μm WAVELENGTH LASERS

In this thesis an extensive study of multiple quantum well (MQW) lasers was reported. For the purposes of this thesis the intrinsic frequency response of two sets of laser structures were characterized. All of the structures were single-step index-guided compressively strained MQW ridge waveguide lasers, designed to have an emission wavelength of approximately 1.3 μm. One group of five structures was studied to examine the effect of varyingQW barrier height from corresponding bandgap wavelengths of 1.2 μm to 1.0 μm while the number of quantum wells was held at ten. The other group of six structures was studied to examine the effect of varyingQW number from 5 to 14 while theQW barrier height was held at a 1.1 μm bandgap wavelength. There were slight differences in the thicknesses and doping levels of the GRINCH regions, and the doping levels used in the barrier layers of the structures in the two groups. However, the width of the wells and barrier layers in all the structures were identical. The device comparison in this study is unique to that of other previous studies in that it simultaneously considers the effect of varying two importantQW physical parameters, the number of wells and the barrier height, in the same basic laser structure.

To begin, the theoretical concepts of intensity noise in semiconductor lasers, the nature of relative intensity noise (RIN) spectra, and the parametric forms that relaxation oscillation frequency and damping factor take with reference to RIN spectra were presented. The dependence of the parameters that influence the relaxation oscillation frequency and damping factor on the intrinsic bandwidth of semiconductors was examined. Specifically, the parameters examined were: the resonance frequency and damping factor of the RIN spectra, the response coefficient D which was characterized from the slope of the resonance frequency versus the root of single facet output power, the response parameter K which was characterized from the slope of the damping factor versus the square of the resonance frequency, the group velocity, the peak photon energy, the optical confinement factor, the mirror loss, and the internal absorption of each device. As well, the differential gain, nonlinear gain coefficient, and the maximum intrinsic bandwidth were to calculated. Finally, the rational for characterizing each parameter and its relative importance to the study was discussed.

Next, details of the laser structures were presented. Accompanying this was some explanation as to how the design variations were expected to impact the parameters being characterized, as well as the intrinsic bandwidth of the laser design being studied in this thesis. This was followed by an explanation of the experimental apparatus and techniques used in the characterization of the laser structures studied.

Finally, the methodology of each parametric characterization and results of these characterizations and how the values of these parameters varied with the device design variations were presented. As well, the results of the calculations of the differential gain, nonlinear gain coefficient, and maximum intrinsic bandwidth using the characterized parameters were presented.

Following the parametric characterizations and calculations there was a discussion of the observed results. Explanations for the lower than expect resonance frequency values observed near threshold in devices from some of the design variations were explored. A brief discussion of the relevance of the D response parameter versus the theoretical maximum intrinsic frequency response to the actual bandwidth behavior of the devices was presented. Discrepancies with theoretical predictions observed in the calculated differential gain values with design variations revealed the possibility that some non ideal behavior, possibly carrier transport effects resulting in non-uniform filling of the quantum wells, was being observed in the structures studied here. As well, the inadequacies of the nonlinear gain coefficient used in the single mode rate equation model adopted by this study were discussed based on the trends in this value with the structural changes explored. A more fundamental parameter representing the nonlinear gain of the amplification system was explored as a replacement for examining the effects of the structural variations on this phenomenon which counteracts the gain process of the laser structure. Then a discussion of the maximum intrinsic bandwidth results explored how the changes in the differential gain and nonlinear gain balanced out with the structural changes explored. Finally, the design optimization possibilities that could be considered based on the discussion of all the parametric results was discussed.

7.1 LIMITATIONS OF SINGLE MODE RATE EQUATION MODEL

Originally this study was to include an examination of how the parameters influencing the intrinsic frequency response of the MQW structures studied here changed with temperature. However it was demonstrated in Fig 5.6 that for operating temperatures greater than 20 °C a deviation in the resonance frequency values measured near threshold from those expected by theory with equations (2.3.13) and (2.3.16) was observed. As was discussed this offset in the resonance frequency values near threshold is possibly an artifact of multiple mode operation resulting from higher spontaneous emission just above threshold. It is quite possible that the spontaneous emission rate increases with temperature increasing the magnitude of this resonance frequency offset. Although it appeared that this effect was negligible at room temperature it served as a further example that using the single mode rate equation model for such characterization as this should be done so with caution. The correlation of any data for above room temperature operation with the single mode rate equation model was impossible necessitating the omission of this data from the study.

Another limitation of the single mode rate equation model is that it assumes uniform filling of the quantum wells in the laser structure. A model which took non-uniform filling of the quantum wells into account would have to be orders of magnitude more complex than that considered here, such as those which include the possible influences of carrier transport effects.[52]-[54] The trends observed in the calculated differential gain with changing cavity length, quantum well number, and barrier height suggested that with the structures considered here non-uniform filling of the quantum wells may have been occurring. In all structures considered, unless the internal quantum efficiency of the device was low, the calculated differential gain was found to decrease rapidly with decreasing carrier concentration beyond a characteristic threshold carrier value. This of course runs completely counter to that expected by theory since as the carrier concentration required to achieve threshold decreases the carrier population is occupying the lower energy region of the conduction band where an increase in carrier concentration is expected to be accompanied by a more rapid change in the Fermi level energy, corresponding to higher differential gain, than at higher energies in the conduction band that would be occupied with a higher threshold condition. Despite the fact that the behavior of the calculated differential gain values with respect to carrier concentration did not agree with theory, there was good theoretical agreement with the differential gain for a given carrier concentration being the same irregardless of quantum well number, as well as the differential gain for a given carrier concentration increasing with increasing barrier height somewhat confirming the validity of the calculated differential gain values.

Many attempts to include the effects of gain saturation into rate equation models involve the inclusion of an equivalent gain scaling factor, as in this study with the inclusion of (1-εs) in equation (2.3.9). However, as discussed earlier, the physical mechanisms responsible for gain nonlinearity are not well understood and the inclusion of any equivalent gain scaling factor is generally accepted as a phenomenological approach.[55] It was found in this study that the calculated nonlinear gain coefficient, ε, showed a dependency on the characterized modal threshold gain which was interpreted as having demonstrated a dependency on the material gain. Therefore it was suggested that the nonlinear gain coefficient, ε, as a gain scaling factor, was possibly inadequate. Attention was then turned to the characterization of the nonlinear gain at threshold, represented by g_s, which demonstrated a fairly linear trend with threshold gain.

7.2 LASER DESIGN OPTIMIZATION

As was discussed in §6.2, the maximum intrinsic bandwidth does not take into account the device heating, and maximum achievable power of the laser. As a result there can be a discrepancy between what the D coefficient values show to be the best structures for modulation bandwidth performance versus f_{max}. These discrepancies can often be accounted for by the dramatic differences that can exist between the current densities required to achieve threshold for the different structures as current density is directly related to internal heating in the laser structures. Despite these possible discrepancies the parameter f_{max} still reveals how key parameters such as photon lifetime, differential gain, and gain saturation compete for influence on the modulation bandwidth of the laser structures.

As mentioned above, the behavior of the linear coefficient ε, referred to as the nonlinear gain, was examined to determine the influence of the structural variations studied here on gain saturation behavior in general. In doing so it was found that the nonlinear gain coefficient demonstrated a dependency on the material gain properties of the structures themselves indicating that representing the material gain dependency on photon density with a linear coefficient was an inadequate approximation. Therefore, rather than relying on the characterization of an approximation of the nonlinear gain, a value for the gain saturation was characterized directly, recognizing that its value represented the nonlinear gain behavior of the laser structure near the threshold condition, as was the case with the calculated differential gain values.

Correlating the calculated differential gain values with the calculated gain saturation it was found that for the range of lower differential gain values the gain saturation is found to increase less rapidly than the differential gain (see Fig 6.14). However in the range of higher differential gain values the gain saturation is found to increase more rapidly than the differential gain. Understanding the competing influence these two parameters have on the modulation bandwidth of a MQW laser it is understandable that attempts to improve the modulation bandwidth performance by improving the differential gain performance of laser structures has been less than successful in the past. However in this particular case the differential gain may be considerably lower than expected from these designs for the lower carrier concentration threshold conditions because of nonuniform filling of the quantum wells. If the differential gain values achieved for the lower threshold carrier concentrations were higher as expected by theory and the nonlinear gain values were low consistent with a low threshold gain condition then clearly the trend between differential gain and nonlinear gain would be reversed with the nonlinear gain becoming smaller for increasing differential gain. In this case the task of design optimization would be much simpler.

When considering the optimization of the basic structural design for improved modulation bandwidth performance it was found that the photon lifetime always has the dominant effect. The magnitude of the photon lifetime is most easily changed with decreasing cavity length indicating that the shorter cavity length designs would appear to always be preferred. Aside from the photon lifetime the combined influence of the optical confinement factor, the gain saturation, and the differential gain was found to have the most consistent influence on the modulation bandwidth performance of the structures. This combined influence was found to be strongest for the shorter length cavity lasers.

The design optimization opportunities available by varying quantum well barrier height were very limited. It is expected that shorter cavity lengths would be used due to the obvious benefits of a shorter photon lifetime. However as cavity length is reduced and mirror losses increase the threshold gain condition for the structures increase resulting in an increase in the carrier concentration at threshold as well as an increase in the gain saturation. At higher threshold gain conditions the impact of the observed decrease in internal quantum efficiency with increasing barrier height results in a noticeable increase in the threshold carrier concentration. The decrease in differential gain resulting from this increase in threshold carrier concentration overwhelms the expected increase in differential gain resulting from increasing the barrier height eliminating any benefit from increasing the barrier height beyond 1.1 μm.

The design optimization opportunities available by varying quantum well number were very limited as well. With these current active region designs it is possible that the quantum wells are not being adequately filled with carriers thus eliminating the possible benefit of increased differential gain with increasing well number. Despite this the change in differential gain with increasing quantum well number was slower than that of the gain saturation resulting in a net benefit from these two parameters to the maximum intrinsic bandwidth of the design. However this benefit was canceled out by the increase in optical confinement. If the design were to be modified to allow for proper filling of the quantum wells it is possible that the increase in differential gain would over power the increase in optical confinement resulting in a clear benefit with increasing quantum well number.

7.3 RECOMMENDATIONS FOR FUTURE WORK

In this study the resonance frequency values measured near threshold for operating temperatures greater than room temperature deviated from the trend expected by theory according to equations (2.3.13) and (2.3.16). It was suggested that this offset in the resonance frequency values near threshold could be an artifact of multiple mode operation resulting from spontaneous emission still present near threshold and that the spontaneous emission rate increases with temperature increasing the magnitude of this resonance frequency offset. One other possibility is that approximations made in the derivation of equations (2.3.13) and (2.3.16) from the original equation (2.3.2) as derived from the single mode rate equation mode used here eliminated terms that become significant at higher temperatures. The term representing the spontaneous emission rate is suspect since its influence in equation (2.3.6) was characterized to show a significant increase with increasing temperature. However this characterization involved some approximation for the calculation of the differential gain from resonance frequency data acquired above room temperature where the offset in resonance frequency values near threshold brought into question the validity of D' parameter values as characterized using equation (2.3.13). Therefore it would be recommended that some modeling of the behavior of the resonance frequency versus current applied above threshold using the single mode rate equation model without the assumptions used in this study be performed to determine whether any of the ignored terms in equation (2.3.2) could account for the observed increasing offset with temperature. It could also be beneficial to attempt some modeling of the resonance frequency behavior above threshold using a more accurate multiple mode rate equation model to determine whether multiple mode operation above threshold could account for this effect. Along with this some investigation into the role that spontaneous emission plays in multiple mode operation above threshold may result in a more accurate form of equation (2.3.6) which could be used in future work to accurately characterize the presence of spontaneous emission near threshold using this simple dc measurement technique. If an understanding of the nature of the resonance frequency offset can be obtained this method of characterizing differential gain and gain saturation could be more confidently used above room temperature.

Based on the trends observed in the calculated differential gain with changing cavity length, quantum well number, and barrier height it was suggested that non-uniform filling of the quantum wells may have been occurring in these structures. If this is the case this particular design presents an excellent opportunity for the study of transient carrier dynamics. Modeling has been performed for other MQW structures taking into account mechanisms such as photon-assisted transport and carrier transport.[53] [54] Modeling in this case coupled with empirically gathered data could be used to validate a purposed carrier dynamics mechanism. Such an improved model could be used to reveal the true differential gain performance realizable from structural modifications as well as to explore novel structural modifications that could potentially overcome carrier dynamic problems in MQW designs. Better understanding of the true achieved differential gain could also lead to an improved understanding of the relationship between differential gain and gain saturation.

It was suggested that the nonlinear gain coefficient, ε, as a gain scaling factor, was possibly inadequate. Characterization of the nonlinear gain at threshold, represented by g_S, demonstrated a fairly linear trend with threshold gain. Further analysis of the behavior of directly characterized nonlinear gain data correlated with characterized material gain could be used to establish a better understanding of the nature of nonlinear gain and its dependencies on device design, as opposed to trying to understand the dependencies of a poorly established linear approximation.

REFERENCES

[1] Morton, P.A.; Temkin, H.; Coblentz, D.L.; Tanbun-Ek, T.; Logan, R.A.; Sciortino, P.F., Jr.; Sergent, A.M., "Enhanced modulation bandwidth of strained MQW lasers", Fourth International Conference on Indium Phosphide and Related Materials, 614-17.

[2] Uomi, K.; Chinone, N., "Proposal on reducing the damping constant in semiconductor lasers by using quantum well structures", Japanese Journal of Applied Physics, Part 2 [LettersB], Vol. 28(8), L1424-5, (1989).

[3] Suemune, I.; Coldren, L.A.; Yamanishi, M.; Kan, Y., "Extremely wide modulation bandwidth in a low threshold current strained quantum well laser", Applied Physics Letters, 53, 1378, (1988).

[4] Arakawa, Y.; Vahala, K.; Yariv, A., "Quantum noise and dynamics in quantum well and quantum wire lasers", Applied Physics Letters, 45, 950-952, (1984).

[5] Arakawa, Y.; Yariv, A., "Theory of gain, modulation response and spectral linewidth in AlGaAs quantum well lasers", IEEE Journal of Quantum Electronics, QE-21, 1666-1674, (1985).

[6] Arakawa, Y.; Yariv, A., "Quantum well lasers - gain, spectra, and dynamics", IEEE Journal of Quantum Electronics, QE-22, 1887-1899, (1986).

[7] Suemune, I.; Coldren, L.A.; Yamanishi, M.; Kan, Y., "Extremely wide modulation bandwidth in a low threshold current strained quantum well laser", Applied Physics Letters, 53, 1378-1380, (1988).

[8] Lester, L.F.; O'Keefe, S.S.; Schaff, W.J.; Eastman, L.F., "Extremely high bandwidth strained-layer InGaAs/GaAs quantum well lasers", Gallium Arsenide and Related Compounds 1992, Proceedings of the Nineteenth International Symposium, 205-10.

[9] Ishikawa, H.; Suemune, I., "Large estimated frequency response increase from deep potential well strained quantum well lasers", IEEE Photonics Technology Letters, 6(11), 1315-17, (1994).

[10] Olshansky, R.; Hill, P.; Lanzisera, V.; Powazinik, W., "Frequency response of 1.3 μm InGaAsP high speed semiconductor lasers", IEEE Journal of Quantum Electronics, QE-23(9), 1410-18, (1987).

[11] Agarwal, G.P.; Dutta, N.K., Long-Wavelength Semionductor Lasers, Van Nostrand Reinhold Electrical/Computer Science and Engineering Series, (1986).

[12] Yasaka, H.; Iga, R.; Noguchi, Y.; Yoshikuni, Y., "Pure effects of strain in strained-layer multiple-quantum-well lasers", IEEE Journal of Quantum Electronics, Vol. 29(4), 1098-103, (1993).

[13] Yasaka, H.; Iga, R.; Noguchi, Y.; Yoshikuni, Y., "Pure strain effects in strained-layer multiple-quantum-well lasers", IEEE Photonics Technology Letters, Vol. 4(8), 826-8, (1992).

[14] Sharfin, W.F.; Rideout, W.; Koteles, E.; Schlafer, J.; Elman, B.; Vassell, M.; Crawford, D.; Benoit, J.; Brosson, P.; Fernier, B., "Effect of carrier transport on modulation bandwidth of quantum well lasers", IOOC-ECOC '91. 17th European Conference on Optical Communication ECOC '91. 8th International Conference on Integrated Optics and Optical Fibre Communication IOOC, vol.1, 133-6, (1991).

[15] Tatham, M.C.; Lealman, I.F.; Seltzer, C.P.; Westbrook, L.D.; Cooper, D.M., "Resonance frequency, damping, and differential gain in 1.5 µm multiple quantum-well lasers", IEEE Journal of Quantum Electronics, Vol. 28(2), 408-14, (1992).

[16] Wong, Y.C.A.; Shore, K.A., "Influence of nonlinear gain on intrinsic bandwidth of quantum well and strained layer semiconductor lasers", IEE Proceedings J [OptoelectronicsB], Vol. 138(6), 413-19, (1991).

[17] Lester, L.F.; O'Keefe, S.S.; Schaff, W.J.; Eastman, L.F., "Modulation characteristics of short cavity strained-layer lasers", Proceedings of the SPIE - The International Society for Optical Engineering, Vol. 1680, 92-100, (1992).

[18] Arakawa, Y.; Takahashi, T., "Effect of nonlinear gain on modulation dynamics in quantum-well lasers", Electronics Letters, 25, 169-70, (1989).

[19] Fukushima, T.; Nagarajan, R.; Ishikawa, M.; Bowers, J.E., "High-speed dynamics in InP based multiple quantum well lasers", Japanese Journal of Applied Physics, Part 1 [Regular Papers & Short NotesB], Vol. 32(1A), 70-83, (1993).

[20] Nagarajan, R.; Ishikawa, M.; Fukushima, T.; Geels, R.S.; Bowers, J.E., "Carrier transport effects in high-speed quantum-well lasers", Proceedings of the SPIE - The International Society for Optical Engineering, Vol. 1634, 119-26, (1992).

[21] Nagarajan, R.; Ishikawa, M.; Bowers, J.E., "Effects of carrier transport of relative intensity noise and modulation response in quantum well lasers", Proceedings of the SPIE - The International Society for Optical Engineering, Vol. 1680, 87-91, (1992).

[22] Nagarajan, R.; Ishikawa, M.; Fukushima, T.; Geels, R.S.; Bowers, J.E., "High speed quantum-well lasers and carrier transport effects", IEEE Journal of Quantum Electronics, Vol. 28(10), 1990-2008, (1992).

[23] Yablonovitch, E., Kane, E.O., "Band structure engineering of semiconductor lasers for optical communications", Journal of Lightwave Technology, 6, 1292-1299, (1988).

[24] Adams, A.R., "Band-stucture engineering for low-threshold high-efficiency semiconductor lasers", Electronics Letters, 22, 249-250, (1986).

[25] Zou, Y.; Osinski, J.S.; Grodzinski, P.; Dapkus, P.D.; Rideout, W.C.; Sharfin, W.F.; Schlafer, J.; Crawford, F.D., "Experimental study of Auger recombination, gain, and temperature sensitivity of 1.5 mu m compressively strained semiconductor lasers", IEEE Journal of Quantum Electronics, Vol. 29(6), 1565-75, (1993).

[26] Tatham, M.C.; Seltzer, C.P.; Perrin, S.D.; Cooper, D.M., "Frequency response and differential gain in strained and unstrained InGaAs/InGaAsP quantum well lasers", Electronics Letters, 27(14), 1278-80, (1991).

[27] Kito, M.; Otsuka, N.; Ishino, M.; Fujihara, K.; Matsui, Y., "Enhanced relaxation oscillation frequency of 1.3 mu m strained-layer multiquantum well lasers", IEEE Photonics Technology Letters, Vol. 6(6), 690-3, (1994).

[28] Mamijoh, T.; Horikawa, H.; Matsui, Y.; Sin, Y.K.; Nakajima, M.; Xu, C.Q.; Ogawa, Y., "Improved operation characteristics of long-wavelength lasers using strained MQW active layers", IEEE Journal of Quantum Electronics, Vol. 30(2), 524-32, (1994).

[29] Nichols, D.; Bhattacharya, P., "Differential gain in InP-based strained layer multiple quantum well lasers", Applied Physics Letters, Vol. 61(18), 2129-31, (1992).

[30] Yasaka, H.; Takahata, K.; Yamamoto, N.; Naganuma, M., "Gain saturation coefficients of strained-layer multiple quantum-well distributed feedback lasers", IEEE Photonics Technology Letters, 3(10), 879-82, (1991).

[31] Ghiti, A.; O'Reilly, E.P., "Nonlinear gain effects in strained-layer lasers", Electronics Letters, 26, 1978-1980, (1990).

[32] Fukushima, T.; Bowers, J.E.; Logan, R.A.; Tanbun-Ek, T.; Temkin, H., "Effect of strain on the resonant frequency and damping factor in InGaAs/InP multiple quantum well lasers", Applied Physics Letters, 58(12), 1244-46, (1991).

[33] Guggenmos, J., "Minimization of laser diode relative intensity noise (RIN) (in optical communication systems)", Proceedings of the SPIE - The International Society for Optical Engineering, Vol. 1044, 260-8, (1989).

[34] Peterman, K.; Arnold, G., "Noise and distortion characteristics of semiconductor lasers in optical fiber communication systems", IEEE Journal of Quantum Electronics, 18(4), 543-55, (1982).

[35] Lau, K.Y.; Yariv, A., "Ultra-high speed semiconductor lasers", IEEE Journal of Quantum Electronics, 21(2), 121-37, (1985).

[36] Su, C.B., "Dynamics of high frequency lasers", Proceedings of the SPIE - The International Society for Optical Engineering, Vol: 1217, 6-13, (1990).

[37] Su, C.B.; Schlafer, J.; Lauer, R.B., "Explanation of low-frequency relative intensity noise in semiconductor lasers", Applied Physics Letters, Vol. 57(9), 849-51, (1990).

[38] Eom, J.; Su, C.B.; LaCourse, J.S.; Lauer, R.B., "The relation of doping level to K factor and the effect on ultimate modulation performance of semiconductor lasers", IEEE Photonics Technology Letters, Vol. 2(10), 692-4, (1990).

[39] Nagarajan, R.; Ishikawa, M.; Bowers, J.E., "Effects of carrier transport on relative intensity noise and critique of K factor predictions of modulation response", Electronics Letters, 28(9), 846-8, (1992).

[40] Evans, J.D., Effects of intentionally introduced mismatch strain on the operating characteristics and temperature performance of InGaAsP/InP long wavelength semiconductor lasers, PhD Thesis, McMaster University, (1993).

[41] Nido, M.; Naniwae, K.; Shimizu, J.; Murata, S.; Suzuki, A., "Analysis of differential gain in InGaAs-InGaAsP compressive and tensile strained quantum-well lasers and its application for estimation of high-speed modulation limit", IEEE Journal of Quantum Electronics, Vol. 29(3), 885-95, (1993).

[42] Ralston, J.D.; Weisser, S.; Esquivias, I.; Larkins, E.C.; Rosenzweig, J.; Tasker, P.J.; Fleissner, J., "Control of differential gain, nonlinear gain and damping factor for high-speed application of GaAs-based MQW lasers", IEEE Journal of Quantum Electronics, Vol. 29(6), 1648-59, (1993).

[43] Zhao, B.; Chen, T.R.; Yariv, A., "The extra differential gain enhancement in MQW lasers", IEEE Photonics Technology Letters, 4, 124-126, (1992).

[44] Cavelier, M.; Lourtioz, J.M.; Xie, J.M.; Chusseau, L., "Gain compression and phase-amplitude coupling in GaInAs quantum well lasers with three, five and seven wells", Electronics Letters, 27(6), 513-14, (1991).

[45] Shimizu, J.; Yamada, H.; Murata, S.; Tomita, A.; Kitamura, M.; Suzuki, A., "Optical-confinement-factor, differential gain, and nonlinear gain coefficient for 1.55 μm InGaAs/InGaAsP MQW and strained-MQW lasers", IEEE Photonics Technology Letters, 3, 773-776, (1991).

[46] Bevington, P.R., Data Reduction and Error Analysis for the Physical Sciences, McGraw-Hill, (1969).

[47] Morton, P.A.; Tanbun-Ek, T.; Logan, R.A.; Sergent, A.M.; Sciortino, P.F.Jr.; Coblentz, D.L., "Frequency Response Subtraction for Simple Measurement of Intrinsic Laser Dynamic Properties", IEEE Photonics Technology Letters, Vol. 4(2), 1041-1135, (1992).

[48] Bierman, R., Report: Small signal laser characterization, BNR Internal Report, February 23, (1995).

[49] H. Lu, High temperature operation of uncoated 1.3 μm ridge waveguide Fabry-Perot lasers utilizing a strained layer MQW active region, BNR Internal memo, Nov, (1993).

[50] van Exter, M.P.; Hamel, W.A.; Woerdman, J.P.; Zeijlmans, B.R.P., "Spectral signature of relaxation oscillations in semiconductor lasers", IEEE Journal of Quantum Electronics, Vol. 28(6), 1470-8, (1992).

[51] Nagarajan, R.; Fukushima, T.; Corzine, S.W.; Bowers, J.E., "Effects of carrier transport on high-speed quantum well lasers", Applied Physics Letters, Vol. 59(15), 1835-1837, (1991).

[52] Ishikawa, T.; Nagarajan, R.; Bowers, J.E., "Analysis of the effects of doping and barrier design on the small-signl modulation characteristics of long-wavelength multiple quantum well lasers", Optical and Quantum Electronics, Vol. 26, S805-S816, (1994).

[53] Lin, C.H.; Tsai, C.Y.; Chua, C.L.; Lo, Y.H., "Effects of transport limited nonuniform pumping for multiple quantum well semiconductor lasers", LEOS '94. Conference Proceedings. IEEE Lasers and Electro-Optics Society 1994 7th Annual Meeting , Vol.1, 121-2.

[54] Tessler, N.; Eisenstein, G., "Transient Carrier Dynamics and Photon-Assisted Transport in Multiple-Quantum-Well Lasers", IEEE Photonics Technology Letters, Vol. 5(3), 291-2, (1993).

[55] Huang, J.; Casperson, L.W., "Tutorial review: Gain and saturation in semiconductor lasers", Optical and Quantum Electronics, 25, 369-90, (1993).

[56] Walpita, L.M., "Solutions for Planar Optical Waveguide Equations By Selecting Zero Elements in a Characteristic Matrix", Journal of Optical Society of America, Vol. 2(4), 595-602, (1985).

[57] Kressel, H.; Butler, J.K., Semiconductor Lasers and Heterojunction LEDs, New York: Academic, (1979).